Universidad de Guanajuato

División de Ciencias e Ingenierías

Two photon state engineering generated in microstructured fibers

An Undergraduate Thesis submitted for evaluation and defense in consideration for academic recognition

Bachelor's degree in Physics

by

Diego Ángel Patiño Ruiz

Supervised By

Dr. LORENA BERENICE VELAZQUEZ IBARRA

Mtro. DANIEL RODRIGUEZ GUILLEN

León, Guanajuato, 2026

Abstract

In this work, spontaneous four wave mixing (SFWM) in photonic crystal fibers (PCFs) is investigated as a source for spectrally engineered photon pairs for photonic applications. A model based on the joint spectral amplitude (JSA) formalism was developed to analyze the influence of fiber geometry dispersion properties and pumping conditions on the spectral correlations. The phase matching function and pump envelope were, then, simulated for two different PCFs configurations, allowing the corresponding joint spectral intensities (JSIs) to be analyzed. The results show that modifications of the fiber geometry and pump wavelength lead to changes in the shape, orientation and localization of the JSI.

To quantify the modal structure of the general states, the JSA was discretized through singular value decomposition. This provides access to the Schmidt Modes, Schmidt coefficients, Schmidt Number, etc. Simulations revealed configurations with Schmidt numbers close to unity and dominant leading Schmidt coefficients. This to verify the potential of SFWM for frequency quantum encoding, with theoretical conditions required for frequency-bin Bell states from two dominant Schmidt modes. Although no fiber configurations satisfied the conditions, the analysis demonstrates the potential and versatility of SFWM as source of structured biphoton states for quantum information processing and maniputation.

Acknowledgment

If you could see your whole life from the start to finish, would you change things?
- Arrival (2016).

La escritura de esta tesis no ha sido solo un gran desafío intelectual, si no emocional, no puedo solo pensar en agradecer una sola persona. La influencia de muchas personas han llevado a este punto.

Obviamente, toda vida mamífera empieza con mamá y papá y yo no soy la excepción. Estoy agradecido con mis padres por acompañarme, amarme y apoyarme incondicionalmente a pesar de que no fui el mejor hijo y mi adolescencia fue una época complicada, pero a pesar de todo aquí estoy: fuera del abismo en el que yo mismo me metí, y con el que batallo a diaro. Pero mejor que nunca, haciendo algo que nunca me vi logrando, estudiando algo que no sabía que me gustaba y con la esperanza de un futuro mejor. Creo que después de muchos años puedo decir que me encontré, y quiero agradecerle a mis padres por soportarme en este proceso, fue muy difícil, pero se logró.

Mamá, te amo, gracias por criarme, gracias por cuidarme, gracias por amarme, gracias por mantenerme, por entenderme, por escucharme y finalmente, gracias por soltarme. Eres una excelente madre y estoy agradecido contigo porque lo hiciste lo mejor que pudiste, te esforzaste como nadie que conozco para darme una buena vida, gracias por darme la oportunidad de estudiar, gracias por criarme, gracias por siempre amarme. Te amo madre, disfruta de la vida cerca del mar.

Papá, te amo, nuestra relación ha sido por no decir otra palabra extraña, sin embargo, eso no quita que mis recuerdos más felices en la infancia sean viendo A Prueba de Todo o House contigo. Te amo padre, nunca dejaré de hacerlo. Gracias por el apoyo en la carrera, gracias por presentarme a mi mayor pasión: la bicicleta. Gracias por darme casa durante una temporada, gracias por cuidarme, gracias por escucharme, gracias por todo padre.

Quiero agradecerle también a mis hermanos: Nadia, Bruno y Magdala, por el simple hecho de existir. Nadia, eres una madre maravillosa. Y a mis pequeños: son unos niños espectaculares, divertidos, gritones, escandalosos, genuinos, quiero verlos felices siempre. Pueden hacer lo que quieran, tienen todo el potencial y el tiempo del mundo para conseguirlo, esfuerzense y diviertanse niños. Los amo a todos ustedes, hermanos, sé que no tenemos la relación más unida, pero eso no quita que los ame.

A mi sobrino Oliver, a mis tíos, tías, primos, primas, abuelos y abuelas. Y aunque mis abuelos maternos no están vivos para ver esto, espero que estén orgullosos.

En mi caso particular, sin ir a explicaciones, hay más madres y más padres. Muchas figuras me han acompañado y formado a lo largo de mi vida, padrastros como Emilio, niñeras como Verito y trabajadoras del hogar como Zenaida y Herminia. Algunas de estas personas que me acompañaron ya no me acompañan físicamente, aunque las llevo conmigo todos los días, por lo cual quiero agradecerles por todo. Sin embargo, una figura que creo de debería reconocerse más en la formación del infante y ser humano es el **profesorado**. Agradezco muchísimo la cantidad de buenos profesor@s que me pudieron acompañar en mi niñez, al los directores Lolita Botella y Rodolfo Horner. Agradezco a mi profesor que me dio mi primera clase de física en la secundaria: Christian. A mi profesora América, que gracias a sus clases de regularización hoy estoy en la División. Cuya gran cantidad de excelentes profesores que me encontré fue impresionante. No puedo agradecer suficiente las clases que me hicieron enamorarme de esta carrera, las clases del Dr. Tejedor, Dr. Torres, Dra. Lorena, Dr. Wiechers, Dr. Gerardo, Dr. Linares, Dr. Ignacio, Dr. Aguayo, Dr. Vargas, Dr. Picón y un gran etcétera. Tal vez no iba a todas las clases y siempre tuve problemas con la autoridad, pero aprendí muchísimo en todas y cada una de sus clases. A lo largo de mi vida académica tuve la suerte de estar rodeado de figuras pacientes, amables y con un genuino interés para que el estudiante aprenda. Además, en este último semestre conocí a mi coasesor de tesis: Daniel, a quien también quiero agradecer muchísimo por el apoyo en esta escritura, y quien es una figura muy prometedora en el área de la informática y física.

Gracias a la persona más maravillosa que conocí en la carrera: Anais, quiero agradecerte por ayudarme a formar lo que probablemente es el vínculo más estable y sano que tengo. Te amo con todo mi corazón, y te espera un futuro brillante.

Al resto de mis amigos: Bruno, Lazcano, Orlando, Eliú, Vane, Oscarín, Betito, entre otros. Muchas gracias todo, son maravillosos, fueron una gran compañía.

A la terapia en general, que me acompaña desde niño, le debo y agradezco mucho. A mi psicólogo actual Gerardo Reyes, me salvaste la vida. Si no fuera por ti probablemente estaría muerto o perdido en una vida que no quiero.

Finalmente quiero agradecerle a todos los que me faltaron, de una manera u otra influyeron en mí. Les mando un abrazo.

Diego Ángel Patiño Ruiz
División de Ciencias e Ingenierías
Universidad de Guanajuato
Guanajuato, México
20 Junio 2026

Table of Contents

List of Figures

Introduction

We live in an era of rapidly evolving technology. The accomplishments achieved by humankind over the past 80 years have been remarkable, particularly in the transmission of information and the rapid advancement of computation. Technological progress in information processing and computation has advanced at an extraordinary pace, driven largely by the continuous growth of computational power and communication technologies [1]. As a result, information science and computation are now at the forefront of emerging fields, among which quantum information and quantum computation stand out as a particularly significant one.

In natural science, Nature has given us a world and we're just to discover its laws. In computers, we can stuff laws into it and create a world.

- Alan Kay [2].

Light plays a crucial role in this context, as it has been central to the early development of quantum technologies. It is no longer merely a means to observe the world, but also a platform for processing information, thanks to advances in photonics and the understanding of the quantum properties of light. In modern laboratories, beams of light can carry information, perform computations, and even enhance data security. One of the most significant developments in optics, and more recently in photonics, is the invention of the laser (Maiman, 1960) [3]. The laser fundamentally changed the way light is studied, as it enables the generation of highly coherent and intense light, while allowing precise control over its initial conditions, making it a powerful tool in laboratory settings, among many other applications [4].

Nevertheless, generating photons with the desired quantum characteristics is far from trivial. In many cases, this requires exploiting the nonlinear properties of optical waveguides. Among the most important, and used, are optical fibers, a third order nonlinear material, which exhibit a wide range of phenomena worthy of study. However, the efficiency of these processes is often limited, as the generated photons exhibit the property of sharing spectral correlations [5]. That is why the development of nonlinear optics has helped other branches of optics. In particular, dispersion engineering is a very promising approach for designing nonlinear-based photonic systems. More recently inverse design methods have been proposed as a new strategy to optimize such systems, reducing computational cost and designing time [6]. Within this framework, spectral correlations can be engineered and controlled by manipulating the degree freedom on experimental parameters, the length of the fiber, pump spectral bandwidth, and the pump wavelength, among others. One such phenomenon, which is the focus of this thesis, is the **Spontaneous Four Wave Mixing** (SFWM) process. Although SFWM can occur in many

types of fiber, this work specifically investigates its behavior in photonic crystal fibers (PCFs) giving a high degree of desinging flexibility, as their properties can be tailored through control of its geometrical structure [6–8]

In recent decades, there has been a strong push to transition from large and complex optical setups to integrated photonic platforms, such as photonic chips and circuits. The goal is to replace bulky, non-scalable table top optical systems with compact and manufacturable devices. Today, millions of optical components can be integrated onto a single photonic chip, bringing together advances in linear and nonlinear optics, quantum optics, photonics, quantum computation, and quantum information, where the quantum information is encoded and processed using quantum states of light. The fundamental unit of quantum information is the **qubit**.

In classical computing, information is encoded in bits, which take values of either 0 or 1. In contrast, a qubit is a two level quantum system that can exist in a superposition of both states. This means that its state can be expressed as a linear combination of $|0\rangle$ and $|1\rangle$, with associated probability amplitudes [2]. Upon measurement, however, the qubit collapses into one of the basis states, recovering a classical outcome. Furthermore, qubits posses quantum entanglement, which enables correlations between quantum systems that have no classical counterpart. This feature allows quantum computers to process information in high dimensional spaces, offering potential advantages in computational power over classical systems. Despite these advantages, qubits are typically fragile and highly susceptible to environmental noise. In many physical implementations, it is necessary to suppress thermal excitations, which requires operating in a regime where $k_B T \ll \hbar\omega$. This condition often forces matter based qubit platforms, such as superconducting circuits, to operate at cryogenic temperatures.

Photonic quantum computing offers a promising alternative. Photons inherently possess quantum properties and, due to their high energies compared to thermal energies at room temperature, optical modes exhibit negligible thermal occupation. As a result, photonic qubits can operate without the need for cryogenic cooling [9], the research employs *master models* and density formalism to describe the evolution of a photonic qubit coupled to a bosonic thermal bath. By solving the equations of motion, it shows how the qubit's state converges toward a thermal equilibrium characterized by the ambient temperature. In contrast, many matter based qubits operate at microwave or lower frequencies, where thermal excitations dominate unless the system is cooled to near absolute zero, increasing both experimental complexity and cost [10].

Photons, as mentioned, possess a variety of quantum degrees of freedom, such as polarization, phase, and time, which have been extensively studied over the past decades.

Among these, polarization has historically been the most widely used; however, frequency-encoded photonic qubits have emerged as an equally promising alternative, particularly for quantum communication [11]. Because frequency-bin encoding is intrinsically coupled to the dispersive nature of the propagation channel, this allows the signal architecture to align with the transmission's natural modes and frequency selectivity of the physical environment. Moreover, because frequency resides in a continuous Hilbert space, it naturally enables the encoding of high-dimensional quantum states (qudits).

The Schmidt decomposition of the Joint Spectral Amplitude (JSA) allows one to identify independent spectral modes that can be directly associated with quantum information carriers [12]. Additionally, frequency-bin states can be generated using compact and integrated photonic sources and are readily manipulated. Frequency-bin encoding is compatible with spectrally heterogeneous matter qubits and supports dense spectral multiplexing, making it a strong candidate for scalable quantum networking architectures [13]. Frequency-bin states are typically measured or decoded through spectral filtering, pulse shaping, or interferometric techniques. However, their implementation and control require fine spectral control, which directly connects to dispersion engineering in photonic systems [14].

Chapter 1

Prelude: Nonlinear Fiber Optics

In this chapter, the theoretical foundations required to describe nonlinear light propagation in optical fibers are developed and understood. Starting from Maxwell's equations, the electromagnetic description of wave propagation in dielectric media, the nonlinear polarization response responsible for optical nonlinear effects. The properties of conventional optical fibers and photonic crystal fibers are then discussed, emphasizing the role of modal confinement, dispersion, and structural parameters. When understanding the system we are working on, we describe Kerr effects, and thus the four wave mixing process. The general expression is derived from the nonlinear polarization, obtaining the coupled amplitude equations that govern the interaction between pump, signal, and idler fields, as well as the conditions for parametric amplification and phase matching.

But, before jumping straight to Fiber Optics, it is useful to first understand light.

Light has attracted the interest of scientists for centuries; in the ancient Greece, light was a subject of study. There are numerous examples for early studies of light, such as Galileo's telescope, Hooke's microscope, Newton's experiments demonstrating that white light is composed of different colors, René Descartes' work on optics described the workings of the eye and suggested improvements for the telescope, among others [15]. A particularly interesting example of the influence and study of optics on mathematics is the *Brachistochrone Problem*. It consists in finding the curve between two points that is traversed in the shortest time by a body that starts at the initial point with zero velocity, posed by Johann Bernoulli in 1696. Although the concept had already been explored incorrectly by Galileo Galilei who proposed the curve was an arc of a circle. By drawing an analogy with the refraction of light and applying Fermat's principle of least time, Bernoulli was able to show that the curve of fastest descent is a cycloid (To understand more see: [16]). However, the modern study of light began with the work of James

Clerk Maxwell and many others before, or along him, such as Michael Faraday, André-Marie Ampère, among others. Maxwell's equations established a connection between magnetism and electricity, thus the electromagnetic theory was born, and a consequence, perhaps even more important, is that it was possible to demonstrate that light behaves like an electromagnetic wave [15]. With the birth of electromagnetic theory came the concepts of electric and magnetic fields. The connection between electromagnetic fields and light was demonstrated in 1845, when it was shown that a magnetic field rotated the plane of polarization of a light ray. But here it is pertinent to ask: What shape does this wave has?

1.1 Classical Electromagnetic Theory

Light propagation on a medium, like all electromagnetic phenomena, is described by **Maxwell's equations**. In the International System of Units Maxwell's equations take the form

Where $\mathbf{E}$ and $\mathbf{H}$ are electric and magnetic field vectors, and $\mathbf{D}$ and $\mathbf{B}$ correspond to electric and magnetic flux densities. Assume a current and charge free medium: $\mathbf{J} = 0$ and $\rho = 0$. The relations of flux densities are

$$\mathbf{D} = \epsilon_0 \mathbf{E} + \mathbf{P}, \tag{1.1}$$

$$\mathbf{B} = \mu_0 (\mathbf{H} + \mathbf{M}). \tag{1.2}$$

where ϵ_0 is the vacuum permittivity and μ_0 is the vacuum permeability. $\mathbf{P}$, $\mathbf{M}$ are the induced electric and magnetic polarizations. Assume also a nonmagnetic medium, then $\mathbf{M} = 0$. These conditions are just the conditions of **optical fibers** [17–19].

To obtain the wave equation that describes light propagating on a dielectric medium, such as an optical fiber, we use the Maxwell's equations one can eliminate $\mathbf{B}$ and $\mathbf{D}$ in favor of $\mathbf{E}$ and $\mathbf{P}$ obtaining

$$\nabla \times \nabla \times \mathbf{E} = -\frac{1}{c^2} \frac{\partial^2 \mathbf{E}}{\partial t^2} - \mu_0 \frac{\partial^2 \mathbf{P}}{\partial t^2}, \tag{1.3}$$

where c is the speed of light in vacuum and satisfies $1/c^2 = \mu_0 \epsilon_0$ [17]. Using the identity

$$\nabla \times (\nabla \times \mathbf{E}) = \nabla(\nabla \cdot \mathbf{E}) - \nabla^2 \mathbf{E}. \tag{1.4}$$

Since we are in a dielectric medium, with no free charges ($\nabla \cdot \mathbf{E} = 0$). Thus, we obtain

$$\nabla^2 \mathbf{E} - \frac{1}{c^2}\frac{\partial^2 \mathbf{E}}{\partial t^2} = \mu_0 \frac{\partial^2 \mathbf{P}}{\partial t^2}. \tag{1.5}$$

This is the wave equation of the electric field propagating in a dielectric media. Including third order nonlinear effects governed by $\chi^{(3)}$. That is, the third order electrical susceptibility, a property of a material that describes how it responds nonlinearly to intense electromagnetic fields [20].

The nonlinear effects of the field are encoded in the polarization induced by the dielectric material, that generates a nonlinear response of the field [20]. The induced polarization consist of two parts

$$\mathbf{P}(\mathbf{r}, t) = \mathbf{P}^{(L)}(\mathbf{r}, t) + \mathbf{P}^{(NL)}(\mathbf{r}, t). \tag{1.6}$$

Where the linear part $\mathbf{P}^{(L)}(\mathbf{r}, t)$ and the nonlinear part $\mathbf{P}^{(NL)}(\mathbf{r}, t)$ are related to the electric field by the general relations [17]

$$\mathbf{P}^{(L)} = \epsilon_0 \int_{-\infty}^{\infty} dt' \, \chi^{(1)}(t - t') \cdot \mathbf{E}(\mathbf{r}, t'), \tag{1.7}$$

$$\mathbf{P}^{(NL)}(\mathbf{r}, t) = \epsilon_0 \iiint_{-\infty}^{\infty} dt_1 dt_2 dt_3 \, \chi^{(3)}(t; \, t_1, t_2, t_3) \; \mathbf{E}(\mathbf{r}, t_1)\mathbf{E}(\mathbf{r}, t_2)\mathbf{E}(\mathbf{r}, t_3). \tag{1.8}$$

We have used the notation: $\mathbf{E} \cdot \mathbf{E} \cdot \mathbf{E} = \mathbf{EEE}$.

1.2 Optical Fibers

An optical fiber is the medium for transmitting light through extremely thin dielectric filaments made of various materials (in the case of interest for this thesis: silica). Light propagates through the center of the fiber, known as the **core**, which is surrounded with an optical material called **cladding**. This cladding traps light within the core due to total internal reflection, due to $n_{core} > n_{cladding}$, where n is the refractive index of the respective material. The refractive index difference between the core and cladding determines the critical angle θ_c. When the incidence angle satisfies $\theta_i > \theta_c$, total internal reflection take place [17]. An optical fiber is considered a waveguide system, where the path of the light is bounded to the limits and effects of the material [18].

Confinement of light

In free space, an electromagnetic wave propagating along the z-direction can be described as a plane wave as [20]

$$\mathbf{E}(\mathbf{r},t) = \mathbf{E}_0 e^{i(\mathbf{k}\cdot\mathbf{z}-\omega t)}, \tag{1.9}$$

where $\mathbf{k} = k_x\hat{e}_x + k_y\hat{e}_y + k_z\hat{e}_z$. In this case, the wavevector is not restricted to a single direction, and the field is spatially uniform in the transverse plane.

However, in an optical fiber, the boundary conditions imposed at the core-cladding system restrict the solution to electromagnetic fields to a discrete set of solutions of Maxwell's equations, these solutions are known as modes [6]. Depending on their confinement properties, modes can be classified as guided, radiative, or evanescent [18]. Guided modes remain confined to the fiber core, although part of their electromagnetic field extends into the cladding as an evanescent tail (this can be associated with light "leakage"). Radiative modes, on the other hand, are not confined and can carry energy away from the waveguide [18].

As a consequence of this confinement, the electric field acquires a non uniform transverse structure, allowing us to separate the transverse structure from the propagation of the field as [17]

$$\mathbf{E}(\mathbf{r},t) = F(x,y)A(z,t)e^{i(\beta z-\omega t)}, \tag{1.10}$$

where β is the **propagation constant** and $F(x,y)$ describes the transverse modal profile. Although light propagates along the fiber axis (z-axis), each mode possesses a characteristic transverse field distribution.

This can be seen in the decomposition of the wave vector: $k^2 = k_x^2 + k_y^2 + \beta^2$, where k_x and k_y describe the transverse spatial variation of the field, while β is the constant associated with the mode along the fiber axis [17, 18]. Each guided mode is characterized by its own dispersion relation: $\beta(\omega) = n(\omega)\omega/c$, depending on the material refraction index, the geometry of the wave, and the confinement. The behavior of light propagating in a fiber is encoded in $\beta(\omega)$. Expanding β in a Taylor series around a central frequency ω_0 [17, 18]:

$$\beta(\omega) = \beta(\omega_0) + \beta_1(\omega-\omega_0) + \frac{\beta_2}{2!}(\omega-\omega_0)^2 + \dots. \tag{1.11}$$

Where $\beta_m = \left[\frac{d^m\beta}{d\omega^m}\right]_{\omega_0}$, and:

- β_0 is the propagation constant evaluated at the frequency ω_0.

- $\beta_1 = \frac{1}{v_g}$, where v_g represents the group velocity of the wave. It describes the propagation speed of the envelope of a wave packet and determines the group delay per unit length.
- β_2 is known as the group velocity dispersion (GVD), because it represents the dispersion of the group velocity (how v_g changes respect to frequency). This measures how far different spectral components are separated from each other [17, 18].

If the electric field possesses a transverse modal structure, then the nonlinear optical interactions depend on how the field intensity is distributed on the crossed section of the fiber. Since guided modes are not perfectly confined and their fields gradually decay away from the fiber core [17, 18], the notion of physical beam area becomes ambiguous. To better characterize the degree of modal confinement, then, defining an effective area is necessary, this directly determines the strength of nonlinear interactions as it allows such interactions to be expressed in terms of an equivalent mode area ($\sim$ transverse modal structure). However, such a definition is far from trivial.

A commonly adopted definition presented, for example, by Agrawal and Okamoto [17, 18], begins with the *modal area* $A = \iint dxdy\,|F(x,y)|^2$ and defines the effective modal area as,

$$A_{\text{eff}} = \frac{(\iint_{-\infty}^{\infty}|F(x,y)|^2 dxdy)^2}{\iint_{-\infty}^{\infty}|F(x,y)|^4 dxdy}, \tag{1.12}$$

where $F(x,y)$, as we stated, describes the mode distribution in the fiber. The numerator corresponds to the square of the transverse modal distribution, whereas the denominator weights the transverse modal distribution by its intensity squared. Thus, A_{eff} quantifies the spatial confinement of the optical intensity in the cross section [18].

In general, in nonlinear fiber optics, light is not treated as a continuous wave but rather as optical pulses. This pulsed regime enables higher peak intensities and precise temporal control, which are essential for processes such as parametric generation [20]. Thus, we will be treating light as high energy pulses.

Another thing to note about optical fibers is that they are centrosymmetric materials. This is a very important property of fibers, as it directly affects the processes that can be obtained.

Centrosymmetric Materials

A material is said to be **centrosymmetric** if its invariant under spatial inversion with respect to an arbitrary point $\mathbf{r}_0$, known as the center of symmetry. $\mathbf{r}_0$ is to be considered

a center of symmetry if it satisfies $\mathbf{r}' = 2\mathbf{r}_0 - \mathbf{r}$. When the origin is chosen at $\mathbf{r}_0 = 0$, represents the transformation: $\mathbf{r} \to -\mathbf{r}$.

The electric field transforms as [17],

$$\mathbf{E}(\mathbf{r}) \to \mathbf{E}(-\mathbf{r}) = -\mathbf{E}(\mathbf{r}), \tag{1.13}$$

Similarly, the polarization satisfies,

$$\mathbf{P}(\mathbf{r}) \to \mathbf{P}(-\mathbf{r}) = -\mathbf{P}(\mathbf{r}). \tag{1.14}$$

Thus, the electric field, and therefore, the polarization, are said to be invariant under spatial inversion. As we know, the induced polarization in a nonlinear medium can be expressed as a power series in the electric field [20],

$$\mathbf{P} = \epsilon_0 \left(\chi^{(1)}\mathbf{E} + \chi^{(2)}\mathbf{E}\mathbf{E} + \chi^{(3)}\mathbf{E}\mathbf{E}\mathbf{E} + \dots \right). \tag{1.15}$$

Under inversion, $\mathbf{E} \to -\mathbf{E}$,

$$\mathbf{P}(-\mathbf{r}) = \epsilon_0 \left(-\chi^{(1)}\mathbf{E} + \chi^{(2)}\mathbf{E}^2 - \chi^{(3)}\mathbf{E}^3 + \dots \right). \tag{1.16}$$

However, $-\mathbf{P}$ has the form,

$$-\mathbf{P} = \epsilon_0 \left(-\chi^{(1)}\mathbf{E} - \chi^{(2)}\mathbf{E}\mathbf{E} - \chi^{(3)}\mathbf{E}\mathbf{E}\mathbf{E} - \dots \right). \tag{1.17}$$

If $\mathbf{P}(-\mathbf{r}) = -\mathbf{P}(\mathbf{r})$, this implies that,

$$\epsilon_0 \left(-\chi^{(1)}\mathbf{E} + \chi^{(2)}\mathbf{E}\mathbf{E} - \chi^{(3)}\mathbf{E}\mathbf{E}\mathbf{E} + \dots \right) = \epsilon_0 \left(-\chi^{(1)}\mathbf{E} - \chi^{(2)}\mathbf{E}\mathbf{E} - \chi^{(3)}\mathbf{E}\mathbf{E}\mathbf{E} - \dots \right). \tag{1.18}$$

As we can see, all even order contributions must vanish in order to preserve inversion symmetry $\chi^{(n)} = 0\,,\ (n = 2, 4, 6, \dots)$. Thus, **in centrosymmetric materials second order nonlinear effects are forbidden** [17, 18]. Since optical fibers are centrosymmetric media, their nonlinear response is dominated by third order effects.

1.3 Photonic Crystal Fibers

A particular type of optical fiber that exhibits a complex microstructure in its transverse plane is the **photonic crystal fiber** (PCF). In these fibers, the core, whose material is

generally silica, is surrounded by a periodic arrangement of air holes ($n \approx n_{\text{air}}$), which effectively reduces the average refractive index of the cladding relative to the solid silica core [17]. The amount of air in the cladding can be quantified through the fill fraction, which is commonly approximated by the ratio d/Λ, where d is the diameter of the air holes and Λ is the pitch of the photonic structure lattice.

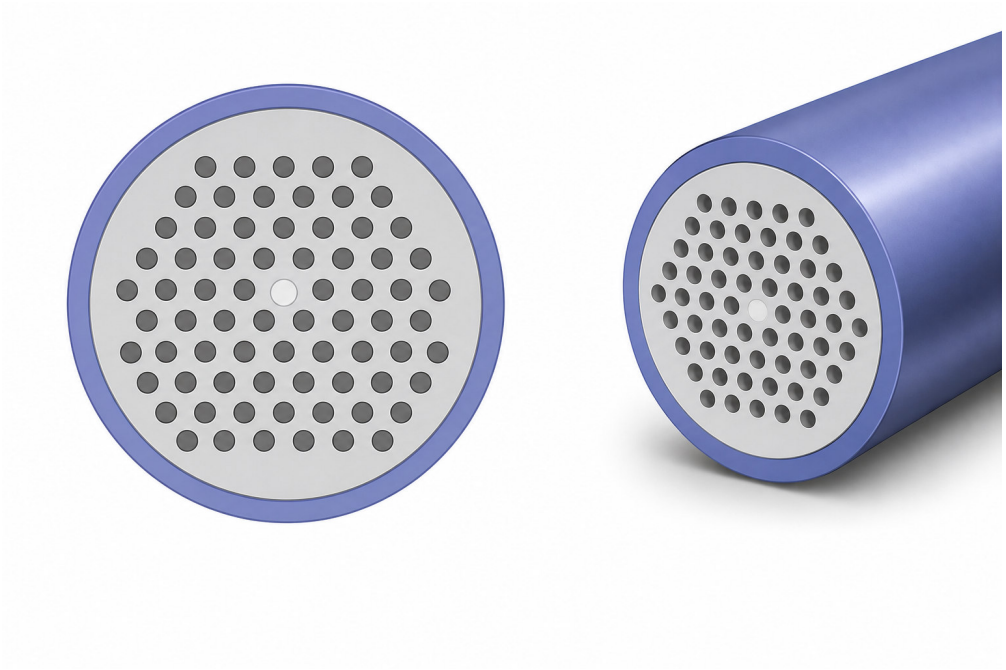

FIGURE 1.1: Structure of a single mode photonic crystal fiber (PCF), showing the solid silica core, silica microestructured cladding, and protective coating.

As previously mentioned, the microstructured geometry of PCFs provides a powerful mechanism for engineering waveguiding properties. The additional geometrical degrees of freedom enable precise control over dispersion and confinement [8].

The optical properties of the PCF are primarily determined by three geometrical parameter: the pitch Λ, the air hole diameter d (radius $r = d/2$), and the number of rings N_r surrounding the core. The pitch corresponds to the center to center distance between adjacent holes, while the air hole diameter determines the amount of air contained within the cladding. Taken together, these quantities define the air-filling fraction (f),

$$f \propto \frac{d}{\Lambda}, \tag{1.19}$$

that provides measure of the refractive index contrast between the silica core and the effective microstructured cladding [17]. The number of rings N_r determines the radial extent of the cladding. A larger number of rings improves mode confinement and reduces leakage losses because the optical field experiences a wider low index barrier before reaching the outer silica region [17].

Birefringence

An important property of certain PCFs is **modal birefringence**. Birefringence is an optical property in which a propagating electromagnetic wave splits into two orthogonally polarized components that travel with different phase velocities [18].

The strength of birefringence is characterized by the dimensionless parameter: $B_m = |n_x - n_y|$, where n_x and n_y are the effective refractive indices of the two orthogonally polarized modes. The axis associated with the lower refractive index is referred to as the **fast axis**, as it corresponds to a higher phase velocity. In contrast, the axis with the higher refractive index is known as the **slow axis** [18]. In practical fibers, birefringence is not perfectly uniform along the propagation direction, but instead varies due to structural imperfections and external perturbations. These variations lead to fluctuations in the propagation constants of the polarization modes. As a result, optical pulses may broaden during propagation due to differential group delays between polarization components. This phenomenon is known as **Polarization Mode Dispersion** (PMD) [17, 18]. It is different from GVD, yet they both contribute in the dispersion of a pulse, but in different domains.

1.4 Physical processes in fibers

Although several physical processes occur during light propagation, in optical fibers, nonlinear effects become relevant when intense optical fields interact with a dielectric medium. In this regime, the induced polarization of the material is no longer proportional to the applied electric field and must be described by nonlinear contributions to the polarization response [20]. The nonlinear response originates from the anharmonic motion of bound electrons under the influence of an external electric field, causing the induced polarization to become a nonlinear function of the electric field.

Instantaneous nonlinear effects arise when the material response follows the optical field without significant delay, resulting in negligible energy transfer between the field and the medium. In contrast, non-instantaneous (or delayed) nonlinear effects involve energy exchange with the medium and are responsible for inelastic processes such as Raman scattering [8, 17]. Nevertheless, this process will no be taken in consideration through the study.

The nonlinear processes studied in this thesis belong primarily to the class of instantaneous third order effects, many of which are collectively known as Kerr effects.

1.4.1 Instant Responses: Kerr effects

One of the most important manifestations of the optical **Kerr effect** is the intensity dependence of the refractive index [20]. For a time varying optical field, the intensity becomes a function of time, such that

$$n(t) = n_0 + n_2 I(t), \tag{1.20}$$

This causes the field to modify the medium, and the medium's response to modify the field, resulting in a variety of interactions during propagation [20]. These interactions are all, in fact, nonlinear, this can be understood by noting that n_0 is the index corresponding to the low-intensity limit, while n_2 known as the *nonlinear refractive index* coefficient which quantifies the change in refractive index induced by the optical intensity ($I(t)$) and its given by [17, 20]

$$n_2 = \frac{3Re[\chi^{(3)}]}{4\epsilon_0 c n_0^2}, \tag{1.21}$$

However, one of the most relevant variables in the manifestation of Kerr-type effects is **phase**. Phase, simply put, determines where in the oscillation cycle of the electric field is located, and therefore its state. The phase between two or more propagating waves determines how they interfere with one another. When the waves maintain the same phase (They are said to be "in phase") then their amplitudes add constructively leading to an improvement of the resultant field. On the other hand, when a phase mismatch exist (They are said to be "out of phase"), the interference becomes partially or in extreme cases completely destructive, reducing the overall amplitude.

Therefore, the relative phase is *fundamental* in the efficiency of wave interactions and parametric gain [17], as we will see later in this Chapter.

Since the refractive index is time dependent, this implies that the phase of the field will also be time dependent as well, because $\beta \rightarrow \beta[n(t)] = \beta(t)$. This leads to a process called *Self Phase Modulation*.

1.4.1.1 Self Phase Modulation

Self phase modulation (SPM) arises from the intensity dependent refractive index associated with the Kerr effect. As a result, the optical field acquires a nonlinear phase shift during propagation.

The Kerr effect introduces an intensity dependent refractive index,

$$n(t) = n_0 + n_2 I(t), \tag{1.22}$$

As a consequence, the optical field accumulates an intensity dependent phase during propagation. After traveling a distance z, the nonlinear phase shift is given by

$$\phi_{\mathrm{NL}}(z,t) = \frac{\omega_0}{c}\, n_2\, I(t)\, z, \tag{1.23}$$

or equivalently,

$$\phi_{\mathrm{NL}}(z,t) = \gamma P(t)\, z, \tag{1.24}$$

where γ is the fiber nonlinear coefficient and $P(t)$ is the instantaneous optical power. Since different temporal portions of the pulse experience different intensities, they accumulate different phase shifts. This temporal variation of the nonlinear phase is known as self phase modulation (SPM) and leads to spectral broadening of the pulse [17].

1.4.1.2 Cross Phase Modulation

When multiple optical fields co-propagate in a nonlinear fiber, the refractive index experienced by each field depends not only on its own intensity but also on the intensities of the other fields, each field has its own Kerr effect associated. This results in an additional nonlinear phase shift arising from the interaction between the co-propagating fields [20]. This phenomenon is known as *cross phase modulation* (XPM).

$$n(t) = n_0 + n_2 \left[I_1(t) + 2I_2(t)\right] \tag{1.25}$$

In contrast to SPM, where a pulse modulates its own phase, XPM arises from the intensity of one field inducing a phase shift on another field at a different frequency. As a result, the temporal intensity variations of one pulse imprint a phase modulation onto the co-propagating pulse, also leading to additional spectral broadening. When the interacting fields are pulses, their group velocities are generally different due to dispersion, leading to pulses that initially overlap gradually separate as they propagate [17]. The nonlinear interaction occurs only over the region where the pulses overlap in time and space, consequently, the strength of XPM depends mostly on the degree of temporal overlap between the pulses (or phase mismatch). The lower dispersion (or closely spaced wavelengths) reduces the group velocity mismatch, increasing the interaction length, enhancing the XPM effect [17].

1.5 Four Wave Mixing

The origin of Four Wave Mixing (FWM) lies in the nonlinear dielectric response of the material to an electromagnetic field. FWM became experimentally accessible once low-loss fibers became available and were studied during the 1980s. Nowadays, low-loss fibers can be engineered and controlled with much greater precision, such as photonic crystal fibers (PCFs) [17].

1.5.1 General form of a nonlinear polarization with an instant response

When one analyzes the third order susceptibility reduces with an instant response, the expression reduces to [17],

$$\chi^{(3)}(t;t_1,t_2,t_3) = \chi^{(3)}\,\delta(t-t_1)\delta(t-t_2)\delta(t-t_3). \tag{1.26}$$

By substituting Eq. 1.26 into Eq. 1.8 one obtains,

$$\begin{aligned}\mathbf{P}^{(NL)}(\mathbf{r},t) &= \epsilon_0 \iiint_{-\infty}^{\infty} dt_1\,dt_2\,dt_3\,\chi^{(3)}[\delta(t-t_1)\delta(t-t_2)\delta(t-t_3)]\,\mathbf{E}(\mathbf{r},t_1)\mathbf{E}(\mathbf{r},t_2)\mathbf{E}(\mathbf{r},t_3)\\ &= \epsilon_0\chi^{(3)}\,[\mathbf{E}(\mathbf{r},t)]^3.\end{aligned} \tag{1.27}$$

Consider the four waves with frequencies ω_m propagating on the z-axis. Thus, the electric field is given by the form [17],

$$E_i(\mathbf{r},t) = \frac{1}{2}\sum_{m=1}^{4}\left[E_{im}\,e^{i(\beta_m z-\omega_m t)} + c.c.\right], \qquad i = x,y,z. \tag{1.28}$$

where E_i denotes the i-th cartesian component and each β_m satisfies $\beta_m = \frac{\tilde{n}_m\omega_m}{c}$. Thus, the nonlinear polarization with an instant response can be written as

$$P_i^{(NL)} = \epsilon_0\sum_{j,k,l}\chi^{(3)}_{ijkl}E_jE_kE_l, \quad (j,k,l) = x,y,z. \tag{1.29}$$

We can also express the non polarization in the same form [17]

$$P_i^{(NL)} = \frac{1}{2}\sum_{m}^{4}\left[P_{im}^{(NL)}e^{i(\beta_m z-\omega_m t)} + c.c.\right]. \tag{1.30}$$

For simplicity, we define: $\phi_m \equiv \beta_m z - \omega_m t,\ m = 1,2,3,4.$

Substituting Eq. (1.28) into Eq. (1.29) generates a cubic product of electric fields, since each field contains both positive and negative frequency components, the expansion gives rise to all possible combinations of three interacting waves [17]. As a result, the nonlinear polarization contains terms oscillating at many different frequencies, corresponding to the various third order nonlinear processes supported by the medium. After straightforward algebra, by substituting Eq. 1.28 in Eq. 1.29, the general expression becomes

$$\begin{aligned} P_i^{(NL)} = \frac{3\epsilon_0}{8} \sum_{jkl}^{3} \sum_{mnp}^{4} \chi_{ijkl}^{(3)} \times \dots \\ \times \Big[(E_{jm} E_{kn} E_{lp}) e^{i(\phi_m + \phi_n + \phi_p)} + (E_{jm} E_{kn}^* E_{lp}) e^{i(\phi_m - \phi_n + \phi_p)} \\ + (E_{jm} E_{kn} E_{lp}^*) e^{i(\phi_m + \phi_n - \phi_p)} + (E_{jm} E_{kn}^* E_{lp}^*) e^{i(\phi_m - \phi_n - \phi_p)} \\ + (E_{jm}^* E_{kn} E_{lp}) e^{i(-\phi_m + \phi_n + \phi_p)} + (E_{jm}^* E_{kn} E_{lp}^*) e^{i(-\phi_m + \phi_n - \phi_p)} \\ + (E_{jm}^* E_{kn}^* E_{lp}) e^{i(-\phi_m - \phi_n + \phi_p)} + (E_{jm}^* E_{kn}^* E_{lp}^*) e^{-i(\phi_m + \phi_n + \phi_p)} \Big]. \end{aligned} \tag{1.31}$$

The eight exponential terms arise from the three electric field factors appearing in the nonlinear polarization. For each factor, either the field itself or its complex conjugate may contribute, yielding two possible choices for the sign of the associated phase term. Since three field factors are involved, this produces $2^3 = 8$ possible sign combinations. Furthermore, each field factor can independently correspond to any of the four interacting waves (pump 1, pump 2, signal, or idler), represented by the indices m, n, and p, giving a total of $4^3 = 64$ possible index combinations. Therefore, the complete expansion of the nonlinear polarization contains $2^3 \times 4^3 = 8 \times 64 = 512$ possible terms. However, in practice, *only the terms that meet the appropriate energy and momentum conditions contribute significantly to the nonlinear interaction* [17].

1.5.2 The FWM process

Four Wave Mixing It is a third order nonlinear process in which three interacting electromagnetic fields induce a nonlinear polarization response that generates a fourth field. The fourth field, as the rest of the process, is governed under **energy conservation** and **momentum conservation** conditions, such that it is generated under the interaction of the three fields [17].

Momentum Conservation Condition:

$$\beta_4 = \beta_1 + \beta_2 - \beta_3. \tag{1.32}$$

Energy Conservation Condition:

$$\omega_4 = \omega_1 + \omega_2 - \omega_3. \tag{1.33}$$

Energy conservation dictates that, at the end of propagation the energy from the fields is transferred to the a field and one companion. By identifying ($\omega_{3,4} \rightarrow \omega_{s,i}$), where s and i represent the signal and idler photon frequencies, respectively. An input *signal* wave mixes with the pump field through Kerr nonlinearity, giving rise to a new frequency component known as the *idler* wave [17].

FWM presents in the next cases:

- Degenerate FWM: $\omega_1 = \omega_2 = \omega_p$. So that $2\omega_p = \omega_s + \omega_i$.
- Non-Degenerate FWM: $\omega_1 = \omega_{p1} \neq \omega_{p2} = \omega_2$. So that $\omega_{p1} + \omega_{p2} = \omega_s + \omega_i$.

1.5.3 Co-polarized scalar model

Considering the scalar case in which all four fields are linearly polarized along the principal axis of birefringent fiber such that they maintain their state of polarization constant along the entire propagation ($\chi^{(3)}_{ijkl} \approx \chi^{(3)}_{xxxx}$ and thus $E_{jm} \rightarrow E_m$). The nonlinear polarization can be written as

$$\begin{aligned} P^{(NL)} = \frac{3\epsilon_0}{8}\chi^{(3)}_{xxxx} \sum_{m,n,p=1}^{4} \Big[& E_m E_n E_p\, e^{i(\phi_m+\phi_n+\phi_p)} + E_m E_n E_p^*\, e^{i(\phi_m+\phi_n-\phi_p)} \\ & + E_m E_n^* E_p\, e^{i(\phi_m-\phi_n+\phi_p)} + E_m E_n^* E_p^*\, e^{i(\phi_m-\phi_n-\phi_p)} \\ & + E_m^* E_n E_p\, e^{i(-\phi_m+\phi_n+\phi_p)} + E_m^* E_n E_p^*\, e^{i(-\phi_m+\phi_n-\phi_p)} \\ & + E_m^* E_n^* E_p\, e^{i(-\phi_m-\phi_n+\phi_p)} + E_m^* E_n^* E_p^*\, e^{-i(\phi_m+\phi_n+\phi_p)} \Big]. \end{aligned} \tag{1.34}$$

This leads to 64 possible combination of phase terms. However, when considering the study of FWM, so the system is constrained by Eq. 1.33 and Eq. 1.32. Since we are looking to describe the generated photon through FWM, we need to extract the terms that oscillate as $e^{i\phi_4}$, that is combination that satisfies: $\phi_4 = \phi_m + \phi_n - \phi_p$.

1. **Self Phase Modulation (SPM)**

   If: $m = n = p = 4 \;\therefore\; \omega_4 + \omega_4 - \omega_4 = \omega_4$.

   Then: $E_4^* E_4 E_4 = E_4 E_4^* E_4 = E_4 E_4 E_4^* = |E_4|^2 E_4$.

The field modifies the refractive index seen by itself through the Kerr nonlinearity, producing an intensity dependent phase accumulation without energy exchange between different frequencies.

2. **Cross Phase Modulation (XPM)**

   If: $m = 4,\ n = p = q \mid q = 1, 2, 3 \ \therefore\ \omega_4 = \omega_4 + \omega_q - \omega_q$.

   Then: $E_4 E_q E_q^* = E_4 E_q^* E_q = E_q^* E_q E_4 = E_q E_q^* E_4 = E_q E_4 E_q^* = E_q^* E_4 E_q$.

   Since $|E_q|^2 E_4 = E_4 |E_q|^2$, it follows that $|E_q|^2 E_4 + E_4 |E_q|^2 = 2|E_q|^2 E_4$.

   This term describes an inter modal nonlinear interaction where the intensity of one field modifies the phase of another co-propagating field. Unlike SPM, here the refractive index change experienced by the wave at ω_4 is induced by the presence of additional fields at different frequencies.

3. **Four Wave Mixing (FWM)**

   If: $(m, n, p) = (1, 2, 3) \ \therefore\ \omega_4 = \omega_1 + \omega_2 - \omega_3 = \omega_2 + \omega_1 - \omega_3$.

   Then: $E_4 = 2E_1 E_2 E_3^*$ and its complex conjugate $E_4^* = 2E_1^* E_2^* E_3$.

   The factor 2 arises because $E_4 = E_1 E_2 E_3^* + E_2 E_1 E_3^*$.

   This solution contributes to **Four Wave Mixing**. Note that E_4^* represents the conjugate interaction process, where the same phase matching condition is satisfied with reversed roles of the fields. Both terms describe the FWM process. In this case, two pump photons effectively mix with a signal photon to generate a new idler frequency.

Then the polarization of the fourth field takes the form [17],

$$\begin{aligned} P_4 &= \frac{3\epsilon_0}{4}\chi^{(3)}_{xxxx}\left[|E_4|^2 E_4 + 2(|E_1|^2 + |E_2|^2 + |E_3|^2)E_4 + 2E_1 E_2 E_3^* + 2E_1^* E_2^* E_3\right] e^{i\phi_4} \\ &= \frac{3\epsilon_0}{4}\chi^{(3)}_{xxxx}\left[|E_4|^2 E_4 + 2\sum_{q\neq 4}|E_q|^2 E_4 + 2E_1 E_2 E_3^* + 2E_1^* E_2^* E_3\right] e^{i\phi_4}. \end{aligned} \tag{1.35}$$

1.5.4 Coupled amplitude equations

We propose the same modal decomposition introduced previously in Eq. 1.10,

$$E_j(\mathbf{r}, t) = F_j(x, y)\tilde{A}_j(z)e^{i(\beta_j z - \omega_j t)}, \quad (j = 1, 2, 3, 4). \tag{1.36}$$

where $F_j(x, y)$ is the transverse modal profile, β_j is the propagation constant, and $\tilde{A}_j(z)$ is a slowly varying amplitude.

For the following analysis, quasi-continuous-wave conditions, corresponding to a steady state regime with long optical pulses, are assumed [17],

$$A(z,t) \to A(z), \qquad \frac{\partial A}{\partial t} \approx 0.$$

In this regime, the temporal dependence of each field component is contained in the carrier factor $e^{-i\omega_j t}$. Thus, each wave corresponds to a single Fourier component centered at frequency ω_j. Therefore, the next relation is satisfied [20].

$$\frac{\partial^2 E_j}{\partial t^2} = -\omega_j^2 E_j.$$

The propagation of the four interacting waves is governed by the nonlinear Helmholtz equation. Since the total field has been decomposed into four monochromatic components (See Eq. 1.28) each frequency component ω_j satisfies the nonlinear Helmholtz equation in the frequency domain [17],

$$\nabla^2 E_j + \frac{\omega_j^2}{c^2}\left[1 + \chi^{(1)}(\omega_j)\right] E_j = -\frac{\omega_j^2}{c^2 \epsilon_0} P_j^{(NL)}. \tag{1.37}$$

The left hand side describes the linear propagation of the guided mode, whereas the nonlinear polarization acts as a source term coupling the interacting waves through the Kerr response.

The transverse modal profile $F_j(x,y)$ is chosen to satisfy the linear eigenvalue equation of the waveguide [18]. As a consequence, after substituting Eq. 1.36 into Eq. 1.37, the transverse linear propagation terms are canceled by the modal eigenvalue relation, leaving an equation that governs the longitudinal evolution of the modal envelopes and their nonlinear coupling through the Kerr response [17].

Furthermore, under the slowly varying envelope approximation (SVEA),

$$\left|\frac{d^2 \tilde{A}_j}{dz^2}\right| \ll \beta_j \left|\frac{d\tilde{A}_j}{dz}\right|, \tag{1.38}$$

the second longitudinal derivative of the envelope can be neglected. This approximation assumes that nonlinear interactions modify the modal amplitudes over characteristic distances much larger than the optical wavelength [20].

Thus, the nonlinear Helmholtz equation reduces to,

$$2i\beta_j F_j e^{i(\beta_j z - \omega_j t)} \frac{d\tilde{A}_j}{dz} = -\frac{\omega_j^2}{c^2 \epsilon_0} P_j^{(NL)}, \tag{1.39}$$

which constitutes the starting point for the derivation of the coupled amplitude equations governing four wave mixing.

The nonlinear polarization (Eq. 1.29) can be written as,

$$P_j^{(NL)} = \frac{3\epsilon_0}{4}\chi^{(3)} \sum_{i,k,l} F_i F_k F_l^* \, \tilde{A}_i \tilde{A}_k \tilde{A}_l^* \, e^{i(\beta_j z - \omega_j t)} e^{i\Delta\beta z}. \tag{1.40}$$

By substituting the nonlinear polarization into the wave equation, one obtains a set of coupled propagation equations for the field amplitudes. The resulting evolution equation contains both phase modulation terms and parametric frequency conversion terms, leading to the general solution,

$$\frac{dA_j}{dz} = \frac{in_2\omega_j}{c}\left[\left(\tilde{f}_{jj}|A_j|^2 + 2\sum_{k\neq j}\tilde{f}_{jk}|A_k|^2\right)A_j + 2\tilde{f}_{ijkl}A_iA_kA_l^*e^{i\Delta\beta z}\right]. \tag{1.41}$$

For the derivation see Appendix A. Here we explain that the contribution proportional to $(|A_j|^2A_j)$ corresponds to self phase modulation (SPM). The terms proportional to $(|A_k|^2A_j)$ describe cross phase modulation (XPM). And the second term $(2\tilde{f}_{ijkl}A_iA_kA_l^*e^{i\Delta\beta z})$ represents the FWM interaction itself.

1.5.5 Approximate analytical solution and parametric amplification

This approach is useful because it provides significant physical insight under the assumption that the pump waves are sufficiently intense to remain undepleted during the process. To further simplify the analysis, we assume that all overlap integrals are approximately equal, i.e., $\tilde{f}_{ijkl} \approx \tilde{f}_{ij} \approx \frac{1}{A_{eff}}$ [17, 18]. In this approximation, we are not concerned with the spatial differences between the waves; we will assume that they occupy essentially the same region of the core, so that the average intensity can be described by a single effective area. In other words, the effective propagation of the fundamental mode HE_{11}. Where,

$$\frac{1}{A_{eff}} = \frac{\iint dxdy|F|^4}{(\iint dxdy|F|^2)^2}. \tag{1.42}$$

We introduce the nonlinear parameter,

$$\gamma_j = \frac{n_2\omega_j}{cA_{eff}} \approx \gamma \tag{1.43}$$

This approximation works well for single mode fibers [17]. Since photonic crystal fibers (PCFs) can be either single mode or multi mode, we will assume a single mode PCF. Then, Eq. 1.41 becomes,

$$\frac{dA_i}{dz} = i\gamma \left[\left(|A_i|^2 + 2\sum_{k\neq i} |A_k|^2 \right) A_i + 2A_j^* A_k A_l e^{i\Delta\beta z} \right], \quad (i = 1, 2, 3, 4). \tag{1.44}$$

Considering only two copropagating pump waves in the fiber, i.e., $A_3 = A_4 = 0$,

$$\frac{dA_i}{dz} = i\gamma \left[(|A_i|^2 + 2\sum_{j\neq i}^{2} |A_j|^2) A_i \right], \quad (i, j = 1, 2). \tag{1.45}$$

This is a simple ordinary differential equation that can be solved by direct integration, with solution,

$$A_i(z) = A_i(0) \exp\left[i\gamma \left(|A_i|^2 + 2|A_j|^2 \right) z \right]. \tag{1.46}$$

As mentioned in Eq. A.11, $P_i = |A_i|^2$ (See Appendix A). Here, this can be specified as $P_i = |A_i(0)|^2$, where $P_{1,2}$ are the input pump powers at $z = 0$. This phase term clearly represents the contributions of SPM and XPM.

If we consider FWM effects, i.e., $A_3 \neq 0$, $A_4 \neq 0$ and the approximation $P_1, P_2 \gg P_3, P_4$, which implies $|A_1|^2, |A_2|^2 \gg |A_3|^2, |A_4|^2$.

Under this condition, it follows: $\gamma_1 \approx \gamma_2 \approx \gamma_3 \approx \gamma_4 \approx \gamma$. Then the equation for A_k is,

$$\frac{dA_k}{dz} = i\gamma \left[(|A_k|^2 + 2\sum_{j=1}^{2} |A_j|^2) A_k + 2A_i A_j A_l^* e^{i\Delta\beta z} \right], \quad (k, l = 3, 4). \tag{1.47}$$

Substituting the expressions for $A_1(z)$ and $A_2(z)$ from Eq. 1.46, we obtain,

$$\frac{dA_k}{dz} = 2i\gamma \left[(P_1 + P_2) A_k + A_1(0) A_2(0) e^{-i\theta} A_l^* \right], \tag{1.48}$$

where $\theta \equiv [\Delta\beta - 3\gamma(P_1 + P_2)]z$ [17]. Analogously with,

$$\frac{dA_l^*}{dz} = -2i\gamma \left[(P_1 + P_2) A_l^* + A_1^*(0) A_2^*(0) e^{i\theta} A_k \right]. \tag{1.49}$$

To find an analytical solution, we propose the transformation,

$$B_k(z) = A_k(z) \exp\left[-2i\gamma (P_1 + P_2) z \right]. \tag{1.50}$$

Since the pump fields undergo the same transformation, i.e., $A_1, A_2 \to B_1, B_2$, it follows that $A_{1,2}(0) = B_{1,2}(0)$. The inverse relation is given by,

$$A_k(z) = B_k(z) \exp\left[2i\gamma(P_1 + P_2)z\right]. \tag{1.51}$$

Then, by applying the derivative to Eq. 1.51, canceling common exponential factor and rearranging terms, we obtain,

$$\frac{dB_k}{dz} = 2i\gamma\, A_1(0)A_2(0)\, B_l^*\, e^{-i\theta} e^{-4i\gamma(P_1+P_2)z}. \tag{1.52}$$

Combining the phase terms gives,

$$\frac{dB_k}{dz} = 2i\gamma\, A_1(0)A_2(0)\, e^{-i\kappa z} B_l^*, \tag{1.53}$$

where $\kappa \equiv \Delta\beta + \gamma(P_1 + P_2)$ is the *effective* phase mismatch term [17, 18].

Notice that B_k depends on B_l^* and vise versa. Thus, the idler photon should be a phase conjugated version of the signal photon, that is, if the pump phases remain relatively constant during the process [17].

To solve Eq. 1.53, we differentiate once more. Then,

$$\frac{d^2B_k}{dz^2} = 2i\gamma A_1(0)A_2(0)\left[(-i\kappa)e^{-i\kappa z}B_l^* + e^{-i\kappa z}\frac{dB_l^*}{dz}\right]. \tag{1.54}$$

Using,

$$\frac{dB_l^*}{dz} = -2i\gamma A_1(0)A_2(0)e^{i\kappa z}B_k. \tag{1.55}$$

By substituting in Eq. 1.54 we get the expression,

$$\frac{d^2B_k}{dz^2} = (-i\kappa)2i\gamma A_1(0)A_2(0)e^{-i\kappa z}B_l^* + 4\gamma^2 A_1(0)^2 A_2(0)^2 B_k. \tag{1.56}$$

Equation 1.53 directly implies that,

$$e^{-i\kappa z}B_l^* = \frac{1}{2i\gamma A_1(0)A_2(0)}\frac{dB_k}{dz}.$$

By substituting this relation into Eq. 1.56, we get the differential equation,

$$\frac{d^2B_k}{dz^2} + i\kappa\frac{dB_k}{dz} - (4\gamma^2 P_1 P_2)B_k = 0. \tag{1.57}$$

This is a second order linear homogeneous differential equation with constant coefficients.

1.5.5.1 Parametric Gain

We propose the solution $B_k(z) = e^{mz}$. Then,

$$\left(m^2 + i\kappa m - 4\gamma^2 P_1 P_2\right) e^{mz} = 0. \tag{1.58}$$

Since $e^{mz} \neq 0$, then m has the known solution,

$$m = \frac{-i\kappa}{2} \pm \sqrt{4\gamma^2 P_1 P_2 - \frac{\kappa^2}{4}}. \tag{1.59}$$

We define $g \equiv \sqrt{4\gamma^2 P_1 P_2 - \frac{\kappa^2}{4}}$.

Thus, the roots can be written as $m = -\frac{i\kappa}{2} \pm g$. This shows that the solution contains an oscillatory phase factor, given by the imaginary part $-\frac{i\kappa}{2}$, and an exponential growth or decay governed by the real parameter g. For convenience, we define the parameter $r \equiv \frac{2\sqrt{P_1 P_2}}{P_0}$, where $P_0 \equiv P_1 + P_2$. Then, $2\sqrt{P_1 P_2} = r P_0$ [17]. These relations allow us to rewrite g as

$$g = \sqrt{(\gamma P_0 r)^2 - \left(\frac{\kappa}{2}\right)^2}. \tag{1.60}$$

Where g is the **parametric gain**, which determines the exponential growth rate of the dignal and idler fields. Its magnitude depends on the nonlinear coupling strength and the phase mismatch between the interacting waves. The maximum gain ($g_{max} = \gamma P_0$) occurs in $\kappa = 0$ or $\Delta\beta = -2\gamma P_0$, which corresponds to a more efficient energy transfer from the pump to the generated fields. The shift in the gain peak from $\Delta\beta = 0$ is due to the contribution of SPM and XPM to the phase mismatch κ [17]. Hence, the general solution takes the form:

$$\begin{aligned} B_k(z) &= \left(a_k e^{gz} + b_k e^{-gz}\right) e^{-i\kappa z/2}, \\ B_l^*(z) &= \left(a_l e^{gz} + b_l e^{-gz}\right) e^{i\kappa z/2}. \end{aligned} \tag{1.61}$$

The form of Eq. 1.61 represents exponential growth:

- If $g > 0$: The amplification grows exponentially.
- If g is pure imaginary: The amplification behavior is oscillatory.

Visualization of the analytical solution

To gain physical insight into the behavior of the generated fields, the analytical solution given by Eq. 1.61 was evaluated numerically for representative parameter values to visualize the different dynamical regimes predicted by the approximate solution and to

illustrate the role of the phase-mismatch parameter (κ) in the evolution of the field amplitudes. The calculations were carried out using representative parameters for silica optical fibers reported and the nonlinear coefficient was chosen within the typical range ($\gamma = 1.5 \times 10^{-5}\,\mathrm{W^{-1}mm^{-1}}$), corresponding to ($1.5 \times 10^{-2}\,\mathrm{W^{-1}m^{-1}}$), while the pump powers were taken as ($P_1 = P_2 = 1\,\mathrm{W}$), values representative of nonlinear optical fiber experiments (Values can be found in [8, 17]). The field amplitudes were initialized with the arbitrary constants $a_k = -1.0$, $b_k = 1.2$, $a_l = 1.5$, and $b_l = -1.1$. The phase mismatch parameter κ was varied in order to explore different dynamical regimes of Eq. 1.61. In Fig. 1.2, the nearly phase-matched regime $\kappa \to 0$ is considered, leading to exponential amplification characterized by hyperbolic growth. In contrast, Fig. 1.3 shows the case of larger phase mismatch ($\kappa > 1$), where the solutions exhibit an oscillatory behavior due to the reduction of the effective parametric gain.

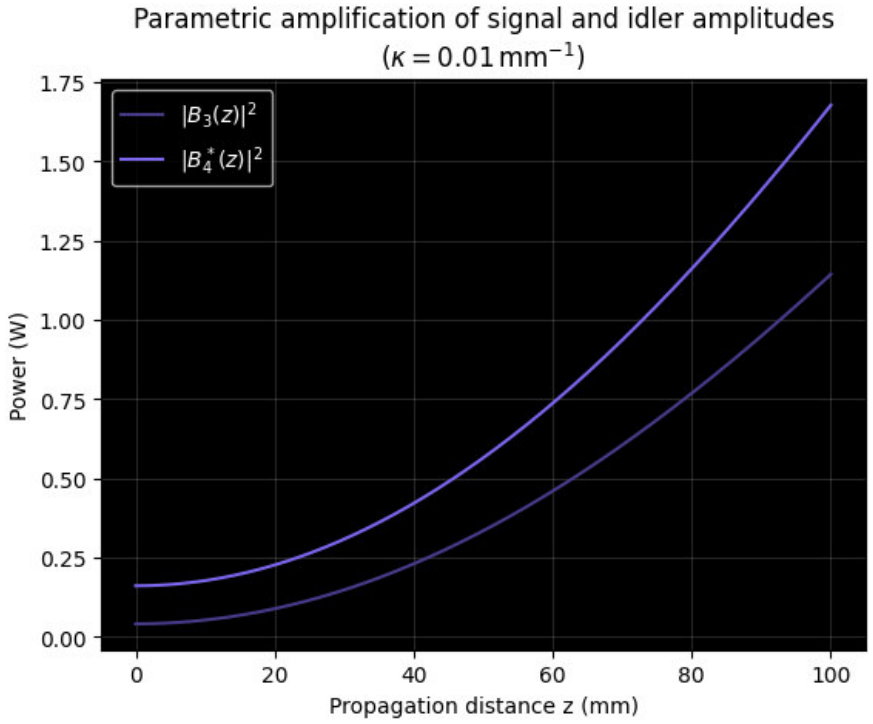

FIGURE 1.2: Nearly phase matched ($\kappa \to 0$), showing exponential amplification due to efficient energy transfer between interacting waves.

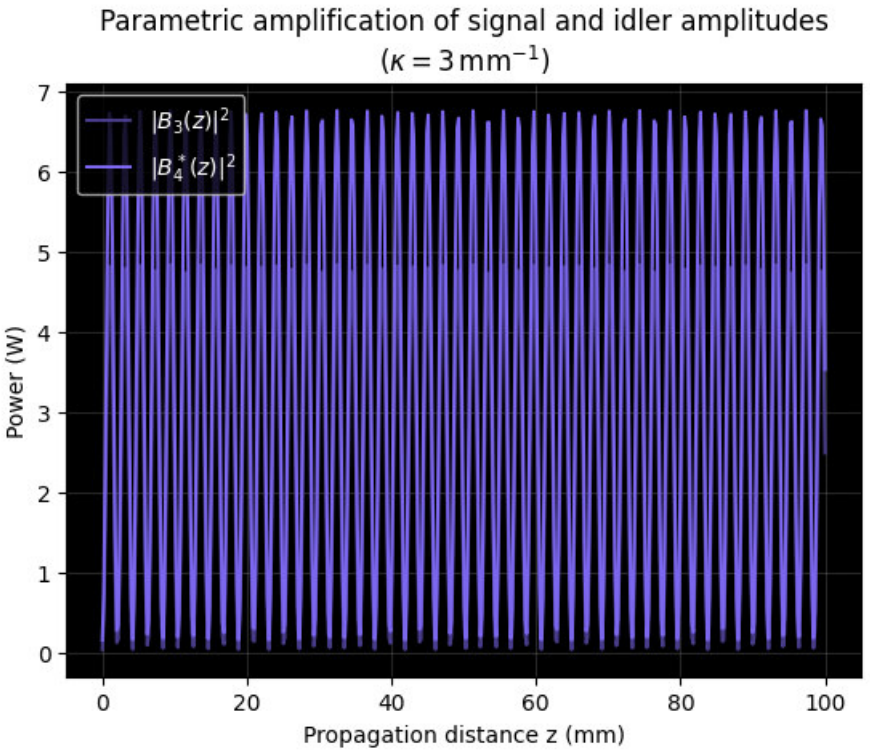

FIGURE 1.3: Nearly phase matched ($\kappa \to 0$), showing exponential amplification due to efficient energy transfer between interacting waves.

This directly implies that when the fields are in phase, or the phase matching condition is satisfied $\kappa \approx 0$, the field interfere constructively and the process is generated. And thus, when $\kappa > 0$ the fields interfere, and the process is never generated.

1.5.6 Phase Matching

Phase matching refers to the condition under which the interacting waves maintain a fixed phase relation as they propagate through a nonlinear medium. Under this condition, the momentum mismatch is minimized, allowing nonlinear contributions generated along the medium to interfere constructively [17]. If phase matching is not satisfied, the contribution of each wave is out of phase and the transference of energy oscillates, instead of growing (As seen in Figures 1.2–1.3) [18]. Phase matching, then, refers to the condition where the phases of two or more waves, such as laser beams or conditions of fibers, are adjusted in such a way that their combined effect is maximized. Therefore, efficient nonlinear interaction requires $\kappa \approx 0$. We can decompose the total phase mismatch as [17]

$$\kappa = \Delta\beta_M + \Delta\beta_W + \Delta\beta_{NL}, \tag{1.62}$$

where:

- $\Delta\beta_M$: material dispersion contribution,
- $\Delta\beta_W$: waveguide dispersion contribution,
- $\Delta\beta_{NL}$: nonlinear phase mismatch.

We write the effective refractive index as $\tilde{n}_j = n_j + \Delta n_j$, where $n_j \equiv n_M(\omega_j)$ is the material refractive index and Δn_j accounts for the waveguide contribution. For degenerate FWM ($\omega_1 = \omega_2 = \omega_p$), the phase mismatch can be written as [17, 18]

$$\kappa = \frac{1}{c}\left[(n_3 + \Delta n_3)\omega_3 + (n_4 + \Delta n_4)\omega_4 - 2(n_1 + \Delta n_1)\omega_1\right]. \tag{1.63}$$

Thus, the different contributions can be identified as:

- $\Delta\beta_M = \frac{1}{c}\left(n_3\omega_3 + n_4\omega_4 - 2n_1\omega_1\right)$,
- $\Delta\beta_W = \frac{1}{c}\left(\Delta n_3\omega_3 + \Delta n_4\omega_4 - 2\Delta n_1\omega_1\right)$,
- $\Delta\beta_{NL} = \gamma(P_1 + P_2)$.

To satisfy $\kappa \approx 0$, these contributions must compensate each other. That means, at the must be at least one negative contribution from one term. The contribution of the material $\Delta\beta_m$ can be expressed in terms of the *Shift Frequency* (Ω_s). Where: $\Omega_s = \omega_1 - \omega_3 = \omega_4 - \omega_1$, if we use the Taylor expantion of $\beta(\omega)$, to the 4-th term:

$$\beta_{3,4} = \beta(\omega_{3,4} = \omega_1 \pm \Omega_s) = \beta_1 + \beta_1'\Omega_s + \frac{\beta_2}{2}\Omega_s^2 + \frac{\beta_3}{6}\Omega_s^3 + \frac{\beta_4}{24}\Omega_s^4. \tag{1.64}$$

Since, $\Delta\beta_M = \beta_3 + \beta_4 - 2\beta_1$, Δk_m takes the form:

$$\Delta\beta_M = \beta_2\Omega_s^2 + \frac{\beta_4}{12}\Omega_s^4. \tag{1.65}$$

Here, β_2 and β_4 denote the dispersion parameters evaluated at the pump frequency ω_1. When the pump wavelength $\lambda_1 = 2\pi c/\omega_1$ is sufficiently far from the zero dispersion wavelength (ZDW) λ_0 of the fiber, the material contribution to the phase mismatch can be approximated as $\Delta\beta_M \approx \beta_2\Omega_s^2$ [17]. Since $\beta_2 > 0$, $\beta_2 \gg \beta_4$ for $\lambda_1 < \lambda_0$, it follows that $\Delta\beta_M$ is positive in the visible and near infrared spectral regions. In single mode fibers, the waveguide contribution $\Delta\beta_W$ is typically much smaller than the material term $\Delta\beta_M$ for co-polarized waves ($\Delta\beta_W \ll \Delta\beta_M$), except in the vicinity of the ZDW, where both contributions become comparable. For a more detailed discussion of phase matching techniques, see Chapter 10 of Agrawal [17].

Chapter 2

Spontaneous Four Wave Mixing

The objective of this Chapter is to develop the quantum description of Spontaneous Four Wave Mixing (SFWM) in nonlinear optical fibers, starting from the classical electromagnetic energy formalism to find the nonlinear interaction through a Hamiltonian framework. This allows for the transition from the macroscopic description of nonlinear propagation to a quantum description of photon pair generation. By applying perturbation theory in the interaction picture, the nonlinear process is described as the creation of correlated *signal* and *idler* photons from the vacuum from the vacuum state. The final result of this approach is the general biphoton state generated by SFWM in an optical fiber, expressed in terms of the joint spectral structure of the emitted photon pair.

> "There may be situations where nature has arranged, or we arrange nature, to be simple and to have so few parts that we can predict exactly what will happen, and thus we can check how our rules work."
>
> — Richard P. Feynman [21]

It is always useful to first understand the classical framework before approaching a problem directly in quantum framework. In the article *"On the Analogy Between Classical and Quantum Mechanics"* [22], Dirac dedicates his entire work to showing that the structure of quantum mechanics is best understood through its relationship to classical mechanics.

Throughout this thesis, this line of thought will be repeated, always beginning by describing the simplest possible case to connect with the process of interest.

2.1 Nonlinear Quantum Framework: Spontaneous Four Wave Mixing

The classical analysis presented in the previous Chapter provided a detailed understanding of four wave mixing in terms of coupled propagation equations and nonlinear polarization. Such a formulation is sufficient to understand the macroscopic behavior of the interacting fields: phase matching, self phase modulation, cross phase modulation, and frequency conversion. The purpose of the following discussion is then, is not to replace the classical picture developed previously, but to reformulate it for quantization, so the physical intuition gained from the classical treatment is preserved.

Spontaneous Four Wave Mixing, on the other hand, is the quantum counterpart of classical Four Wave Mixing. Although both correspond to the same third order nonlinear interaction ($\chi^{(3)}$) and obey the same phase matching and energy conservation conditions, they differ in the origin of the generated fields. In classical FWM, weak signal and idler fields are assumed to be present at the input and are parametrically amplified through the nonlinear interaction. In contrast, SFWM is initiated by vacuum fluctuations: the signal and idler modes are initially in the vacuum state and are *spontaneously* populated inside the nonlinear medium by the annihilation of two pump photons, leading to the generation of correlated signal and idler photon pairs. Throughout this process, the pump field is treated as a strong classical electromagnetic field [8], while the quantum nature of the interaction emerges inside the nonlinear medium manifest in the generated signal and idler photons at the output.

Usually a quantum description requires that the dynamics be expressed in a Hamiltonian framework [23]. In the case of SFWM in optical fibers, an important question naturally arises: *what is the form of the Hamiltonian that describes this nonlinear interaction?* In general, the Hamiltonian associated with SFWM is highly complex due to the nonlinear coupling between electromagnetic modes, this motivates the use of perturbation theory, which we will properly discussed in more detail later.

However, as stated, the process is initially classical. So, let us begin with finding the general Hamiltonian that describes nonlinear electromagnetic interactions.

2.1.1 Electromagnetic Energy and Hamiltonian Formalism

Following the classical electromagnetic formulation presented in [24] [Born, Wolf (1999)]. Electromagnetic theory interprets light intensity as the energy flux carried by the electromagnetic field. Maxwell's equations in SI is,

$$\nabla \times \mathbf{H} - \frac{\partial \mathbf{D}}{\partial t} = \mathbf{J}, \tag{2.1}$$

$$\nabla \times \mathbf{E} + \frac{\partial \mathbf{B}}{\partial t} = 0. \tag{2.2}$$

By taking the scalar product of $\mathbf{E}$ on the first equation and of the second equation respect to $\mathbf{H}$, obtaining,

$$\mathbf{E} \cdot (\nabla \times \mathbf{H}) - \mathbf{H} \cdot (\nabla \times \mathbf{E}) = \mathbf{J} \cdot \mathbf{E} + \mathbf{E} \cdot \frac{\partial \mathbf{D}}{\partial t} + \mathbf{H} \cdot \frac{\partial \mathbf{B}}{\partial t}. \tag{2.3}$$

Using the vector identity:

$$\nabla \cdot (\mathbf{E} \times \mathbf{H}) = \mathbf{H} \cdot (\nabla \times \mathbf{E}) - \mathbf{E} \cdot (\nabla \times \mathbf{H}). \tag{2.4}$$

The left side becomes,

$$\mathbf{E} \cdot (\nabla \times \mathbf{H}) - \mathbf{H} \cdot (\nabla \times \mathbf{E}) = -\nabla \cdot (\mathbf{E} \times \mathbf{H}). \tag{2.5}$$

Substituting Eq. 2.5 into Eq. 2.3. Assuming an electric field and a magnetic field propagating on a medium with volume V and integrating over the volume to obtain the electric and magnetic field densities, we obtain,

$$\iiint_V dV \left[\left(\mathbf{E} \cdot \frac{\partial \mathbf{D}}{\partial t} + \mathbf{H} \cdot \frac{\partial \mathbf{B}}{\partial t} \right) + (\mathbf{J} \cdot \mathbf{E}) + \nabla \cdot (\mathbf{E} \times \mathbf{H}) \right] = 0. \tag{2.6}$$

Applying Gauss's theorem [25],

$$\iiint_V \nabla \cdot \mathbf{F} \, dV = \iint_S \mathbf{F} \cdot \hat{\mathbf{n}} \, dS, \tag{2.7}$$

and assuming a free current medium ($\mathbf{J} = \mathbf{0}$), give us the expression

$$\iiint_V \left(\mathbf{E} \cdot \frac{\partial \mathbf{D}}{\partial t} + \mathbf{H} \cdot \frac{\partial \mathbf{B}}{\partial t} \right) dV + \iint_S (\mathbf{E} \times \mathbf{H}) \cdot \hat{\mathbf{n}} \, dS = 0. \tag{2.8}$$

Using the relations [24, 25],

$$\mathbf{E}\cdot\frac{\partial\mathbf{D}}{\partial t}=\frac{1}{2}\frac{\partial}{\partial t}(\mathbf{E}\cdot\mathbf{D}),\qquad \mathbf{H}\cdot\frac{\partial\mathbf{B}}{\partial t}=\frac{1}{2}\frac{\partial}{\partial t}(\mathbf{H}\cdot\mathbf{B}). \tag{2.9}$$

In SI units, the electric and magnetic energy densities are defined as [26],

$$W_e\equiv\frac{1}{2}(\mathbf{E}\cdot\mathbf{D}),\qquad W_m\equiv\frac{1}{2}(\mathbf{H}\cdot\mathbf{B}). \tag{2.10}$$

The total electromagnetic energy inside the volume V is [8],

$$W(t)=\iiint_V (W_e+W_m)\,dV. \tag{2.11}$$

Since the integration volume V is fixed in time, we obtain de following relation,

$$\iiint_V \frac{\partial}{\partial t}(W_e+W_m)\,dV=\frac{\partial}{\partial t}\iiint_V (W_e+W_m)\,dV=\frac{dW(t)}{dt}. \tag{2.12}$$

Then, finally obtaining the corresponding expression for **Poynting's theorem**,

$$\frac{dW}{dt}+\iint_S(\mathbf{E}\times\mathbf{H})\cdot\hat{\mathbf{n}}\,dS=0. \tag{2.13}$$

The Poyinting theorem expresses the conservation of energy for the electromagnetic fields, stating that the variation of the electromagnetic field, stating that variation of the electromagnetic energy stored within a given volume arises from either the energy flux crossing its boundary or the energy exchanged between the field and the material. $\mathbf{S}$ is the Poynting vector, describes the flow of electromagnetic energy and, in the case of a propagating wave, indicates the direction of energy transportas an ideal optical fiber, no electromagnetic energy is dissipated as heat, and the total electromagnetic energy is conserved during propagation [8, 25]. Consequently, the total energy of the electromagnetic field can be identified with the Hamiltonian of the system,

$$H=\int_V (W_e+W_m)\,dV. \tag{2.14}$$

2.1.2 The Hamiltonian that describes Spontaneous Four Wave Mixing

Recall that the electromagnetic response of the medium is described by [26, 27],

$$\mathbf{D}=\epsilon_0\mathbf{E}+\mathbf{P},\qquad \mathbf{B}=\mu_0\mathbf{H}+\mathbf{M}. \tag{2.15}$$

As mentioned, in optical fibers, the magnetic response is typically negligible, such that $\mathbf{M} = \mathbf{0}$ [17]. Analogous to the previous nonlinear analysis, we consider two pumps propagating with collinear polarization propagating through a fiber. And a colinear polarization with the form,

$$\mathbf{P} = \mathbf{P}^{(L)} + \mathbf{P}^{(NL)} = \epsilon_0 \chi^{(1)} \mathbf{E} + \epsilon_0 \chi^{(3)} \, \mathbf{EEE}, \quad \chi^{(3)} = \chi^{(3)}_{xxxx}, \tag{2.16}$$

and a field with the form [28],

$$\mathbf{E}(\mathbf{r}, t) = (E_1 + E_2 + E_s + E_i)\, \hat{\mathbf{x}}. \tag{2.17}$$

As is been demonstrated, each field can be decomposed into its positive and negative frequency components as,

$$E_\alpha = \frac{1}{2}\left(E_\alpha^{(+)} + E_\alpha^{(-)}\right), \qquad (\alpha = 1, 2, s, i). \tag{2.18}$$

Defined analogous to Eq. 1.28,

$$E_\alpha^{(+)} = E\, e^{i(\beta_\alpha z - \omega_\alpha t)}, \qquad E_\alpha^{(-)} = E^* e^{-i(\beta_\alpha z - \omega_\alpha t)}. \tag{2.19}$$

In a quantum framework the positive frequency component is associated with photon annihilation processes, whereas the negative frequency component is associated with photon creation processes in the quantized description [29].

Substituting the field decomposition into the nonlinear polarization expansion leads to,

$$\mathbf{P} = \epsilon_0 \chi^{(1)} E_\alpha + \frac{1}{8} \epsilon_0 \chi^{(3)} E_\alpha E_\beta E_\gamma. \tag{2.20}$$

Focusing only on contributions to $\mathbf{D}$ oscillating at frequency ω_1 that satisfies the SFWM energy conservation relations $\omega_1 = \omega_2 - \omega_s - \omega_i$ and $\omega_1 = \omega_s + \omega_i - \omega_2$. Proceeding analogously to the nonlinear analysis, we identify the resonant that contributes to the cases

- $\omega_1 = \omega_1 - \omega_1 + \omega_1$: There are three permutations of the form $E_1 E_1 E_1^* \sim |E_1|^2 E_1$, corresponding to SPM,

$$3E_1 E_1 E_1^* \sim 3|E_1|^2 E_1.$$

- $\omega_1 = \omega_2 - \omega_2 + \omega_1$: There are 3! permutations of the form $E_2 E_2^* E_1 \sim |E_2|^2 E_1$, corresponding to XPM, resulting in

$$6E_2 E_2^* E_1 \sim 6|E_2|^2 E_1.$$

  Combining both SPM and XPM contributions in Eq. 2.20 leads to,

$$\frac{3}{4}\epsilon_0 \chi^{(3)} \left(|E_1|^2 + 2|E_2|^2\right) E_1.$$

- $\omega_1 = \omega_2 - \omega_s - \omega_i$: Including the complex conjugate terms there are $(3!) + (3!)$ permutations of: $6E_2^{(+)} E_s^{(-)} E_i^{(-)} + 6E_2^{(-)} E_s^{(+)} E_i^{(+)}$. These terms describe the SFWM interaction itself and this contribution takes the form,

$$\frac{3}{4}\epsilon_0 \chi^{(3)} \left(2E_2^{(+)} E_s^{(-)} E_i^{(-)} + 2E_2^{(-)} E_s^{(+)} E_i^{(+)}\right). \tag{2.21}$$

As we have learn, it is useful to separate the SFWM interaction terms from the linear, SPM, and XPM contributions. This is achieved by defining,

$$\eta_e \equiv 1 + \chi^{(1)} + \frac{3}{4}\chi^{(3)} \left(|E_1|^2 + 2|E_2|^2\right) = n^2. \tag{2.22}$$

We define, $\epsilon \equiv \epsilon_0 \eta_e$ that represents the effective dielectric constant and n is the refractive index of the medium [8]. By decomposing $\mathbf{D}$ into positive and negative frequency components, we can write the positive frequency component of the dielectric displacement as,

$$\mathbf{D}_1^{(+)} = \epsilon E_1^{(+)} + \frac{3}{4}\epsilon_0 \chi^{(3)} 2E_2^{(+)} E_s^{(-)} E_i^{(-)}. \tag{2.23}$$

And finally, the complete dielectric displacement vector is obtained by adding the corresponding negative frequency contribution. Since $\mathbf{D}_1 = \frac{1}{2}\left[\mathbf{D}_1^{(+)} + \mathbf{D}_1^{(-)}\right]$, then we can write the expression,

$$\mathbf{D}_1 = \frac{1}{2}\left[\epsilon \left(E_1^{(+)} + E_1^{(-)}\right) + \frac{3}{4}\epsilon_0 \chi^{(3)} \left(2E_2^{(+)} E_s^{(-)} E_i^{(-)} + 2E_2^{(-)} E_s^{(+)} E_i^{(+)}\right)\right]. \tag{2.24}$$

From the definition of the electric energy density in Eq. 2.10 and using the constitutive relation $\mathbf{D} = \epsilon \mathbf{E} + \mathbf{P}^{(3)} + \cdots$, the electric energy density can be written as

$$W_e = \frac{1}{2}\epsilon E^2 + \frac{1}{2}\mathbf{E} \cdot \mathbf{P}^{(3)}, \tag{2.25}$$

where the first term corresponds to the linear energy of the electromagnetic field, while the second term contains the nonlinear interaction responsible for the coupling between the optical modes.

For the SFWM process, the nonlinear polarization is identified by Eq. 2.21 and thus can be written as,

$$\mathbf{P}^{(3)}_{\text{SFWM}} = \frac{3}{4}\epsilon_0\chi^{(3)}\left(2E_2^{(+)}E_s^{(-)}E_i^{(-)} + 2E_2^{(-)}E_s^{(+)}E_i^{(+)}\right)\hat{\mathbf{x}}. \tag{2.26}$$

Finally, identify the energy density (**Hamiltonian**) associated with the SFWM process as,

$$W_{e,(SFWM)} = \frac{3}{4}\epsilon_0\chi^{(3)}E_1^{(+)}E_2^{(+)}E_s^{(-)}E_i^{(-)}. \tag{2.27}$$

This quantity represents the interaction energy per unit volume stored in the nonlinear medium [8, 26]. The corresponding Hamiltonian is obtained by integrating the energy density over the interaction volume,

$$H_{SFWM}(t) = \int_V W_{e,(SFWM)}(\mathbf{r},t)\,dV. \tag{2.28}$$

It is important to emphasize that E_1 and E_2 are treated as classical pump fields, whereas E_s and E_i are quantized fields.

Therefore, the quantum Hamiltonian ($H \to \hat{H}$) representing SFWM process is,

$$\hat{H}(t) = \frac{3}{4}\epsilon_0\chi^{(3)}\int_V \left[E_1^{(+)}(\mathbf{r},t)E_2^{(+)}(\mathbf{r},t)\hat{E}_s^{(-)}(\mathbf{r},t)\hat{E}_i^{(-)}(\mathbf{r},t)\right]\,dV. \tag{2.29}$$

In the free field regime, each electromagnetic mode evolves independently under the action of the free Hamiltonian [29]. However, nonlinear processes such as SFWM introduce a weak coupling between pump, signal, and idler modes, allowing the exchange of energy and momentum among them [8, 26]. Since this nonlinear interaction is typically much weaker than the free evolution of the field, it can be treated as a perturbation to the free field dynamics [23, 30].

2.1.3 Perturbation Theory and the Interaction Picture

The interaction picture (or Dirac Picture) is an intermediate formulation between the Schrödinger and Heisenberg representation, designed to facilitate perturbation theory. In this picture, dynamics are divided between states and operators; operators evolve only under the free Hamiltonian denoted as $\hat{H}_0$, while states incorporate interaction

through the full evolution operator. This contrasts with the Schrödinger picture, where states evolve and operators are fixed, and with Heisenberg picture, where the opposite operators evolve and states are fixed [31]. Despite these differences in the designation of time dependence, the three descriptions are completely equivalent and lead to the same physical predictions. Guaranteeing the invariance of observables under the change or representation [30].

A convenient framework for describing weak nonlinear interactions is provided by *perturbation theory* in *the interaction picture*. In this representation, the free evolution generated by the unperturbed Hamiltonian is treated exactly as previously described, while the nonlinear interaction is incorporated through a perturbative Interaction Hamiltonian [23]. In SFWM, the interaction is sufficiently weak that the generated quantum fields may be regarded as small perturbations to the free electromagnetic field [26, 27], and thus is an ideal process to study in this framework.

The Interaction Picture, also known as the *Dirac picture*, provides the natural framework for perturbation theory (we use the subscript S to indicate the Schrödinger picture and the subscript H to indicate the Heisenberg picture). In the Schrödinger picture, the state vectors evolve in time while the operators remain fixed. Conversely, in the Heisenberg picture, the operators carry the time dependence while the state vectors remain constant. Both formulations yield identical physical predictions and are therefore completely equivalent descriptions of quantum dynamics [23, 27, 32].

For an arbitrary operator $\hat{q}$, in the Heisenberg picture operator is defined as

$$\hat{q}_H(t) = \hat{U}_0^\dagger(t, t_0)\, \hat{q}_S\, \hat{U}_0(t, t_0),$$

where $\hat{U}(t, t_0)$ is the time evolution operator [32].

In the interaction picture, the operators evolves only under the free Hamiltonian $\hat{H}_0$, such that [31],

$$\hat{q}_I(t) = \hat{U}_0^\dagger(t, t_0)\, \hat{q}_S\, \hat{U}(t, t_0), \qquad \hat{U}_0(t, t_0) = \exp\left[-\frac{i}{\hbar}\hat{H}_0(t - t_0).\right] \tag{2.30}$$

Accordingly, the interaction picture state vector is defined as $|\psi(t)\rangle_I = \hat{U}^\dagger(t, t_0)\, |\psi(t)\rangle_S$ [31, 32]. These definitions ensure that physical observables remain invariant under the choice of representation and statistical properties are conserved between pictures [31].

Perturbation theory consists of treating the interaction Hamiltonian as a small correction to a known and solvable free Hamiltonian. Thus, the total Hamiltonian may be

decomposed as,

$$\hat{H} = \hat{H}_0 + \hat{H}_I, \tag{2.31}$$

where $\hat{H}_I$ contains the nonlinear interaction terms responsible for the SFWM process [26]. Explicitly,

$$\hat{H}_0 = \hat{H}_A + \hat{H}_F, \tag{2.32}$$

here, $\hat{H}_A$ and $\hat{H}_F$ represent the Hamiltonians of the noninteracting atomic medium and the free electromagnetic field, respectively [27].

In the interaction picture, the interaction Hamiltonian evolves as (See Eq. 2.30),

$$\hat{H}_I(t) = \hat{U}_0^\dagger(t, t_0)\hat{H}_I\hat{U}_0(t, t_0).$$

The quantum state associated with any process is obtained from the general expression

$$|\psi(t)\rangle_I = \hat{U}_I(t, t')\,|\psi(t')\rangle_I\,.$$

That satisfies [31],

$$i\hbar\frac{d}{dt}\hat{U}_I(t, t') = \hat{H}_I(t')\hat{U}_I(t, t'). \tag{2.33}$$

Using the *Dyson expansion* to solve the differential equation [31, 32],

$$\hat{U}_I(t) = \hat{T}\exp\left[\frac{1}{i\hbar}\int_0^t dt'\hat{H}_I(t')\right] \approx 1 + \frac{1}{i\hbar}\int_0^t dt'\hat{H}_I(t'), \tag{2.34}$$

where, $\hat{T}$ denotes the time ordering operator, which arranges products of the time dependent operators in chronological order (To see more detail about this operator see [31]). Thus, the state $|\psi(t)\rangle_I$ may be written as,

$$|\psi(t)\rangle_I = \hat{U}_I(t, t')\,|\psi(t')\rangle_I\,, \quad \hat{U}_I(t, t') = 1 + \frac{1}{i\hbar}\int_{t_0}^t dt'\hat{H}_I(t'). \tag{2.35}$$

The SFWM process can be interpreted as the generation of a signal-idler photon pair from the vacuum state $|0\rangle$, through previous nonlinear interactions inside the fiber. Therefore, the interaction Hamiltonian must contain terms capable of creating such photon pairs. This suggests a contribution of the form: $\hat{H}_I \sim \hat{a}_s^\dagger\hat{a}_i^\dagger$, where $\hat{a}_s^\dagger$ and $\hat{a}_i^\dagger$ are the creation operators associated with the signal and idler modes, respectively. If we consider that the process succeded to the Hamiltonian interaction acting on the vacuum state must generate a two-photon state: $\hat{H}_I\,|0\rangle = |1\rangle_s\,|1\rangle_i$. We can identify that Eq. 2.29

precisely generates this biphotonic state, since the creation of two photons is encoded in the creation operators that form the electric field operator $\hat{E}^{(+)}_{s,i}$.

2.2 Description of the biphoton state generated by SFWM

Now that we know the form of the interaction Hamiltonian and how it evolves it time, we can find the form of the state generated by spontaneous four wave mixing.

In a quantum context, the generated state must be associated with a Hilbert space composed of the signal and idler Hilbert subspaces. Specifically, let $\mathcal{H}^{(s)}$ and $\mathcal{H}^{(i)}$ denote the Hilbert spaces corresponding to the signal and idler modes, respectively. The complete biphoton system is therefore described in the tensor product space as,

$$\left(\mathcal{H}^{(s)} \otimes \mathcal{H}^{(i)}\right) \subseteq \mathcal{H}^{(I)}. \tag{2.36}$$

The tensor product describes the joint biphoton state generated during the nonlinear interaction (See more about Hilbert Spaces in Appendix C). Then, the vacuum state of the combined system is written as $|0\rangle = |0\rangle_s |0\rangle_i$. It is understood that we are in the interaction frame, due to Eq. 2.36, so the subscript will not be explicitly written from now on, except to distinguish whether it is the free or interaction Hamiltonian.

In SFWM biphoton state context, we can revise Eq. 2.35 as,

$$|\psi(t)\rangle = \left[1 + \frac{1}{i\hbar}\int_0^t dt'\, \hat{H}_I(t')\right] |0\rangle_s |0\rangle_i \,. \tag{2.37}$$

Since $\hat{H}_I(t)$ has the form given by Eq. 2.29, substituting into Eq. 2.37 give us the general expression,

$$|\psi(t)\rangle = \left[1 + \frac{1}{i\hbar}\int_0^t dt' \left\{\frac{3}{4}\epsilon_0\chi^{(3)}\int_V \left[E_1^{(+)}(\mathbf{r},t')E_2^{(+)}(\mathbf{r},t')\hat{E}_s^{(-)}(\mathbf{r},t')\hat{E}_i^{(-)}(\mathbf{r},t')\right]dV\right\}\right] |0\rangle_s |0\rangle_i \,.$$

We define, similar to the spacetime coordinate, $x' \equiv (\mathbf{r}', t')$, so that the previous expression may be written in the compact form,

$$|\psi(t)\rangle = \left[1 + \frac{3\epsilon_0\chi^{(3)}}{4i\hbar}\int_V d^3\mathbf{r}' \int_0^t dt'\, E_1^{(+)}(x')E_2^{(+)}(x')\hat{E}_s^{(-)}(x')\hat{E}_i^{(-)}(x')\right] |0\rangle_s |0\rangle_i \,. \tag{2.38}$$

Here, the integration extends over the volume of the interaction and the time interval of the interaction $0 \leq t' \leq t$. For convenience, we define,

$$|\psi(t)\rangle = |0\rangle_s |0\rangle_i + |\Psi^{(2)}\rangle \,. \tag{2.39}$$

This state represents a quantum superposition between the vacuum component and the two photon component generated through the SFWM interaction. The term $|0\rangle_s |0\rangle_i$ corresponds to the vacuum state, i.e., the absence of generated photons, and $|\Psi^{(2)}\rangle \sim |1\rangle_s |1\rangle_i$ represents the successful generation of a correlated signal-idler photon pair. Physically, this structure reflects the probabilistic character of spontaneous nonlinear processes: the vacuum component remains the most likely outcome, while pair generation occurs with a much smaller probability [27, 30]. The coexistence of both amplitudes in the same quantum state is a direct consequence of the coherent unitary evolution governed by the interaction Hamiltonian.

The biphoton state, then, is defined as,

$$|\Psi^{(2)}\rangle \equiv \frac{3\epsilon_0 \chi^{(3)}}{4i\hbar} \left[\int_V d^3\mathbf{r}' \int_0^t dt' \, E_1^{(+)}(x') E_2^{(+)}(x') \hat{E}_s^{(-)}(x') \hat{E}_i^{(-)}(x') \right] |0\rangle_s |0\rangle_i \,. \tag{2.40}$$

To find the forms of $E_{1,2}^{(+)}$ and $\hat{E}_{s,i}^{(-)}$, we use the forms given in [8], that followed the work presented by Mandel and Wolf in *Optical Coherence and Quantum Optics* [26].

The signal and idler electric fields, written in SI units, takes the form,

$$\hat{E}_\lambda^{(+)}(\mathbf{r}, t) = i \sqrt{\frac{\hbar \omega_\lambda}{\epsilon_0 n^2 V}} \, \hat{a}_\lambda \mathbf{u}_\lambda(\mathbf{r}) e^{-i\omega_\lambda t}, \quad \lambda = s, i. \tag{2.41}$$

Where the spatial mode function is written as $\mathbf{u}_\lambda(\mathbf{r}) = f_\lambda(x, y) e^{i\beta_\lambda z}$ [26]. Therefore,

$$\hat{E}_\lambda^{(+)}(\mathbf{r}, t) = i \sqrt{\frac{\hbar \omega(\beta_\lambda)}{\epsilon_0 n^2 V}} \, \hat{a}(\beta_\lambda) f_\lambda(x, y) e^{i\beta_\lambda z} e^{-i\omega(\beta_\lambda)t}. \tag{2.42}$$

By imposing periodic boundary conditions over a quantization length L_Q, the propagation constant becomes discretized according to $\beta_\lambda = \frac{2\pi m}{L_Q}$, where $m \in \mathbb{Z}$. Consequently, the mode spacing is $\delta_k \equiv \frac{2\pi}{L_Q}$ [26]. If the effective quantization volume is written as $V \equiv A_{\text{eff}} L_Q$ and we define [17],

$$\Theta_\lambda = \iint |f_\lambda(x, y)|^2 dx dy, \tag{2.43}$$

Obtaining the relations,

$$V = \Theta_\lambda L_Q, \qquad \sqrt{\frac{\hbar\omega(\beta_\lambda)}{\epsilon_0 n^2 V}} \to \sqrt{\frac{\hbar\omega(\beta_\lambda)\delta_k}{2\pi\epsilon_0 n^2 \Theta_\lambda}}, \qquad l(\beta_\lambda) = \sqrt{\frac{h\omega_\lambda}{2\pi\epsilon_0 n_\lambda^2}}. \tag{2.44}$$

This relations follows the standard quantization procedure for electromagnetic fields in dielectric media presented in [27] and [26], and adapted to guided optical modes in fibers in [8] and [33] (We'll discuss the physical meaning of $l(\beta)$ in the next chapter). In this formalism, the electromagnetic field is decomposed into a discrete set of longitudinal propagation modes satisfy periodic boundary conditions over the quantization length L_Q. The transverse spatial dependence is described by the normalized modal profile $f_\lambda(x, y)$, while the longitudinal and temporal evolution is contained in the phase factor $\exp[-i(\omega_\lambda t - \beta_\lambda z)]$ but in time domain. In optical fibers, this normalization constant is naturally generalized through the effective modal area and the longitudinal quantization length [17, 26]. Therefore, the negative frequency component of the electric field operator takes the form [8],

$$\hat{E}_\lambda^{(-)}(\mathbf{r}, t) = -i\sqrt{\frac{\delta_k}{\Theta_\lambda}} f_\lambda^*(x, y) \exp\left[i(\omega_\lambda t - \beta_\lambda z)\right] l(\beta_\lambda)\, \hat{a}_\lambda^\dagger. \tag{2.45}$$

Classical fields, on the other hand, are treated as classical pumps, i.e., coherent electromagnetic fields [27]. These fields can be expressed in terms of their Fourier components such as,

$$E^{(+)}(\mathbf{r}, t) = \int d^3\mathbf{k} \tilde{E}(\mathbf{k}) e^{i(\mathbf{k}\cdot\mathbf{r} - \omega t)}. \tag{2.46}$$

For guided propagation in a fiber, we decompose the wavevector into the transverse and longitudinal components $\mathbf{k} \to (\mathbf{k}_\perp, \beta)$. Therefore,

$$E_\rho^{(+)}(\mathbf{r}, t) = A_\rho f_\rho \int d\beta_\rho \alpha(\omega_\rho) e^{i(\beta_\rho z - \omega_\rho t)}, \qquad (\rho = 1, 2), \tag{2.47}$$

where $\alpha(\omega_\rho)$ is the spectral amplitude of the pump and we absorb normalization constants into A_ρ.

Although the transverse profile $f_\rho(x, y)$ is, in general, frequency dependent, in single-mode fibers the differences between the transverse distributions of the interacting fields are sufficiently small to be neglected in practice [8, 17, 33]. If V stands for the volume of the fiber, we can separate it like we have been doing: $\iiint_V d^3\mathbf{r} = \iint_A dxdy \int_0^L dz$. We use the approximation: $f_\rho \approx f_\lambda \approx f_\lambda^* \approx f(x, y)$ (Similar to the nonlinear classic framework). And also, bearing in mind that while $|\psi(t)\rangle$ will be represented in time domain yet, the fields are in frequency fourier domain: $E_\rho(\mathbf{r}, t)$, $E_\lambda(\mathbf{r}, t) \to E_\rho(\mathbf{r}, \omega_\rho)e^{-i\omega_\rho t}$, $E_\lambda(\mathbf{r}, \omega_\lambda)e^{-i\omega_\lambda t}$.

Using Eq. 2.47 and Eq. 2.45 in Eq. 2.38, the state can be written as,

$$|\psi(t)\rangle = \Bigg\{1 + \frac{3\epsilon_0\chi^{(3)}}{4i\hbar}\Bigg[\int_0^L dz\, e^{i(\beta_1+\beta_2-\beta_s-\beta_i)z}\iint_A dxdy|f(x,y)|^4 \\ \ldots \times \int_0^t \left(\iint d\omega_1 d\omega_2 \alpha(\omega_1)\alpha(\omega_2)e^{-i(\omega_1+\omega_2-\omega_s-\omega_i)t'}\right)dt'\Bigg] \times \ldots \\ \ldots \times \left(-\frac{A_1A_2\delta_k}{\sqrt{\Theta_s\Theta_i}}\, l(\beta_s)l(\beta_i)\hat{a}^\dagger(\beta_s)\hat{a}^\dagger(\beta_i)\right)\Bigg\}|0\rangle_s|0\rangle_i\,. \tag{2.48}$$

We know that

$$\int_0^t dt' \iint \omega_1\omega_2\,\alpha(\omega_1)\alpha(\omega_2)e^{-i(\omega_1+\omega_2-\omega_s-\omega_i)t'} \to \ldots \\ \ldots \to \iint \omega_1\omega_2\,\alpha(\omega_1)\alpha(\omega_2)\int_0^t dt' e^{-i(\omega_1+\omega_2-\omega_s-\omega_i)t'}.$$

The temporal integral appearing in the perturbative expansion is key in establishing energy conservation during the interaction. For finite interaction times, this integral produces a sinc shaped spectral response centered at $\omega_1+\omega_2 = \omega_s+\omega_i$. As the interaction time becomes much longer than the optical time scale, the sinc function becomes increasingly narrow and approaches a Dirac delta distribution, in the distributional sense. Consequently, only frequency combinations satisfying $\Delta\omega = \omega_1+\omega_2-\omega_s-\omega_i$ contributes significantly to the process, enforcing energy conservation between the annihilated pump photons and the generated signal and idler pair. This result follows directly from the Fourier transform relation between long temporal interactions and spectral selectivity, this is standard result of time dependent perturbation theory [27, 31]. Thus it satisfies

$$\int_0^t dt'\, e^{-i\Delta\omega t'} = e^{-i\Delta\omega t/2}\, t\,\mathrm{sinc}\left(\frac{\Delta\omega t}{2}\right) \Rightarrow \lim_{t\to\infty} t\,\mathrm{sinc}\left(\frac{\Delta\omega t}{2}\right) = 2\pi\delta(\Delta\omega). \tag{2.49}$$

We define: $\Omega \equiv \omega_s+\omega_i$, so: $\delta(\Delta\omega) \to \delta(\omega_1+\omega_2-\Omega)$. Therefore,

$$\int d\omega_1\alpha(\omega_1)\int d\omega_2\alpha(\omega_2)\delta(\omega_1+\omega_2-\Omega) = \int d\omega_1\alpha(\omega_1)\alpha(\Omega-\omega_1). \tag{2.50}$$

We can approximate, because the area is the same and also simmetric, such that $(\Theta_s\Theta_i)^{-1/2} \approx (\Theta^2)^{-1/2} = \Theta^{-1} = (\iint dxdy|f(x,y)|^2)^{-1}$. Then,

$$\frac{\iint dxdy|f(x,y)|^4}{\iint dxdy|f(x,y)|^2} = \frac{\Theta}{A_{eff}}. \tag{2.51}$$

It can be proven that (See Appendix B),

$$\int_0^L dz\, e^{i\Delta\beta z} = L\,\mathrm{sinc}\left(\frac{L}{2}\Delta\beta\right) e^{i\frac{L}{2}\Delta\beta}. \tag{2.52}$$

Simplifications lead to,

$$\frac{3i\chi^{(3)}\epsilon_0}{4\hbar}\frac{\Theta A_1 A_2}{A_{eff}} 2\pi L\delta_k \left(l(\beta_s)l(\beta_i)\int d\omega\, \alpha(\omega)\alpha(\Omega-\omega)\,\mathrm{sinc}\left[\frac{L}{2}\Delta\beta\right] e^{i\frac{L}{2}\Delta\beta}\right)\hat{a}^\dagger(\beta_s)\hat{a}^\dagger(\beta_i).$$

As we know from Eq. A.9 (See Appendix A), we can then simplify more,

$$A_\rho = \sqrt{P_\rho \frac{2}{\epsilon_0 c n_\rho \Theta}} \Rightarrow A_1 A_2 = \frac{2}{\epsilon_0 c\sqrt{n_1 n_2}\Theta}\sqrt{P_1 P_2}. \tag{2.53}$$

Even in the degenerate case the pump powers are kept as independent parameters for generality. Therefore,

$$\frac{3i\chi^{(3)}\epsilon_0}{4\hbar}\frac{\Theta A_1 A_2}{A_{eff}} 2\pi L\delta_k \rightarrow \frac{3i\chi^{(3)}}{4\hbar}\frac{2\sqrt{P_1 P_2}}{n_1 c A_{eff}} 2\pi L\delta_k. \tag{2.54}$$

To facilitate comparison with the standard nonlinear fiber formalism, the third order susceptibility is expressed in terms of the nonlinear coefficient γ. Notice that Eq. 1.43 is equivalent to the expression,

$$\gamma(\omega) = \frac{3}{4}\frac{\chi^{(3)}\omega}{\epsilon_0 n^2(\omega) c^2 A_{eff}}. \tag{2.55}$$

Thus, one can rewrite,

$$\frac{3}{4}\frac{\chi^{(3)}}{A_{eff}}\frac{1}{c\,n(\omega_1)} = \gamma(\omega_1)\left(\frac{\epsilon_0 c\, n(\omega_1)}{\omega_1}\right). \tag{2.56}$$

Substituting this relation into Eq. 2.54 yields,

$$\frac{3i\chi^{(3)}}{4\hbar}\frac{2\sqrt{P_1 P_2}}{n_1 c A_{eff}} 2\pi L\delta_k = i\frac{2(2\pi)\epsilon_0 c n(\omega_1)}{\hbar\omega_1} L\,\gamma(\omega_1)\sqrt{P_1 P_2}\,\delta_k. \tag{2.57}$$

After all these simplifications, the state may be written as,

$$
\begin{aligned}
|\psi(t)\rangle = & \underbrace{|0\rangle_s |0\rangle_i}_{\text{Vaccum}} + \dots \\
& \cdots + \Bigg\{ \underbrace{\left(i\frac{2(2\pi)\epsilon_0 c n(\omega_1)}{\hbar\omega_1} L\gamma(\omega_1)\sqrt{P_1 P_2}\delta_k \right)}_{\text{Overal SFWM interaction strength}} \times \dots \\
& \dots \times \underbrace{\left(l(\beta_s)l(\beta_i) \int d\omega\, \alpha(\omega)\alpha(\Omega-\omega)\, \text{sinc}\left[\frac{L}{2}\Delta\beta\right] e^{i\frac{L}{2}\Delta\beta} \right)}_{\text{Spectral correlations}} \Bigg\} \times \dots \\
& \dots \times \underbrace{\left[\hat{a}^\dagger(\beta_s)\hat{a}^\dagger(\beta_i) |0\rangle_s |0\rangle_i \right]}_{\text{Creation of two photons}} .
\end{aligned}
\tag{2.58}
$$

We define [8],

$$
\zeta \equiv i\frac{2(2\pi)\epsilon_0 c n(\omega_1)}{\hbar\omega_1} L\gamma(\omega_1)\sqrt{P_1 P_2}\delta_k, \tag{2.59}
$$

where ζ characterizes the overall strength of the SFWM interaction and sets the scale of the biphoton generation amplitude. Since it is proportional to the nonlinear coefficient γ, the pump powers, and the interaction length, larger values of $|\zeta|$ correspond to a higher probability of photon pair generation. Although ζ controls the overall efficiency of pair generation, it does not affect the spectral structure of the biphoton state [8]. The spectral properties of the generated are contained in Eq. 2.60, as it will be proven. The present work is primarily concerned with the spectral structure and correlations of the generated state. We define the expression,

$$
G(\beta_s, \beta_i) \equiv l(\beta_s)l(\beta_i) \int d\omega\, \alpha(\omega)\alpha(\Omega-\omega)\, \text{sinc}\left[\frac{L}{2}\Delta\beta\right] e^{i\frac{L}{2}\Delta\beta}, \tag{2.60}
$$

where $G(\beta_s, \beta_i)$ is known as the **Joint Spectral Function** (JSF). This definition follows the conventions used in [8] and [33].

Therefore,

$$
|\Psi^{(2)}(t)\rangle = \zeta \sum_{\beta_s,\beta_i} G(\beta_s,\beta_i)\hat{a}^\dagger(\beta_s)\hat{a}^\dagger(\beta_i) |0\rangle_s |0\rangle_i = \zeta \sum_{\beta_s,\beta_i} G(\beta_s,\beta_i) |1(\beta_s)\rangle_s |1(\beta_i)\rangle_i .
\tag{2.61}
$$

Equation 2.61 reveals the presence of **spectral correlations** between the signal and idler photons. These correlations are fully encoded in the Joint Spectral Function $G(\beta_s, \beta_i)$.

The function $G(\beta_s, \beta_i)$ acts as a *weight function* that determines the probability amplitude associated with each pair of modes (β_s, β_i). In this sense, it defines the spectral structure of the generated biphoton state and specifies which combinations of frequencies are favored or suppressed by the nonlinear interaction.

Chapter 3

Joint Spectral Amplitude

In this Chapter we derive and analyze the spectral structure of the biphoton state previously discussed. Transformation of the SFWM state into the frequency domain and reduction of the expression of the joint spectral function to the Joint Spectral Amplitude (JSA) allows for a better description of the frequency correlations between the generated signal and idler photons. Then, an analytical expression for the JSA is obtained by approximating the pump spectra as Gaussian functions and linearizing the phase mismatch around the central frequencies, allowing the spectral contribution to be separated into the pump envelope and the phase matching function. This analytical expression of the JSA relies on the previous knowledge of the central signal and idler frequencies satisfying the phase matching condition. Thus, these parameters were obtained from numerical simulations of the microstructured fibers through dispersion engineering. The resulting dispersion profiles were then used to evaluate the Joint Spectral Intensity (JSI) and compare the spectral properties of different PCF configurations.

3.1 The Joint Spectral Function

We can reparameterize the $G(\beta_s, \beta_i)$ (Eq. 2.60) in function of frequencies since: $\beta_j = \beta(\omega_j)$ $(j = s, i)$, such that,

$$\begin{aligned} &G(\beta_s, \beta_i) \rightarrow G(\omega_s, \omega_i) = l(\omega_s) l(\omega_i) F(\omega_s, \omega_i), \\ &\text{Such that, } \; F(\omega_s, \omega_i) \equiv \int d\omega \, \alpha(\omega) \alpha(\Omega - \omega) \text{sinc}\,(\Delta)\, e^{i\Delta}, \end{aligned} \tag{3.1}$$

where we have defined for simplification $\Delta \equiv \frac{L}{2}\Delta\beta$. The function $l(\omega)$ is known as the quantum mode normalization factor [8] and can be rewritten as,

$$l(\omega) = \left[\frac{\hbar\omega}{2\pi\epsilon_0 n^2(\omega)}\right]^{1/2} \sim \alpha\left(\frac{\omega}{n^2(\omega)}\right)^{1/2}, \tag{3.2}$$

where $\alpha \equiv \sqrt{\frac{\hbar}{2\pi\epsilon_0}}$. The appearance of $l(\omega)$ is a consequence of the quantization of the electromagnetic field and the use of creation operators in the interaction Hamiltonian. Since quantum mechanics requires properly normalized field operators, normalization factors naturally arise within this formalism. Let us take the natural logarithm of $l(\omega)$, in order to separate the expression such that,

$$\ln[l(\omega)] = \frac{1}{2}\ln(\omega) - \ln[n(\omega)] + \ln\alpha$$

Differentiating with respect to ω gives us the relation,

$$\frac{1}{l}\frac{dl}{d\omega} = \frac{1}{2\omega} - \frac{1}{n}\frac{dn}{d\omega}.$$

Notice that the left side represents the rate of change of l. For a finite spectral interval $\Delta\omega$ we have $\Delta l = l(\omega+\Delta\omega) - l(\omega) \approx \frac{dl}{d\omega}\Delta\omega$, such that,

$$\frac{\Delta l}{l} \approx \frac{1}{l}\frac{dl}{d\omega}\Delta\omega \approx \left(\frac{1}{2\omega} - \frac{1}{n}\frac{dn}{d\omega}\right)\Delta\omega.$$

In general, $l(\omega)$ depends only weakly on frequency compared to the spectral variations introduced by the pump envelope and the phase matching function [8]. Therefore, over the bandwidth of interest $\Delta\omega$, its relative variation satisfies,

$$\frac{1}{l(\omega)}\frac{dl(\omega)}{d\omega}\Delta\omega \ll 1. \tag{3.3}$$

This condition implies that $l(\omega)$ behaves as a slowly varying spectral envelope and may be treated as approximately constant over the relevant bandwidth [8].

Then we will know the F function as the **Joint Spectral Amplitude** (JSA) function. In practice the physical quantity that can be measured is actually the **Joint Spectral Intensity** (JSI), defined as [7, 28]

$$I(\omega_s, \omega_i) \equiv |F(\omega_s, \omega_i)|^2. \tag{3.4}$$

3.2 Closed analytical solution to the JSA

Eq. 3.1 defines the JSA as an integral and one can numerically resolve the convolution and evaluate the integral to obtain a solution, however, a detailed understanding of the factors governing the spectral correlations of the biphoton state, and their dependence on the physical parameters of a particular configuration, requires expressing the JSA in a closed analytical form [8]. Nevertheless, the integral in the equation does not have a known simplified analytical solution, and obtaining it is no trivial task. However, the lack of direct analytical solutions to an expression has never stopped physicists from finding ways to work out approximate solutions. Particularly in this case, to better understand the spectral correlations in the biphoton state, we approximate the spectral envelope $\alpha(\omega)$, assumed to be normalized of the pump fields by Gaussian functions as [7, 28, 33],

$$\alpha(\omega) = \frac{1}{\sqrt{\pi\sigma}} \exp\left[-\frac{(\omega-\bar{\omega})^2}{\sigma^2}\right]. \tag{3.5}$$

Introducing frequency detunings: $\nu_j \equiv \omega_j - \bar{\omega}_j$ allows us to express all the spectral quantities in relation to their corresponding central frequencies. Considering a general configuration involving two pump fields, characterized by central frequencies $\bar{\omega}_1$, $\bar{\omega}_2$ and bandwidths σ_1, σ_2. In terms of the detuning variables, the corresponding spectral envelopes can be written as,

$$\alpha_1(\nu_p) = \frac{1}{\sqrt{\pi\sigma_1}} \exp\left[-\frac{\nu_p^2}{\sigma_1^2}\right], \quad \alpha_2(\nu_s+\nu_i-\nu_p) = \frac{1}{\sqrt{\pi\sigma_2}} \exp\left[-\frac{(\nu_s+\nu_i-\nu_p)^2}{\sigma_2^2}\right], \tag{3.6}$$

where ν_p denotes the integration variable associated with the pump frequency [7, 8]. Energy conservation in the degenerate limit, as established, when $\bar{\omega}_1 = \bar{\omega}_2 = \bar{\omega}_p$, then the energy conservation condition reduces to $2\omega_p = \omega_s + \omega_i$. Even when considering this degenerate limit configuration, it is convenient to retain the index 1 and 2 to keep track of the origin of each contribution throughout the derivation, because degeneration is imposed on central frequencies, but in the mathematical development it is treated as different contributions associated with each pump.

The product in Eq. 3.1 becomes a product of Gaussian functions. Since *the product of Gaussian distributions is itself Gaussian*, the resulting spectral structure remains analytically tractable [34]. Thus to further simplify the expression, we use the identity *Fourier integral representation of the sinc function* [28] (See Appendix B),

$$\mathrm{sinc}(x) \approx \frac{1}{2}\int_{-1}^{1} e^{ix\xi} d\xi \quad \therefore \quad \mathrm{sinc}(\Delta)e^{i\Delta} \;\rightarrow\; \frac{1}{2}\int_{-1}^{1} d\xi \exp\left[i(1+\xi)\Delta\right]. \tag{3.7}$$

Next, when expanding the propagation constant $\beta(\omega)$ around the central frequencies $\bar{\omega}_j$, keeping only first-order terms we obtain [8, 17],

$$\begin{aligned}\Delta\beta &= \beta^1(\bar{\omega}_1)\nu_p + \beta^1(\bar{\omega}_2)(\nu_s + \nu_i - \nu_p) - \beta^1(\bar{\omega}_s)\nu_s - \beta^1(\bar{\omega}_i)\nu_i \\ &= \nu_p\left[\beta^1(\bar{\omega}_1) - \beta^1(\bar{\omega}_2)\right] + \nu_s\left[\beta^1(\bar{\omega}_2) - \beta^1(\bar{\omega}_s)\right] + \nu_i\left[\beta^1(\bar{\omega}_2) - \beta^1(\bar{\omega}_i)\right].\end{aligned} \tag{3.8}$$

We can write the phase mismatch as $L\Delta\beta = \tau_p\nu_p + \tau_s\nu_s + \tau_i\nu_i$ [7, 28], by identifying the group-delay mismatch parameters as,

$$\begin{aligned}\tau_\lambda &\equiv L\left[\beta^1(\bar{\omega}_2) - \beta^1(\bar{\omega}_\lambda)\right], \quad (\lambda = s, i), \\ \tau_p &\equiv L\left[\beta^1(\bar{\omega}_1) - \beta^1(\bar{\omega}_2)\right].\end{aligned} \tag{3.9}$$

These coefficients describe the relative group delays between the interacting fields ($\beta^{(1)} = \beta^1 = 1/v_g$), and therefore encode the temporal walk-off in the nonlinear interaction. These are called group-delay mismatches with dimensions $[\tau] = \left[\text{Length} \times \frac{\text{Time}}{\text{Length}}\right] = [\text{Time}]$ [17]. In the context of SFWM, τ describes the relavite delay between the pump and the generated signal and idler fields [8]. Thus, τ_s and τ_i represent the relative time delays acumulated between the pump, signal and idler fields through the propagation.

Then, the expression may be written as

$$\frac{1}{2}\int_{-1}^{1} d\xi\, \exp\left[\frac{i}{2}(1+\xi)\left(\tau_p\nu_p + \tau_s\nu_s + \tau_i\nu_i\right)\right]. \tag{3.10}$$

Combining the previous results into Eq. 3.1, and expressing the joint spectral amplitude in terms of the detuning variables, such as $F(\omega_s, \omega_i) \to F(\nu_s, \nu_i)$, we obtain

$$\begin{aligned}F(\nu_s, \nu_i) = \frac{1}{2}A\int_{-1}^{1} d\xi\, \exp\left[\frac{i}{2}(1+\xi)\left(\tau_s\nu_s + \tau_i\nu_i\right)\right] \times \ldots \\ \ldots \times \int d\nu_p \exp\left[-\frac{\nu_p^2}{\sigma_1^2} - \frac{(\nu_s + \nu_i - \nu_p)^2}{\sigma_2^2} + iC\,\nu_p\right],\end{aligned} \tag{3.11}$$

where we have made the definitions $A \equiv \frac{1}{\pi\sqrt{\sigma_1\sigma_2}}$, $C \equiv \frac{1+\xi}{2}\tau_p$. To further simplifications, we notice that the remaining integral ν_p is Gaussian and can be evaluated analytically to find the simplified gaussian form.

We begin by expanding the exponent, such that,

$$\int d\nu_p \exp\left[-\nu_p^2\left(\frac{1}{\sigma_1^2} + \frac{1}{\sigma_2^2}\right) + \nu_p\left(\frac{2(\nu_s + \nu_i)}{\sigma_2^2} + iC\right) - \frac{(\nu_s + \nu_i)^2}{\sigma_2^2}\right]. \tag{3.12}$$

Then define the parameters,

$$a \equiv \frac{\sigma_1^2 + \sigma_2^2}{\sigma_1^2 \sigma_2^2}, \quad b \equiv \frac{2(\nu_s + \nu_i)}{\sigma_2^2} + iC, \tag{3.13}$$

so the integral takes the standard gaussian form,

$$\int d\nu_p \, e^{-a\nu_p^2 + b\nu_p}. \tag{3.14}$$

And therefore, Eq. 3.11 takes the form,

$$\begin{aligned} F(\nu_s, \nu_i) = \frac{1}{2} A \int_{-1}^{1} d\xi \, \exp\left[\frac{i}{2}(1+\xi)\left(\tau_s \nu_s + \tau_i \nu_i\right)\right] \times \dots \\ \dots \times \exp\left[-\frac{(\nu_s + \nu_i)^2}{\sigma_2^2}\right] \int d\nu_p \, e^{-a\nu_p^2 + b\nu_p}. \end{aligned} \tag{3.15}$$

After straightforward algebraic simplifications and by using the standard Gaussian integral (see Chapter 13 of [35]), we obtain the expression,

$$\int_{-\infty}^{\infty} e^{-ax^2 + bx} \, dx = \sqrt{\frac{\pi}{a}} \exp\left(\frac{b^2}{4a}\right), \qquad \forall \, b \in \mathbb{C}. \tag{3.16}$$

By using Eq. 3.16 in Eq 3.15, then factorizing and separating ν_s and ν_i we obtain,

$$\begin{aligned} &\exp\left[\frac{i}{2}(1+\xi)\left(\frac{\sigma_1^2}{\sigma_1^2 + \sigma_2^2}(\tau_p \nu_s + \tau_p \nu_i) + (\tau_s \nu_s + \tau_i \nu_i)\right)\right] = \dots \\ &\cdots = \exp\left\{\frac{i}{2}(1+\xi)\left[\nu_s\left(\tau_p \frac{\sigma_1^2}{\sigma_1^2 + \sigma_2^2} + \tau_s\right) + \nu_i\left(\tau_p \frac{\sigma_1^2}{\sigma_1^2 + \sigma_2^2} + \tau_i\right)\right]\right\}. \end{aligned} \tag{3.17}$$

Then we define $T_\lambda \equiv \tau_\lambda + \frac{\sigma_1^2}{\sigma_1^2 + \sigma_2^2}\tau_p$ and, then, define the linearized phase mismatch as $L\Delta\beta_{\text{lin}} \equiv T_\lambda \nu_\lambda$ [8]. Thus, after reorganizing, we can rewrite the expression as,

$$\exp\left(\frac{i}{2}(1+\xi)[\nu_\lambda T_\lambda]\right). \tag{3.18}$$

Here, T_λ is the effective time delay between the generated field ($\lambda = s, i$) and the effective pump pulse that drives the nonlinear interaction once the spectral overlap of the pumps is taken into account [36]. Thus, when integrating, even when factoring the signal and idler pumps ($\nu_{s,i}$), the JSA depends on an effective superposition of both pumps, since T_λ has information on the term $\frac{\sigma_1^2}{\sigma_1^2 + \sigma_2^2}$, and the effective delay emerges after spectrally combining both pumps.

To finish, for simplification, we define $B \equiv \frac{\sqrt{\sigma_1^2 + \sigma_2^2}}{\sigma_1 \sigma_2 \tau_p}$ [8].

All the previous simplifications lead to the analytical expression for the joint spectral amplitude to take the form [7, 8],

$$F(\nu_s,\nu_i) = \underbrace{\frac{1}{\pi\sqrt{\sigma_1\sigma_2}}\exp\left(-\frac{(\nu_s+\nu_i)^2}{\sigma_1^2+\sigma_2^2}\right)}_{\text{pump envelope}}\times \\ \times\underbrace{\frac{\sqrt{\pi}\sigma_1\sigma_2}{2\sqrt{\sigma_1^2+\sigma_2^2}}\int_{-1}^{1}d\xi\,\exp\left[i\frac{L\Delta\beta_{\text{lin}}}{2}(1+\xi)\right]\exp\left[-\frac{(1+\xi)^2}{(4B)^2}\right]}_{\text{phase matching function}}. \tag{3.19}$$

For convenience and convention, we make the definitions,

$$\alpha(\nu_s,\nu_i) \equiv \frac{1}{\pi\sqrt{\sigma_1\sigma_2}}\exp\left(-\frac{(\nu_s+\nu_i)^2}{\sigma_1^2+\sigma_2^2}\right), \tag{3.20}$$

$$\phi(\nu_s,\nu_i) \equiv \frac{\sqrt{\pi}\sigma_1\sigma_2}{2\sqrt{\sigma_1^2+\sigma_2^2}}\int_{-1}^{1}d\xi\,\exp\left[i\frac{L\Delta\beta_{\text{lin}}}{2}(1+\xi)\right]\exp\left[-\frac{(1+\xi)^2}{(4B)^2}\right]. \tag{3.21}$$

Finally, the JSA can be written as

$$F(\nu_s,\nu_i) = \alpha(\nu_s,\nu_i)\,\phi(\nu_s,\nu_i). \tag{3.22}$$

Where the function $\alpha(\nu_s,\nu_i)$ corresponds to the **spectral envelope of the pump** and reflects the constraints imposed by energy conservation and pump bandwidth. On the other hand, $\phi(\nu_s,\nu_i)$ is the **phase matching function**, which contains the dispersive properties of the fiber through the linearized phase mismatch.

Degenerate case

By imposing the degenerate pump conditions,

$$\bar{\omega}_1 = \bar{\omega}_2 = \bar{\omega}_p, \qquad \sigma_1 = \sigma_2 = \sigma,$$

$\tau_p = 0$ vanishes and the general SFWM expressions reduce to,

$$F(\nu_s,\nu_i) = \tilde{\alpha}(\nu_s,\nu_i)\tilde{\phi}(\nu_s,\nu_i). \tag{3.23}$$

Where the pump envelope, phase matching function are then given by [8]

$$\tilde{\alpha}(\nu_s,\nu_i) = \frac{1}{\pi\sigma}\exp\left[-\frac{(\nu_s+\nu_i)^2}{2\sigma^2}\right], \quad \tilde{\phi}(\nu_s,\nu_i) = \sqrt{\frac{\pi}{2}}\sigma\,\text{sinc}\left(\frac{L\Delta\beta_{\text{lin}}}{2}\right)e^{i\frac{L\Delta\beta_{\text{lin}}}{2}}. \tag{3.24}$$

Hence, $\tilde{\alpha}(\nu_s,\nu_i)$ and $\tilde{\phi}(\nu_s,\nu_i)$ correspond to the **degenerate spectral envelope** and the **degenerate phase matching function**, respectively. To conclude, the JSA can

be expressed in this interpretation as the product of the pump envelope function and the phase matching function.

Nevertheless, it is important to understand the limits of this approximation. The linearization of $\Delta\beta$ used is equivalent to,

$$\Delta\beta(\omega_s,\omega_i) \approx \Delta\beta_0 + \left|\frac{\partial\Delta\beta}{\partial\omega_s}\right|_0 \nu_s + \left|\frac{\partial\Delta\beta}{\partial\omega_i}\right|_0 \nu_i + \left|\frac{\partial\Delta\beta}{\partial\omega_p}\right|_0 \nu_p. \tag{3.25}$$

Consequently, *prior knowledge of the central signal and idler frecuencies* $(\bar{\omega}_s,\bar{\omega}_i)$ *that satisfies* $\Delta\beta(\bar{\omega}_s,\bar{\omega}_i)=0$ *is required* [8]. In the present work, these frequencies were obtained numerically from the dispersion properties of the photonic crystal fiber. Specifically, **the effective refractive index $n_{\text{eff}}(\omega)$ is calculated using a reduced numerical model based on the finite difference frequency domain method**, from which **the propagation constant is acquired through** $\beta(\omega)=n_{\text{eff}}(\omega)\omega/c$. To find this solutions, a finite difference mode solver was used in the frequency domain with a reduced model. This solver was created by my thesis co-advisor, *Daniel Rodríguez Guillén* (More about dispersion engineering in [37]. But that is not this specific solver). Then, **the chromatic dispersion parameter** was numerically obtained from the second order dispersion coefficient through the relation [17],

$$D(\lambda) = -\frac{2\pi c}{\lambda^2}\beta_2, \tag{3.26}$$

where $\beta_2 = \frac{d^2\beta}{d\omega^2}$. As discussed in Chapter 1, β_2 quantifies how different spectral components of an optical pulse separate from each another during the propagation [20]. When $\beta_2 > 0$ (and thus $D < 0$), higher frequency components travel more slowly than lower frequency components, causing the pulse to broaden. This regime is known as *normal dispersion* [17]. In contrast, when $\beta_2 < 0$ (and thus $D > 0$), higher frequency components travel faster, leading to the *anomalous dispersion* regime, in which SFWM can be more efficiently phase matched [17]. In the particular case where $\beta_2 = 0$, or equivalently $D = 0$, the transition between the normal and anomalous dispersion regimes occurs the corresponding wavelengths are known as *zero dispersion wavelengths* (ZDWs), mentioned in Chapter 1 when discussing Phase Matching.

The dispersion profiles presented in Figures 3.1–3.2 correspond to two PCF configurations with different geometrical parameters: $\Lambda_1 = 1.53\,\mu$m, $r_1 = 0.32\,\mu$m, and 10 rings, versus $\Lambda_2 = 2.2\,\mu$m, $r_2 = 0.33\,\mu$m, and 12 rings. Using $d = 2r$, the air-filling fraction changes from $d_1/\Lambda_1 \approx 0.42$ to $d_2/\Lambda_2 \approx 0.30$ (See Eq. 1.19). This reduction implies a lower air content in the cladding, which increases its effective refractive index (n_{eff}) and reduces the contrast with the core. Thus, a weaker modal confinement and a larger effective mode area A_{eff} are expected. In contrast, the number of rings mainly affects

confinement losses rather than A_{eff} itself: for periodic PCFs, the effective mode area depends primarily on d/Λ and λ/Λ, while the confinement loss decreases as the number of rings increases [17].

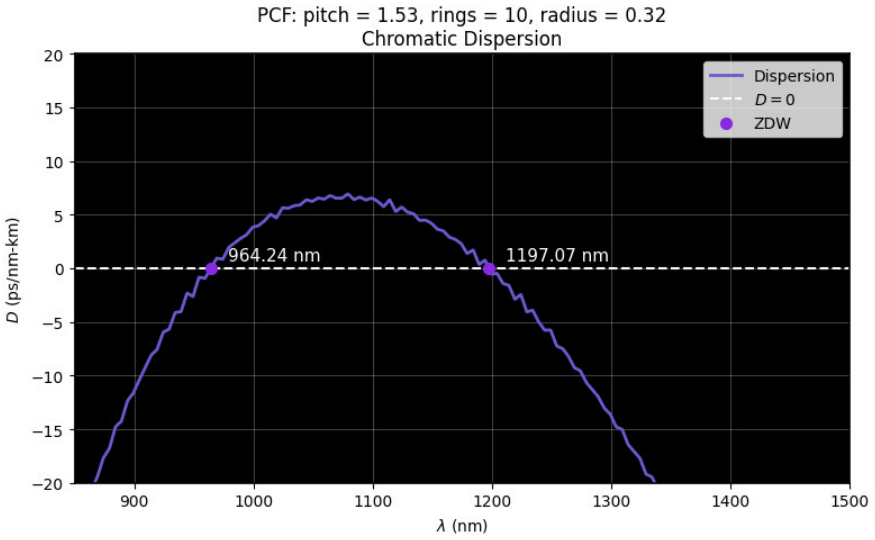

FIGURE 3.1: Fiber 1 (pitch = 1.53 μm, rings = 10, radius = 0.32 μm) exhibits ZDW at 964.24 nm and 1197.07 nm.

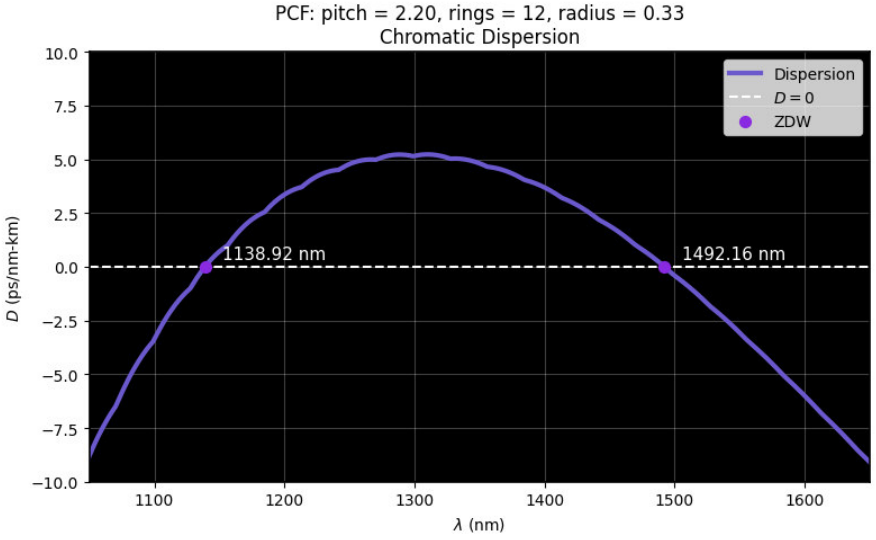

FIGURE 3.2: Fiber 2 (pitch = 2.2 μm, rings = 12, radius = 0.33 μm) exhibits ZDW at 1138.92 nm and 1492.16 nm.

These dispersion profiles determine the phase matching conditions of the SFWM process and therefore the spectral regions where photon pair generation is expected to occur [20]. In particular, the anomalous dispersion region (ADR) (where $D > 0$) identified for each fiber provide operating windows where phase matching can be achieved for a range of pump wavelengths.

TABLE 3.1: Comparison of the geometrical parameters and dispersion properties of the photonic crystal fibers considered in this work. ADR denotes the width of the anomalous dispersion region. Defined as ADR $\equiv$ ZDW$_2$ − ZDW$_1$.

Fiber	Pitch (μm)	Rings	Radius (μm)	ZDW$_1$ (nm)	ZDW$_2$ (nm)	ADR (nm)
1	1.53	10	0.32	964.24	1197.07	232.83
2	2.20	12	0.33	1138.92	1492.16	353.24

Table 3.1 shows that Fiber 2 exhibits a broader anomalous dispersion region (ADR) and a second zero dispersion wavelength, ZDW$_2$, located near 1550 nm. Compared with Fiber 1, both zero dispersion wavelengths are shifted toward longer wavelengths and the anomalous dispersion region becomes wider.

3.3 Modeling the Joint Spectral Amplitude

To better understand the theoretical concepts in the preceding paragraphs, the emphasis was placed on understanding momentum and energy conservation conditions in this particular process. Phase mismatch was evaluated considering only the contribution of linear dispersion, using: $\Delta\beta = \beta(\omega_p) + \beta(\omega_s + \omega_i - \omega_p) - \beta(\omega_s) - \beta(\omega_i)$, where energy conservation is implicitly enforced through the pump frequencies [8]. Nonlinear corrections associated with SPM and XPM, commonly represented by a term proportional to $2\gamma P_p$ [17], were neglected, so that the phase matching analysis reflects exclusively the linear dispersive properties of the fiber.

Let us then begin by presenting the phase matching curve, considering a degenerate pump, and then, the phase matching functions, simulated through Eq. 3.24.

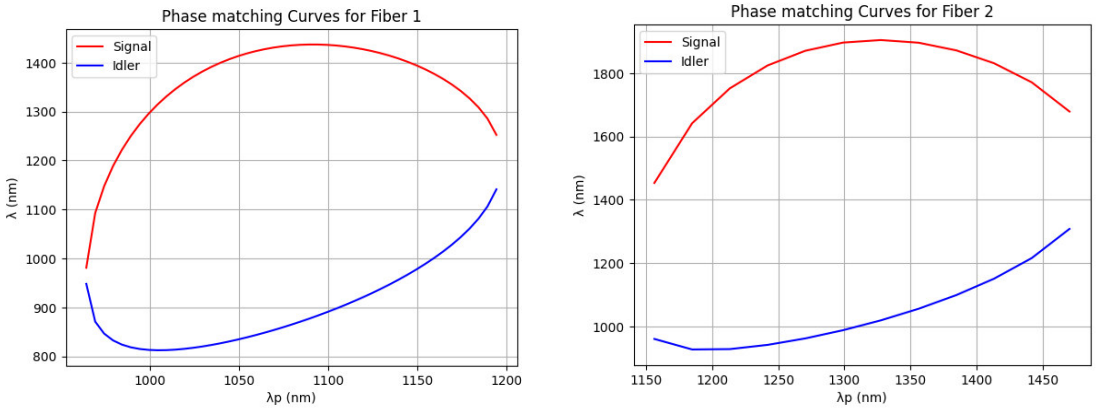

(A) Phase matching curve for Fiber 1. (B) Phase matching curve for Fiber 2.

FIGURE 3.3: Comparison of the phase matching curves obtained for the PCF.

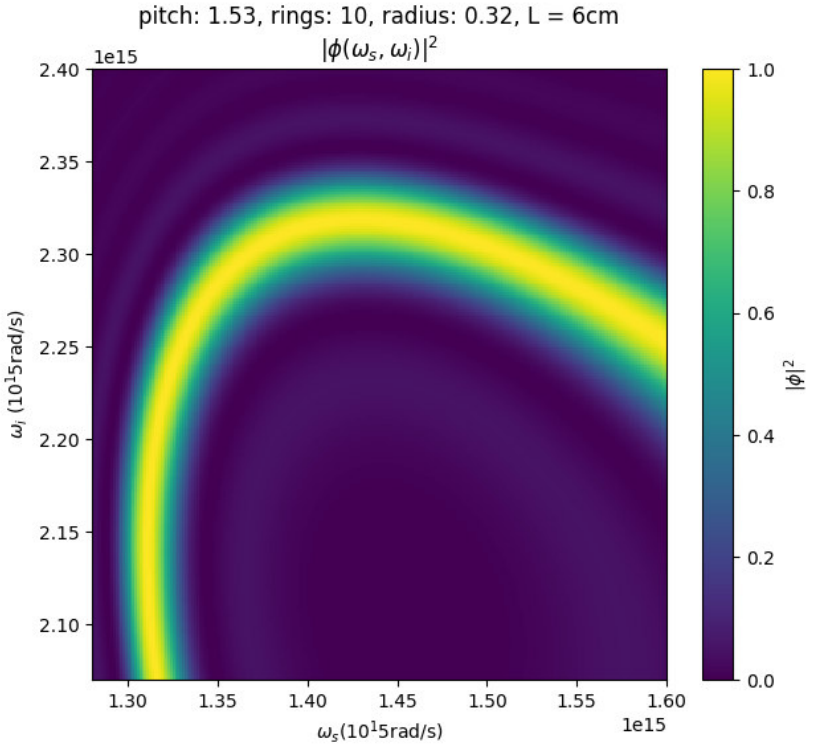

FIGURE 3.4: Phase matching function for Fiber 1: pitch: 1.53 μm, rings: 10, radius: 0.32 μm, L: 6 cm.

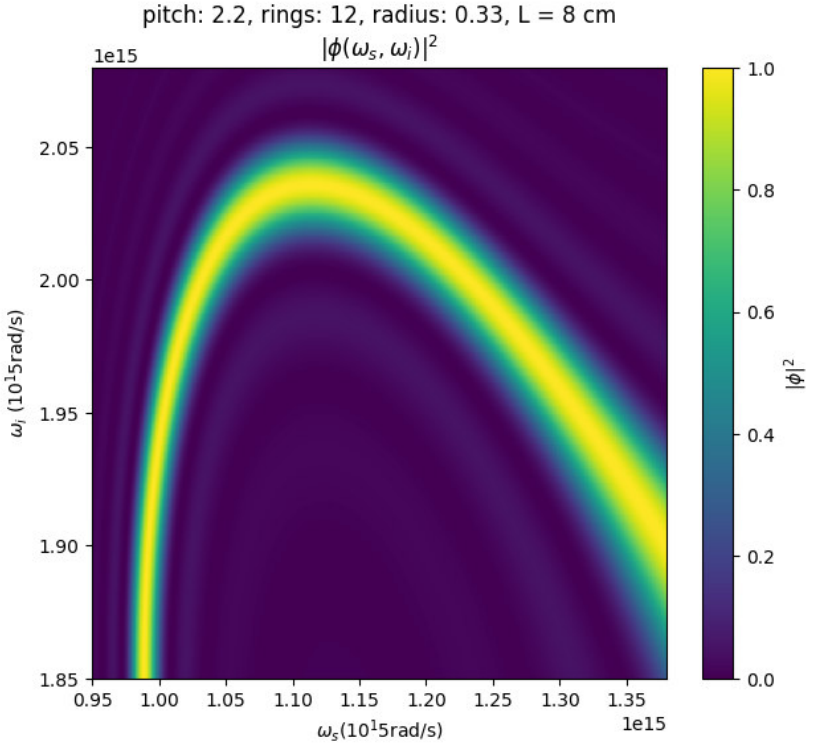

FIGURE 3.5: Phase matching function for Fiber 2: pitch: 2.2 μm, rings: 12, radius: 0.33 μm, L = 8 cm.

A comparison between Figures 3.4–3.5 and more specifically Figures 3.3a–3.3b shows that both fibers exhibit a similar phase matching structure. Nevertheless, modification of the geometrical parameters produces a clear spectral displacement of the phase matching region, consistent with the shift of the ZDWs reported in Table 3.1. As a consequence, the generated signal and idler photons become more spectrally separated, while the overall the phase matching curves remains essentially unchanged. It is also worth noting that Fiber 2 preserves a well defined phase matching structure despite being 20 mm longer than Fiber 1.

As we know, the final spectral properties of the generated state are determined by the combined action of the phase matching function (ϕ) and the pump envelope (α) [8]. To further investigate the impact of the geometrical modifications on the generated photon pairs, the phase matching contours are examined together with the pump envelope. This allows visualization of the regions where both conditions overlap and, consequently, where the joint spectral intensity (JSI) is expected to be concentrated.

3.3.1 Joint Spectral Intensity

Fiber 1

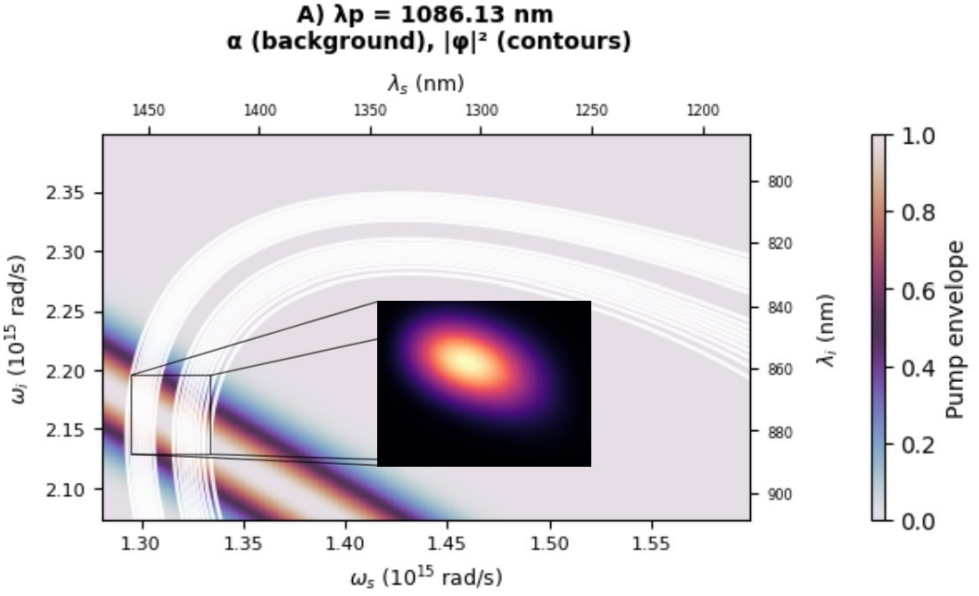

FIGURE 3.6: Phase matching landscape for SFWM in a fiber for a pump wavelength of $\lambda_p = 1086.13\,\text{nm}$ and a spectral width σ_p of $3 \times 10^{15}\,\text{rads}/s$. The background color map with contour lines shows the phase mismatch as a function of the signal and idler wavelengths.

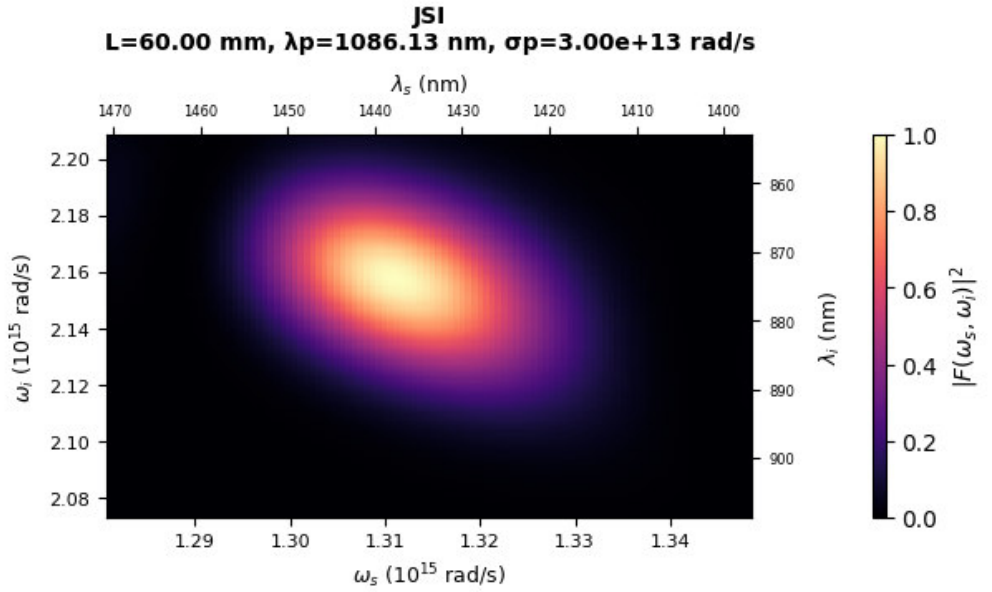

FIGURE 3.7: The JSI exhibits a compact elliptical distribution with a negative inclination.

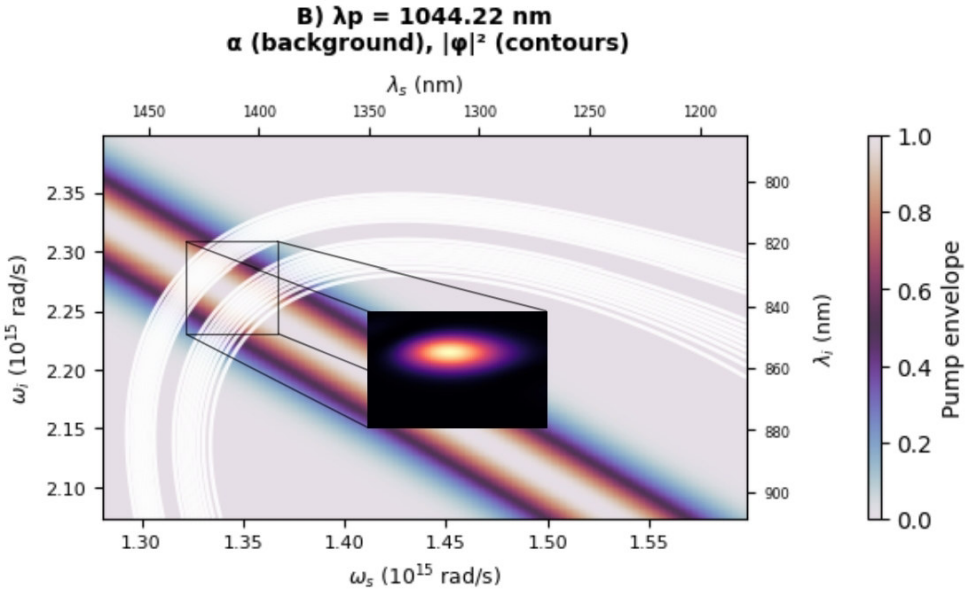

FIGURE 3.8: Phase matching landscape for SFWM in a fiber for a pump wavelength of $\lambda_p = 1044.22\,\text{nm}$ and a spectral width σ_p of $3 \times 10^{15}\,\text{rads}/s$. The background color map with contour lines shows the phase mismatch as a function of the signal and idler wavelengths.

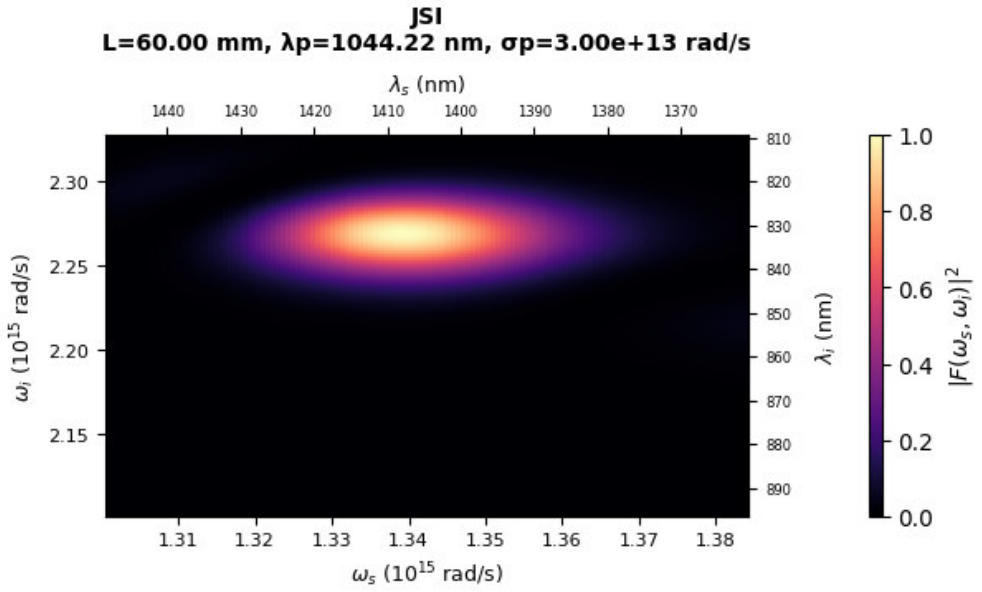

FIGURE 3.9: The JSI becomes a more elongated horizontal elliptical distribution.

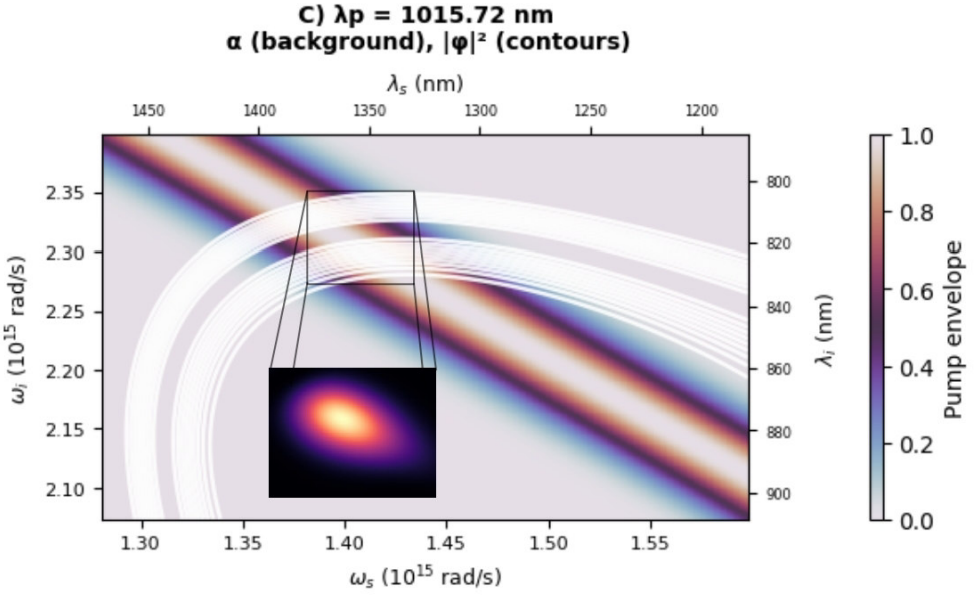

FIGURE 3.10: Phase matching landscape for SFWM in a fiber for a pump wavelength of $\lambda_p = 1015.72\,\text{nm}$ and a spectral width σ_p of $3 \times 10^{15}\,\text{rads}/s$. The background color map with contour lines shows the phase mismatch as a function of the signal and idler wavelengths.

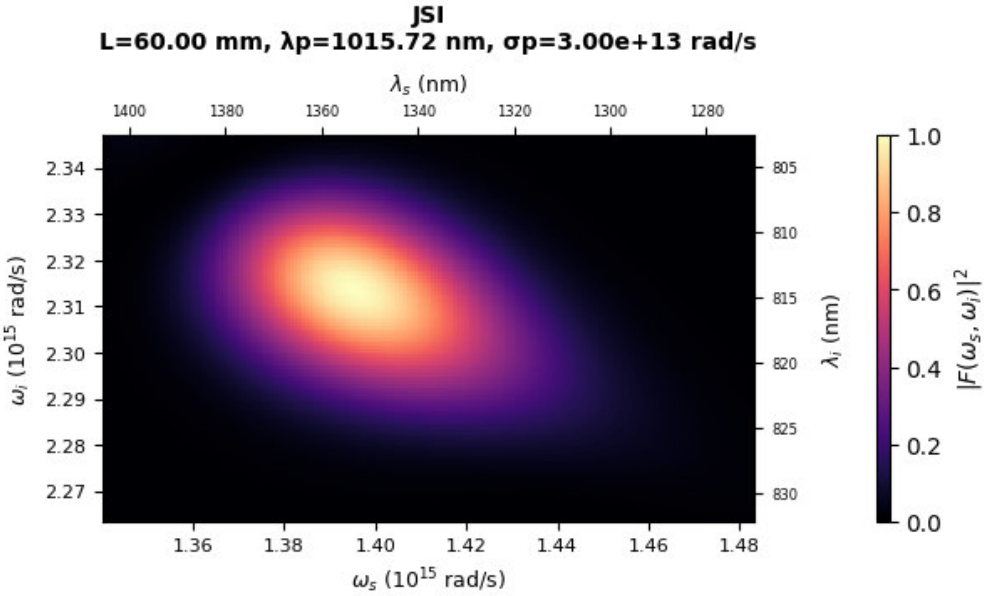

FIGURE 3.11: The JSI returns to a compact elliptical distribution with negative inclination, but an pseudo-elongated form.

Although all three configurations remain localized around a single dominant spectral peak, the shape of the JSI undergoes a clear qualitative evolution as the pump wavelength is tuned. In case A, the distribution exhibits an elliptical profile with a negative inclination, indicating a relatively balanced correlation between signal and idler frequencies. In case B, the JSI becomes noticeably stretched along the signal axis (ω_s), resulting in a horizontally elongated elliptical distribution. Finally, in case C, the distribution partially recovers a similar form to case A. Note that the reshaping of the JSI, with change in size and direction, occur despite the pump bandwidth being kept fixed at $\sigma_p = 3.0 \times 10^{15}$ rad/s. The changing behavior arises from variation of the phase matching landscape, that reconfigures the effective correlation between signal and idler frequencies in each configuration [7].

For Fiber 1, τ_s increases monotonically from near zero to a maximum value of approximately 3.88, followed by decrease into negative values, spanning the range [~ 0, 3.88]. In contrast, τ_i exhibits a more gradual evolution, transitioning from positive to negative values with a nearly monotonic trend over the same spectral interval. This resulting in the ratio τ_s/τ_i showing a strong non uniform behavior. Starting from values of order unity, increasing up to values above 10^1, and exhibiting sign changes associated with the zero crossing of τ_i. Overall, Fiber 1 displays a structured but highly asymmetric group delay landscape dominated by the interplay between the variation of τ_s and the sign changing of τ_i.

Fiber 2

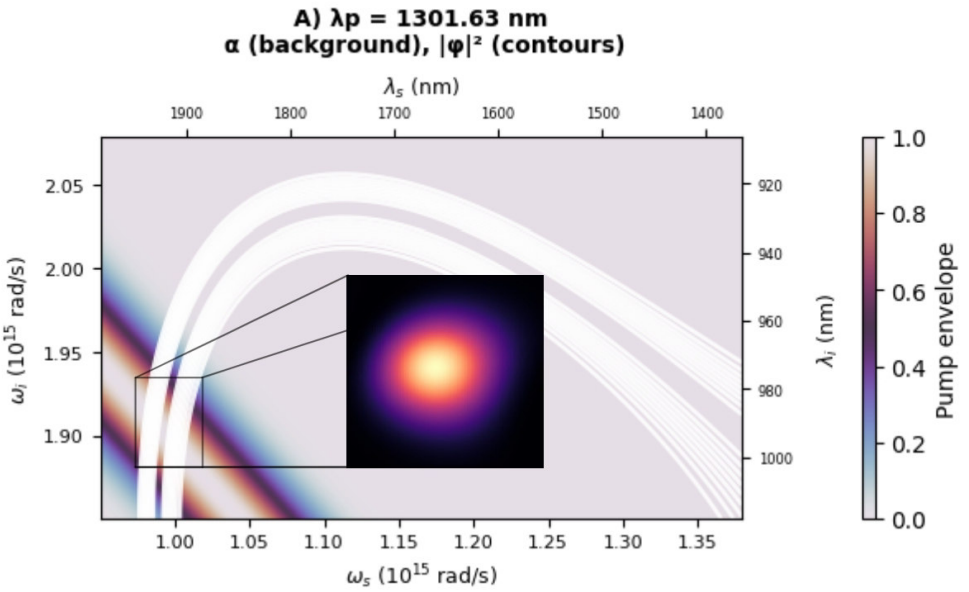

FIGURE 3.12: Phase matching landscape for SFWM in a fiber for a pump wavelength of $\lambda_p = 1301.63\,\text{nm}$ and a spectral width σ_p of $3 \times 10^{15}\,\text{rads}/s$. The background color map with contour lines shows the phase mismatch as a function of the signal and idler wavelengths.

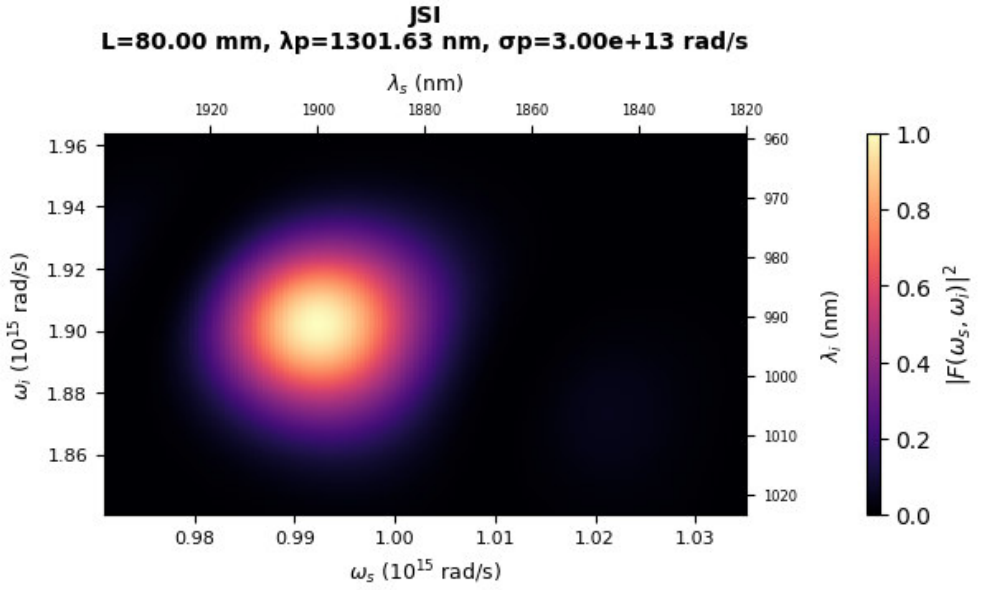

FIGURE 3.13: The JSI presents a centered pseudo circular spectral distribution with a single peak behaviour.

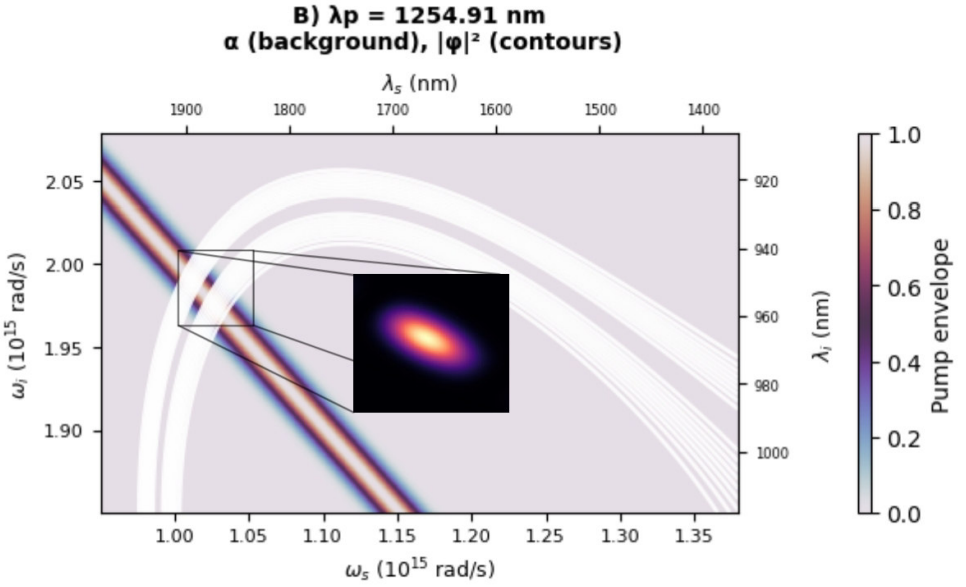

FIGURE 3.14: Phase matching landscape for SFWM in a fiber for a pump wavelength of $\lambda_p = 1254.91\,\text{nm}$ and a spectral width σ_p of $1 \times 10^{15}\,\text{rads}/s$. The background color map with contour lines shows the phase mismatch as a function of the signal and idler wavelengths.

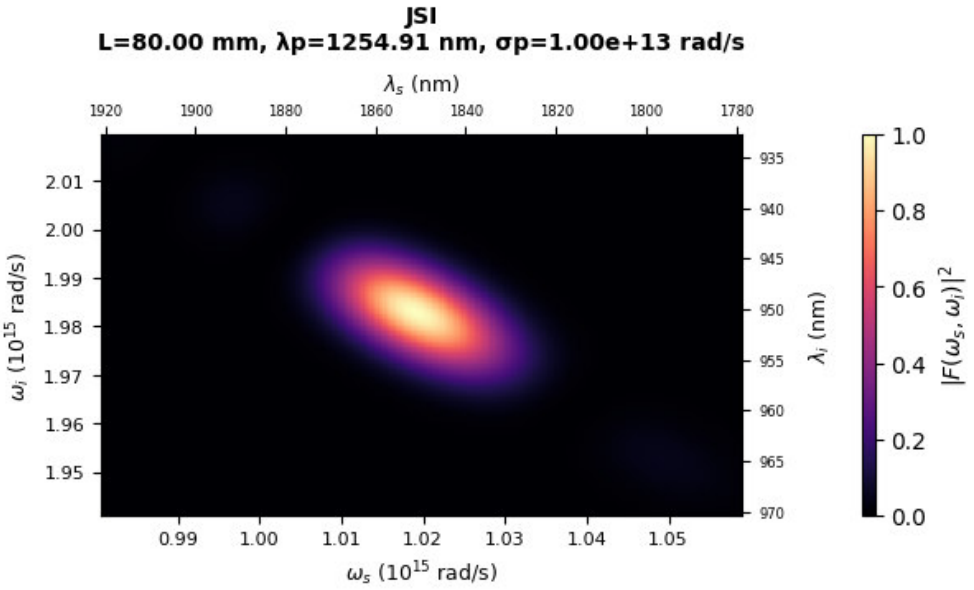

FIGURE 3.15: The JSI rotates toward a diagonal orientation, forming a compact elliptical distribution localized around a spectral peak.

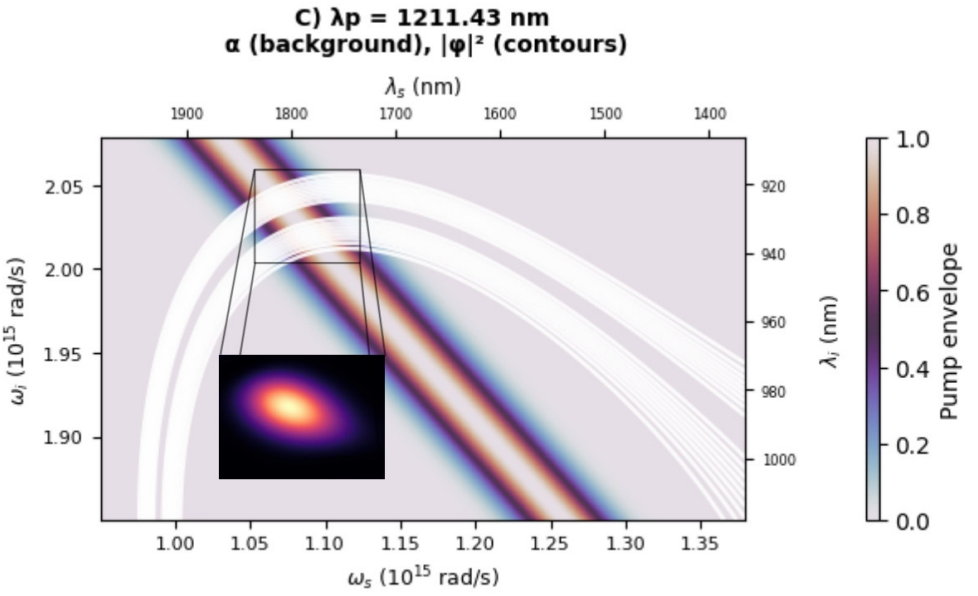

FIGURE 3.16: Phase matching landscape for SFWM in a fiber for a pump wavelength of $\lambda_p = 1211.43\,\text{nm}$ and a spectral width σ_p of $2 \times 10^{15}\,\text{rads}/s$. The background color map with contour lines shows the phase mismatch as a function of the signal and idler wavelengths.

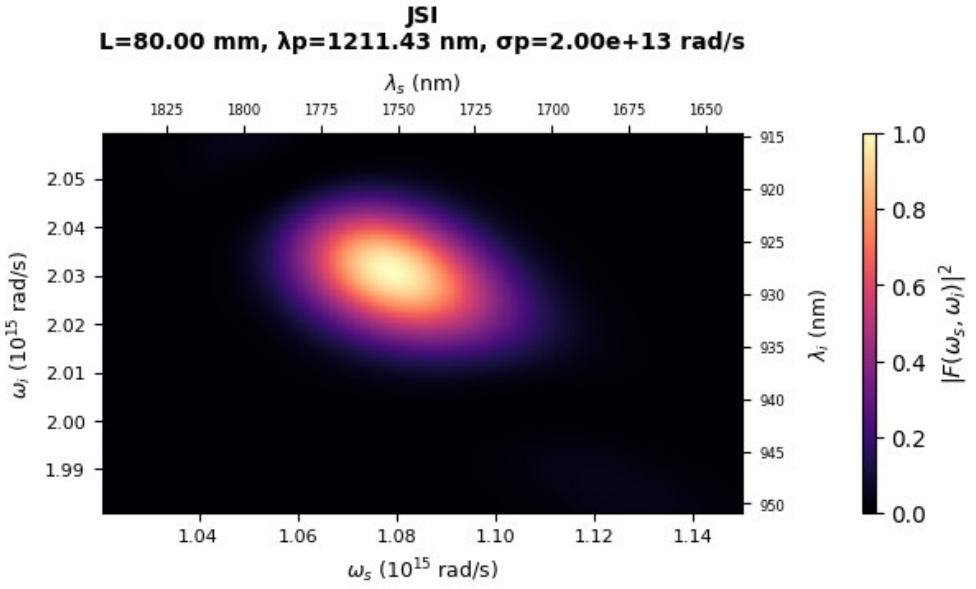

FIGURE 3.17: Finally, the JSI evolves into more horizontally elliptical distribution with little inclination.

In contrast to Fiber 1, Fiber 2 exhibits a systematic geometric evolution of the JSI as the pump wavelength is varied. As shown in cases A–C, the spectral distribution undergoes a continuous transformation from an initially nearly isotropic profile, to a diagonally oriented compact ellipse, and finally to a predominantly horizontally elongated distribution

with reduced inclination. This evolution reflects a progressive rotation and reshaping of the phase matching region in the spectral plane.

For Fiber 2, τ_s exhibits a compact and symmetric evolution, ranging approximately from ~ 0 to 4.29 and reaching a well defined maximum near the center of the spectrum. The corresponding τ_i spans the ranges $[-2.63, 1.08]$ and crosses zero close to the central spectral region, with an overall smoother variation compared to Fiber 1. Consequently, the ratio τ_s/τ_i displays localized sharp enhancements reaching values on the order of 10^2, directly associated with the near-vanishing of τ_i, followed by rapid sign changes. Despite these features, the underlying joint spectral amplitude remains stable and preserves a tilted elliptical phase matching structure, indicating no physical instability.

TABLE 3.2: Table of values $\lambda_{p,s,i}$ resulted from each case

Fiber	L **(mm)**	**Case**	λ_p (nm)	λ_s (nm)	λ_i (nm)
1	60	A	1086	1434	873
		B	1044	1405	830
		C	1015	1349	813
2	80	A	1301	1899	990
		B	1254	1848	950
		C	1211	1744	927

When comparing Table 3.1 with the simulated pump wavelengths listed in this table, it can be verified that all pump configurations employed in the photonic crystal fibers lie within their respective anomalous dispersion regions bounded by the corresponding ZDWs. Thus, all numerical simulations were performed in the regime where $\beta_2 < 0$, ensuring consistency with the phase matching conditions expected for efficient SFWM.

The normalization of the JSA, and thus, JSI is discused in the next chapter, when discussing tools to quantify spectral correlations.

Chapter 4

From Joint Spectral Amplitude to Frequency-Bin Quantum Information

In this chapter, the previously simulated biphoton states generated in the photonic crystal fibers are analyzed in terms of their spectral correlation properties. Using the Schmidt decomposition of the numerically obtained JSAs, the Schmidt coefficients and corresponding Schmidt modes were extracted to quantify the modal structure, spectral purity, and degree of correlation of the generated photon pairs.

The Schmidt number, normalized second order correlation function, and heralded photon purity were obtained for the different fiber and pump configurations. A diagnosis was made on the distribution of Schmidt coefficients among the available modes. Based on this analysis, two relevant regimes were explored: the generation of highly pure heralded photons through dominant single Schmidt modes, and a theoretical proposal for frequency-bin Bell state generation using specific Schmidt mode combinations and Schmidt coefficient distributions. Although the latter represents a theoretical characterization rather than a demonstrated numerical result, it provides a possible connection between SFWM sources and frequency-encoded quantum information applications.

4.1 Normalized Second Order Correlation Function and Schmidt Number

Although the JSA derived in Eq. 3.24 contains the complete information of the generated biphoton state, its analytical form alone does not provide a direct quantitative

measure of the spectral correlations between signal and idler photons. In particular, visual inspection of the JSA and/or the phase matching function can provide valuable qualitative insight, but it is often insufficient to determine whether the generated state is highly correlated, nearly factorable, or suitable for the generation of spectrally pure heralded photons. To characterize these properties quantitatively, it is necessary to introduce quantities capable of describing the correlation structure of the biphoton quantum state. Before we introduce the quantum description of photon-pair correlations, it is useful and instructive to revisit the classical theory of optical coherence, since many of the concepts employed in quantum optics, including correlation functions and coherence measures, among many others, originate from the statistical description of classical electromagnetic fields [27].

4.1.1 Normalized Second Order Correlation Function

The normalized second order correlation function is constructed from the first and second order coherence functions of the quantized electromagnetic field. A detailed discussion of these quantities and their physical interpretation can be found in the standard texts of Mandel and Wolf [26] and Gerry and Knight [29]. In particular, Gerry and Knight derive these correlation functions by considering a quantized electromagnetic field incident on a 50:50 beam splitter, with photodetectors located at positions x_1 and x_2. Within this framework, the first order correlation function $G^{(1)}$ characterizes the field coherence and is related to single photon detection probabilities, whereas the second order correlation function $G^{(2)}$ describes joint detection events and therefore quantifies photon-photon correlations.

The **normalized second order correlation function** is defined as [26, 27, 29]

$$g^{(2)}(x_1, x_2; x_2, x_1) = \frac{G^{(2)}(x_1, x_2; x_2, x_1)}{G^{(1)}(x_1, x_1)G^{(1)}(x_2, x_2)}. \tag{4.1}$$

Where, the first order correlation function has the form,

$$G^{(1)}(x_1, x_2) = \left\langle \hat{E}^{(-)}(x_1)\, \hat{E}^{(+)}(x_2) \right\rangle, \tag{4.2}$$

this quantity measures the degree of field coherence between two space time points [26]. And the second order correlation function,

$$G^{(2)}(x_1, x_2; x_2, x_1) = \left\langle \hat{E}^{(-)}(x_1)\hat{E}^{(-)}(x_2)\, \hat{E}^{(+)}(x_2)\hat{E}^{(+)}(x_1) \right\rangle, \tag{4.3}$$

describes the probability of coincident photodetection events and therefore provides information about the statistical properties of the optical field [26].

For stationary field statistics, the properties are invariant under time translations, implying that the correlation functions depend only on the time difference between detection events. Defining $\tau = t_2 - t_1$ where τ represents the temporal delay between two photodetection events, the normalized second order correlation function can be written as [29],

$$g^{(2)}(\tau) = \frac{\langle \hat{E}^{(-)}(t)\hat{E}^{(-)}(t+\tau)\hat{E}^{(+)}(t+\tau)\hat{E}^{(+)}(t)\rangle}{\langle \hat{E}^{(-)}(t)\hat{E}^{(+)}(t)\rangle\langle \hat{E}^{(-)}(t+\tau)\hat{E}^{(+)}(t+\tau)\rangle}. \tag{4.4}$$

For statistically independent detection events, $g^{(2)}$ satisfies $g^{(2)}(\tau) = 1$.

For a single mode field propagating in a fiber in the $z-$axis, with general form [17],

$$\hat{E}^{(+)}(z,t) = iE_0\hat{a}e^{i(\beta z - \omega t)}, \tag{4.5}$$

it can be shown that Eq. 4.6 follows by substituting Eq. 4.5 into Eq. 4.4,

$$g^{(2)}(0) = \frac{\langle \hat{a}^\dagger\hat{a}^\dagger\hat{a}\hat{a}\rangle}{\langle \hat{a}^\dagger\hat{a}\rangle^2}. \tag{4.6}$$

It is useful to write the normalized second order coherence function in the Fock representation, where the quantum state of the electromagnetic field is expanded in the photon number basis $\{|n\rangle\}$ and each state contains a well defined number of photons [27, 29]. In this basis, the number operator is defined as $\hat{n} = \hat{a}^\dagger\hat{a}$, with eigenvalue equation

$$\hat{n}\,|n\rangle = n\,|n\rangle\,. \tag{4.7}$$

Using the commutation relation $[\hat{a}, \hat{a}^\dagger] = 1$. Eq. (4.6) can be rewritten as [26, 29]

$$g^{(2)}(0) = \frac{\langle \hat{n}(\hat{n}-1)\rangle}{\langle \hat{n}\rangle^2}. \tag{4.8}$$

Expressing the result in terms of the photon number variance commonly written as $\langle(\Delta\hat{n})^2\rangle = \langle\hat{n}^2\rangle - \langle\hat{n}\rangle^2$, one obtains the following expression

$$g^{(2)}(0) = 1 + \frac{\langle(\Delta\hat{n})^2\rangle - \langle\hat{n}\rangle}{\langle\hat{n}\rangle^2}. \tag{4.9}$$

Therefore, we can conclude that $g^{(2)}(0)$ provides a direct measure of photon number

fluctuations and reveals how the photon statistics deviate from a Poissonian distribution [29],

$$g^{(2)}(0) = \begin{cases} 1, & \text{Coherent state (Poissonian statistics),} \\ 2, & \text{Thermal state (Super Poissonian),} \\ 0, & \text{Single photon Fock state.} \end{cases} \tag{4.10}$$

A coherent state is the quantum state that most closely resembles a classical electromagnetic wave and exhibits Poissonian photon statistics. A thermal state describes incoherent radiation with super Poissonian fluctuations, while a single photon Fock state contains exactly one photon. A thorough derivation of thermal photon number statistics may be found in Chapter 2.5 of [29]. Complementary discussions, particularly in connection with squeezed states and quantum fluctuations are available in [27].

In the context of SFWM operated in the low gain regime, the reduced state of the individual signal or idler field exhibits thermal photon number statistics since photons are always created in signal and idler pairs [27].

4.1.2 Schmidt Decomposition and Schmidt Number

The **Schmidt Decomposition** provides a canonical representation of bipartite pure states in terms of orthonormal mode pairs, making it a central tool for quantifying correlations in quantum photonic systems [2]. The formal mathematical definition of the Schmidt decomposition in quantum photonic information is,

> Suppose that $|\psi\rangle$ is a pure state of a composite system $(A \otimes B) \Rightarrow \exists$ the orthonormal states $|i_A\rangle \in A$ and $|i_B\rangle \in B$, such that,
>
> $$|\psi\rangle = \sum_i \sqrt{\lambda_i}\ |i_A\rangle \otimes |i_B\rangle\,, \tag{4.11}$$
>
> where $\lambda_i \geq 0$ and $\sum_i \lambda_i = 1$ [2, 38].

Where, the coefficients λ_i are known as **Schmidt Coefficients**.

Spectral correlations are fully captured by the distribution of these coefficients, which determine state purity and the effective number of accessible modes.

By defining $\bar{n}_n \equiv \langle \hat{a}_n^\dagger \hat{a}_n \rangle$, where $\bar{n}_n$ is the mean photon number in mode n, Eq. 4.6 can be written as the form,

$$g^{(2)} = 1 + \frac{\sum_n \bar{n}_n^2}{\left(\sum_n \bar{n}_n\right)^2}. \tag{4.12}$$

This expression can be obtained from Eq. 4.9 by decomposing the total photon number operator as $\hat{n} = \sum_n \hat{n}_n$ and assuming that the Schmidt modes are statistically independent. Furthermore, each Schmidt mode is described by a thermal photon number distribution, for which $\mathrm{Var}(\hat{n}_n) = \bar{n}_n + \bar{n}_n^2$. Under these conditions, Eq. 4.9 reduces to Eq. 4.12, where $\bar{n} = \sum_n \bar{n}_n$ is the total mean photon number [29, 30].

Assuming an independent low gain regime population of Schmidt modes, as mentioned, where $\bar{n}_n \propto \lambda_n$, then we define $\bar{n}_n \equiv \lambda_n \bar{n}$ and since the relation $\sum_n \lambda_n = 1$ must always be satisfied [2], Eq. 4.12 becomes,

$$g^{(2)} = 1 + \sum_n \lambda_n^2. \tag{4.13}$$

The **Schmidt number** is defined as [2]

$$K = \frac{1}{\sum_n \lambda_n^2}. \tag{4.14}$$

Therefore, the degree of spectral entanglement is quantified through the Schmidt number [27]. Finding the final expression

$$g^{(2)} = 1 + \frac{1}{K}. \tag{4.15}$$

Notice, from the expression, that in the particular case where the state $|\Psi^{(2)}\rangle$ has only one nonzero Schmidt coefficient, the Schmidt number satisfies $K = 1$, and the state is **factorable**. The presence of multiple nonzero Schmidt coefficients ($K > 1$) indicates the existence of correlations between the subsystems in the Schmidt basis [26, 27, 29].

While the global bipartite state remains pure, the reduced state of each subsystem, obtained via partial trace, is in general a mixed state (See Appendix C). This structure implies that, in the process of SFWM, the number and distribution of Schmidt coefficients determine the spectral mode structure and the purity of the generated photons [12, 14]. A single dominant Schmidt mode corresponds to a spectrally pure, effectively single mode emission. In contrast, a multimode structure leads to a mixed reduced state for each subsystem, which reduces the degree of coherence in the corresponding single-photon state.

4.2 Quantum Information Regime

At this point, the problem is naturally formulated in terms of *continuous frequency variables*, where the spectral correlations between signal and idler are fully characterized by

the numerically obtained JSA. This final chapter focuses on integrating all the concepts and formalism developed for the construction of a biphoton state in a photonic crystal fiber with an emphasis on its potential applications in **quantum information** science.

However, many applications of quantum information and technologies are formulated in a different language. Of course, it is a quantum language, but in general quantum communication, computing and information processing are typically described in terms of **finite dimensional quantum systems** that live in **discrete Hilbert spaces** [2, 38]. The biphotonic state represented in Eq. 3.22, Eq. 3.23 are all described by the continuous spectral variable ω, and therefore, live in a continuous Hilbert space.

A question arises: *How can a biphoton state generated in a continuous spectral space be connected to a discrete quantum state?* And *How can this biphoton state can be employed in quantum information?*

Beginning with a brief introduction to the fundamental concepts of quantum information, let us begin with the must basic definition in quantum information: the **qubit**.

A brief introduction to the qubit concept

A qubit is a mathematical abstract object that represents the state vector of a specific quantum system. Such system is defined in [2, 38], as

> **Definition**: A **qubit** is a quantum system described by a two dimensional Hilbert space ($\mathcal{H} \cong \mathbb{C}^2$) named **qubit space**. The qubit state encodes all the information of the system, the consecuence of ***Postulate 1*** (See Appendix C). The orthonormal basis the qubit space is $\{|0\rangle, |1\rangle\}$.
>
> An observable can be represented as the measurement outcome of the operator $\hat{\sigma}_z$. Such that
>
> $$\hat{\sigma}_z |0\rangle \mapsto +1, \quad \hat{\sigma}_z |1\rangle \mapsto -1. \tag{4.16}$$

A consequence of quantum mechanics postulates is that any pure state of a two level system can be written as a linear combination of the computational basis [38]

$$|\psi\rangle = a|0\rangle + b|1\rangle, \quad a, b \in \mathbb{C}, \quad |a|^2 + |b|^2 = 1. \tag{4.17}$$

Therefore, a qubit is not a physical object, but a mathematical structure. Any physical system whose effective dynamics can be restricted to a two dimensional Hilbert space can function as a qubit. Examples of this are many, photon polarization, electron spin,

two vibrational states of a molecule, the presence or absence of a photon in an optical mode, frequency-coded states, two states of magnetic flux, etc. [2, 38].

4.3 Frequency domain representation of the biphoton state

From Eq. 3.1, we define the biphoton state generated by SWFM in the frequency domain as,

$$|\Psi^{(2)}\rangle = \iint d\omega_s \, d\omega_i \, F(\omega_s, \omega_i) \, |\omega_s\rangle \, |\omega_i\rangle \, , \tag{4.18}$$

where $|\Psi^{(2)}\rangle \in \mathcal{H}^s \otimes \mathcal{H}^i$. It is also common to write the expression in terms the creation operators, such as [14, 28],

$$|\Psi^{(2)}\rangle = \iint d\omega_s \, d\omega_i \, F(\omega_s, \omega_i) \, \hat{a}_s^\dagger(\omega_s) \hat{a}_i^\dagger(\omega_i) \, |vac\rangle \, . \tag{4.19}$$

$|vac\rangle$ is the vacuum state, this notation is used, so a distinction is made from the $|0\rangle$ qubit representation. Since ω is a **continuous variable**, the frequency basis $\{|\omega\rangle\}$ satisfies the relations [23],

$$\langle\omega|\omega'\rangle = \delta(\omega - \omega'), \quad \int d\omega \; |\omega\rangle \, \langle\omega| = \hat{I}. \tag{4.20}$$

Thus, the bipartite basis is that represent the signal and idler photon ($\{|\omega_s\rangle \otimes |\omega_i\rangle\}$) also satisfies the relations,

$$\langle\omega_s|\omega_s'\rangle = \delta(\omega_s - \omega_s'), \quad \langle\omega_i|\omega_i'\rangle = \delta(\omega_i - \omega_i'). \tag{4.21}$$

By projecting Eq 4.18 in $\{|\omega_s\rangle \otimes |\omega_i\rangle\} = \{|\omega_s\rangle \, |\omega_i\rangle\}$, and using Eq. 4.21, to reduce the expression the JSA naturally emerges,

$$(\langle\omega_s| \, \langle\omega_i|) \, |\Psi^{(2)}\rangle = \iint d\omega_s' \, d\omega_i' \; \langle\omega_s|\omega_s'\rangle \, \langle\omega_i|\omega_i'\rangle \; F(\omega_s', \omega_i') = F(\omega_s, \omega_i). \tag{4.22}$$

Thus, the JSA can be interpreted as the wavefunction of the biphoton state in the frequency representation; therefore, it fully characterizes the probability amplitudes and correlations between signal and idler photons.

To move from a continuous space to a discrete space

To find a discrete representation of our state, we will make use of the Schmidt decomposition seen in the previous chapter, and it will be shown how an ideal discrete basis for constructing useful states in quantum information naturally arises.

4.3.1 Discrete Schmidt modes

Since the biphoton state admits Schmidt Decomposition [14], then Eq. 4.18 can be expressed in terms of a discrete orthonormal mode basis through the Schmidt decomposition. These modes are known as **Schmidt modes** or **Schmidt Functions** and are represented by the complex functions $[u_n(\omega_s),\ v_n(\omega_i)] \in \mathbb{C}$ [38]. The Schmidt modes define orthogonal spectral wavepacket modes of the electromagnetic field, each corresponding to a well defined single photon excitation in a distinct temporal spectral degree of freedom [39, 40]. The biphoton state, then, takes the form,

$$|\Psi^{(2)}\rangle = \iint d\omega_s d\omega_i \left(\sum_n \sqrt{\lambda_n}\, u_n(\omega_s) v_n(\omega_i) \right) |\omega_s\rangle\, |\omega_i\rangle\,. \tag{4.23}$$

Thus,

$$F(\omega_s, \omega_i) = \sum_n \sqrt{\lambda_n}\, u_n(\omega_s)\, v_n(\omega_i). \tag{4.24}$$

This representation of the JSA does not changes the correlation structure. Rather, it allows to reorganize correlations into a discrete set of orthonormal pairs $\{(u_n,\, v_n)\}$, each weighted by the set of Schmidt coefficients $\{\lambda_1, \lambda_2, \ldots, \lambda_n\}$. The coefficients λ_n quantify the contribution of each pair of modes so that the complete set of Schmidt coefficients provides a compact description of the correlation structure of the state [41]. This connects directly with the fact that the **Schmidt Number** allows one to quantify the correlations of the state (See Eq. 4.14).

Therefore, the biphoton state may be written in terms of this orthonormal base $\{|u_n\rangle_s\ |v_n\rangle_i\}$ as

$$|\Psi^{(2)}\rangle = \sum_n \sqrt{\lambda_n}\, |u_n\rangle_s\, |v_n\rangle_i\,, \tag{4.25}$$

with the **Schmidt Vectors** defined as

$$|u_n\rangle = \int d\omega_s\, u_n(\omega_s)\, |\omega_s\rangle\,, \quad |v_n\rangle = \int d\omega_i\, v_n(\omega_i)\, |\omega_i\rangle\,. \tag{4.26}$$

The biphoton state generated by SFWM is a pure state when both photons are considered jointly. However, when analyzing the photons separated, the state is considered mixed (See Appendix C), due to spectral correlations [7, 28].

Describing such situations requires focusing on a subsystem rather than on the complete biphoton state. The density operator formalism provides the appropriate framework, allowing the description of reduced and conditional states obtained after measurement or by disregarding part of the system.

4.3.2 Heralding photon method

The density operator provides a convenient framework for describing both the complete biphoton state and the reduced states associated with individual heralded photons. The density operator representing the biphoton state in the frequency domain ($\hat{\rho} = |\Psi^{(2)}\rangle \langle\Psi^{(2)}|$) takes the form,

$$\hat{\rho}^{(2)} = \iint d\omega_s \, d\omega_i \iint d\omega_s' \, d\omega_i' \, F(\omega_s, \omega_i) \, F^*(\omega_s', \omega_i') \, \left(|\omega_s\rangle \langle\omega_s'|\right) \otimes \left(|\omega_i\rangle \langle\omega_i'|\right) . \tag{4.27}$$

In addition to obtaining reduced states by tracing out one subsystem, it is also possible to define conditional states through measurement. This procedure is commonly known as **heralding**.

Heralding a photon is the detection of one photon (for instance, the idler) and this provides information about the presence of its partner, effectively conditioning the state of the remaining subsystem [29]. The **heralded state** is obtained by projecting onto a measurement outcome in the idler subsystem. In contrast with the reduced state obtained by tracing over the idler subsystem, *the heralded state retains conditional information about the correlations present in the biphoton state* [12, 26]. *Mathematically*, this is described by a projection onto the idler mode followed by a partial trace (see Appendix C) over the idler degrees of freedom, in simpler words: the idler is not described, only the signal photon is described (measured). This yields a *conditional state of the signal*, i.e., the state of the signal subsystem given that a detection event has occurred in the idler mode.

Since both reduced density operators share the same Schmidt eigenvalue spectrum, quantities related to the Schmidt number are independent of the subsystem chosen [2, 27]. Therefore, without loss of generality, we trace over the signal (idler) degrees of freedom,

such as,

$$\begin{aligned}\hat{\rho}^s &= \mathrm{Tr}_i[\hat{\rho}^{(2)}] \\ &= \int d\omega_i \ \langle\omega_i|\, \hat{\rho}^{(2)}\, |\omega_i\rangle \\ &= \int d\omega_i \iint d\omega_s\, d\omega_i' \iint d\omega_s'\, d\omega_i''\, F(\omega_s,\omega_i')\, F^*(\omega_s',\omega_i'')\, \big(|\omega_s\rangle\, \langle\omega_s'|\big) \underbrace{\big(\langle\omega_i|\omega_i'\rangle\, \langle\omega_i''|\omega_i\rangle\big)}_{\langle\omega_i|\omega_i'\rangle=\delta(\omega_i-\omega_i')}.\end{aligned}$$

Resulting, in,

$$\hat{\rho}^s = \iint d\omega_s\, d\omega_s'\ |\omega_s\rangle\, \langle\omega_s'| \int d\omega_i\, F(\omega_s,\omega_i)\, F^*(\omega_s',\omega_i). \tag{4.28}$$

In this particular case, no mode selective measurement is performed on the idler subsystem, the heralding process reduces to a *non resolved detection* [29]. Thus, $\hat{\rho}^s$ is the effective quantum state of the signal photon when the idler is not observed.

The reduced density operator matrix has the form [2],

$$\hat{\rho}^s(\omega_s,\omega_s') = \int d\omega_i F(\omega_s,\omega_i)\, F^*(\omega_s',\omega_i). \tag{4.29}$$

For each frequency ω_s, the function maintains ω_i fixed. This is represented as $F(\omega_s,\cdot)$, where "$\cdot$" is used to characterize that ω_i is the free argument of the function. This can be seen as the quantity

$$F(\omega_s,\omega_i)F^*(\omega_s',\omega_i), \tag{4.30}$$

is the comparison of two different quantum amplitudes. Integrating over ω_i may be interpreted as coherently summing all the possibilities of the idler frequencies. Thus the integration over ω_i quantifies the spectral coherence retained between the signal frequency components ω_s and ω_s' after tracing out the idler subsystem [26].

We define the **kernel** [42] as

$$K_s(\omega_s,\omega_s') \equiv \int d\omega_i\, F(\omega_s,\omega_i)\, F^*(\omega_s',\omega_i). \tag{4.31}$$

From a mathematical perspective, for each fixed value of ω_s, the function $F(\omega_s,\cdot)$ is treated as a vector in the Hilbert space $L^2(\mathbb{R})$ of square integrable functions in idler frequency domain. The kernel $K_s(\omega_s,\omega_s')$ then, can be interpreted as the inner product between two of such vectors [38, 43].

Thus, $\hat{\rho}^s$ can be written in terms of the kernel as,

$$\hat{\rho}^s = \iint d\omega_s \, d\omega'_s \, K_s(\omega_s, \omega'_s) \; |\omega_s\rangle \, \langle \omega'_s| \, . \tag{4.32}$$

Thus, $\hat{\rho}^s$ matrix elements in the basis $\{|\omega_s\rangle\}$, are given by $K_s(\omega_s, \omega'_s)$ (in analogy with the discrete case: $\hat{\Omega} = \sum_{ij} \hat{\Omega}_{ij} \, |i\rangle \, \langle j|$).

Apply this operator over an arbitrary vector in the frequency representation: $|\phi\rangle$ such that $|\phi\rangle = \int d\omega'_s \, \phi(\omega'_s) \, |\omega'_s\rangle$. Then, we obtain,

$$\hat{\rho}^s \, |\phi\rangle = \iint d\omega_s d\omega'_s \; K_s(\omega_s, \omega'_s) \; |\omega_s\rangle \underbrace{\langle \omega'_s| \left(\int d\omega''_s \, \phi(\omega''_s) \, |\omega''_s\rangle \right)}_{\langle \omega'_s | \omega''_s \rangle = \delta(\omega'_s - \omega''_s)} . \tag{4.33}$$

$$\hat{\rho}^s \, |\phi\rangle = \int d\omega_s \, |\omega_s\rangle \int d\omega'_s \; K_s(\omega_s, \omega'_s) \, \phi(\omega'_s). \tag{4.34}$$

The reduced density operators admits Schmidt Decomposition, thus it can be written as [2, 12],

$$\hat{\rho}^s = \sum_n \lambda_n \, |u_n\rangle \, \langle u_n| \, . \tag{4.35}$$

with $\sum_n \lambda_n = 1$. By identifying $|\phi\rangle \to |u_n\rangle$ and projecting over $|\omega_s\rangle$ we get,

$$\langle \omega_s| \, \hat{\rho}^s \, |u_n\rangle = \int d\omega'_s \, K_s(\omega_s, \omega'_s) \, u_n(\omega'_s). \tag{4.36}$$

If we impose the eigenvalue equation $\hat{\rho}^s \, |u_n\rangle = \lambda_n \, |u_n\rangle$, the next relation must be satisfied:

$$\int d\omega'_s \, K_s(\omega_s, \omega'_s) \, u_n(\omega'_s) = \lambda_n \, u_n(\omega_s). \tag{4.37}$$

This defines the eigenvalue problem associated with the reduced density operator. Its solutions identify the natural spectral modes in which the SFWM source emits photon pairs [14].

4.3.2.1 Integral operator eigenvalue problem

The reduced density operator defines a second kind **homogeneous Fredholm integral equation**, with form

$$\int K(s,t) \, g(t) \, dt = \lambda \, g(s). \tag{4.38}$$

Such kernels are known as Hilbert–Schmidt (L_2) kernels, where the integration domain may be finite or infinite [42].

$$\iint |K(s,t)|^2 ds dt < \infty. \tag{4.39}$$

The kernel $K_s(\omega_s, \omega_s')$ satisfies the Hermiticity condition $K_s(\omega_s, \omega_s') = K_s^*(\omega_s', \omega_s)$ [14]. By the spectral theorem, its eigenfunctions form a complete orthonormal basis of the associated Hilbert space and its eigenvalues satisfy, [2, 42]

$$\sum_n |\lambda_n|^2 < \infty. \tag{4.40}$$

By substituting the Schmidt decomposition of the JSA (Eq- 4.24) into the kernel definition (Eq. 4.31) reveals that the spectral decomposition of the reduced density operator coincides with the Schmidt decomposition of the biphoton state.

$$K_s(\omega_s,\, \omega_s') = \sum_{nm} \sqrt{\lambda_n \lambda_m}\, u_n(\omega_s) u_m^*(\omega_s') \int d\omega_i\, v_n(\omega_i) v_m^*(\omega_i). \tag{4.41}$$

Since Schmidt modes are orthonormal, they satisfy the relation

$$\int d\omega_i\, v_n(\omega_i) v_m^*(\omega_i) = \delta_{nm}. \tag{4.42}$$

Thus, Eq. 4.41 takes the form

$$K_s(\omega_s,\, \omega_s') = \sum_n \lambda_n\, u_n(\omega_s)\, u_n^*(\omega_s'). \tag{4.43}$$

In braket notation:

$$K_s(\omega_s, \omega_s') \;\sim\; \hat{K}^s_{nn'} = \sum_n \lambda_n \left|u_n\right\rangle \left\langle u_n'\right|. \tag{4.44}$$

We can identify then, the relation

$$\hat{\rho}^s_{nn'} = \hat{K}^s_{nn'}. \tag{4.45}$$

This is proof that $u_n(\omega_s)$ are the eigenfunctions of $\hat{\rho}^s$, and thus, λ_n are the eigenvalues of $\hat{\rho}^s$. In other word, **we have proven that diagonalizing the reduced density operator** (Eq. 4.29) **is equivalent to performing the Schmidt decomposition of the biphoton state** (Eq. 4.18). The modal structure of the generated photon pair is thus completely determined by the spectrum of the reduced density operator [2, 38, 44].

In the numerical simulations developed in this thesis, the JSA is represented by a discretized matrix, as seen in the previous chapter. The Schmidt decomposition of the continuous JSA then becomes equivalent to a Singular Value Decomposition (SVD) of

the corresponding matrix representation (see Appendix D). The singular values numerically obtained from the SVD are the Schmidt coefficients, from which quantities such as the Schmidt number and the purity of the heralded photon can be directly calculated [7, 8, 14].

4.4 Numerical Approach

The integral eigenvalue problem associated with the Schmidt decomposition of the biphoton state (Eq 4.37) cannot, in general, be solved analytically for arbitrary JSA. Thus, we use a numerically simulated JSA discretized matrix.

4.4.1 JSA discretized matrix

The JSA discretized matrix is represented as

$$F(\omega_s, \omega_i) \longrightarrow F_{ij}, \tag{4.46}$$

where the indices i and j label discrete signal and idler frequency, respectively. The JSA is constructed on the discrete mesh by calculating the phase matching and the spectral profile of the pumping pulse, modeled as a Gaussian (or combination of Gaussians), centered at the pumping frequency (ω_{p0}) with bandwidth σ_p, such that it promotes energy conservation $2\omega_p = \omega_s + \omega_i$ [7].

Simultaneously, the phase matching term $\phi(\omega_s, \omega_i)$) is obtained by evaluating the phase mismatch $\Delta\beta(\omega_s, \omega_i) = \beta(\omega_p) + \beta(\omega_s + \omega_i - \omega_p) - \beta(\omega_s) - \beta(\omega_i)$, equivalent to, $2\beta(\omega_p) - \beta(\omega_s) - \beta(\omega_i)$ for the degenerated case [8]) and calculating $\phi = \mathrm{sinc}(\Delta\beta L/2)\ \exp(i\Delta\beta L/2)$, where (L) is the length of the nonlinear medium [7, 8]. Finally, the discrete JSA is obtained by multiplying the pumping profile α by the phase matching term ϕ.

$$F_{ij} = \alpha_{ij}\ \phi_{ij}. \tag{4.47}$$

Next, normalization of F_{ij} is performed. Since $\langle \Psi^{(2)} | \Psi^{(2)} \rangle = 1$, then

$$\iint d\omega_s d\omega_i\ |F(\omega_s, \omega_i)|^2 = 1, \tag{4.48}$$

which can be interpreted as the joint spectral probability density of detecting a signal-idler pair at frequencies (ω_s, ω_i) [2, 8, 44]. We approximate this expression in a discrete

framework as a Riemann Sum [45, 46]

$$\iint d\omega_s d\omega_i \, |F(\omega_s, \omega_i)|^2 \approx \sum_{ij} |F_{ij}|^2 \, \Delta\omega_s \, \Delta\omega_i \approx 1, \tag{4.49}$$

where $\Delta\omega_{s,i}$ is defined as

$$\Delta\omega_s = \frac{\omega_s^{\max} - \omega_s^{\min}}{N-1}, \qquad \Delta\omega_i = \frac{\omega_i^{\max} - \omega_i^{\min}}{N-1}, \tag{4.50}$$

and N is the number of points on the grid ($N \sim 3000$), since the grid is symmetrical $N_s = N_i = N$. And thus, the normalized JSA takes the normalized form,

$$F_{ij} \to \frac{F_{ij}}{\sqrt{\sum_{nm} |F_{nm}|^2 \, \Delta\omega_s \, \Delta\omega_i}}. \tag{4.51}$$

This accurately describes the joint probability amplitude of the photon pair in a discrete form [44].

4.4.2 Single Value Decomposition and obtaining Schmidt coefficients

Numerical singular value decomposition is applied, which is equivalent to the Schmidt decomposition of the continuous state (See Appendix D).

We begin factoring F in the form

$$F = U \Sigma V^\dagger, \tag{4.52}$$

where U and V are unitary matrices whose columns contain the left and right singular vectors. Σ is the diagonal matrix containing the singular values s [2, 44]. In this decomposition, each singular vector in the columns of U corresponds to a discretized Schmidt mode $u_n(\omega_s)$ and, respectively, with $v_n(\omega_i)$.

The singular values are orderer from largest to smallest and are related to the Schmidt coefficients as,

$$\lambda_n = s_n^2, \quad \text{such that:} \quad \sum_n \lambda_n = 1. \tag{4.53}$$

It is important to emphasize that the Schmidt decomposition was performed on the complex JSA, $F(\omega_s, \omega_i) = \alpha(\omega_s, \omega_i)\Phi(\omega_s, \omega_i)$, rather than on the JSI, and was carried out in the frequency domain (ω) rather than in wavelength (λ).

The wavelength representation adopted in Figures 3.7–3.17 is used solely for visualization and qualitative analysis of the spectral correlations, as it is the conventional

representation in experimental optics. Thus, the phase matching function does include the spectral phase factor $\exp(i\Delta kL/2)$ through $\phi = \mathrm{sinc}(\Delta kL/2)\exp(i\Delta kL/2)$, ensuring that the full phase information of the biphoton state is preserved in the matrix used for the singular value decomposition [7]

Relationship with the reduced density operator and purity measures

It can bee shown that the numerical SVD factorization is, in fact, equivalent to solving the Fredholm integral equation for the reduced density operator of the signal photon (Eq. 4.37 to Eq. 4.44). If the reduced density Kernel operator is defined in discrete form as

$$K_s(\omega_s, \omega_s') = \int d\omega_i \, F(\omega_s, \omega_i) F^*(\omega_s', \omega_i) \rightarrow K^s_{ii'} = \sum_j F_{ij} F^*_{i'j}, \tag{4.54}$$

or in operator notation as,

$$\hat{K}^s = \hat{F}\hat{F}^\dagger = \hat{U}\hat{\Sigma}^2\hat{U}^\dagger. \tag{4.55}$$

An analogous construction holds for the idler subsystem,

$$\hat{\rho}^i = \hat{K}^i = \hat{F}^\dagger\hat{F} = \hat{V}\hat{\Sigma}^2\hat{V}^\dagger, \tag{4.56}$$

showing that both reduced density operators share the same non zero eigenvalue spectrum. Therefore, the Schmidt coefficients λ_n correspond to the eigenvalues of either reduced density operator, independently of whether the signal or idler subsystem is traced out. The choice of subsystem only determines the Schmidt modes.

Therefore, the SVD of the JSA directly yields the spectral mode decomposition of the biphoton state and, consequently, the reduced density operator of the heralded photon. As we have established, the Schmid coefficients are the eigenvalue of the reduced density matrix $\hat{\rho}^s$. Thus,

$$(\hat{\rho}^s)^2 = \sum_n \lambda_n^2 \left|u_n\right\rangle \left\langle u_n\right|. \tag{4.57}$$

By tracing over $(\hat{\rho}^s)^2$,

$$\mathrm{Tr}[(\hat{\rho}^s)^2] = \sum_n \lambda_n^2 = \frac{1}{K} \tag{4.58}$$

From the Schmidt coefficients λ_n, the purity of the heralded state is obtained as,

$$P = \mathrm{Tr}\left[(\hat{\rho}^s)^2\right] = \sum_n \lambda_n^2 = \frac{1}{K}. \tag{4.59}$$

The reason is that purity answers the following question: *how close is a density matrix to itself when it represents a pure state?* Recall that for a pure state $\hat{\rho} = |\psi\rangle\langle\psi|$, one

has [2],

$$\hat{\rho}^2 = |\psi\rangle\langle\psi|\,|\psi\rangle\langle\psi| = |\psi\rangle\langle\psi| = \hat{\rho},$$

so a pure state is idempotent ($\hat{\rho}^2 = \hat{\rho}$), that is, an operation can be applied multiple times and produce the exact same result.

Taking the trace then gives $\mathrm{Tr}(\hat{\rho}^2) = \mathrm{Tr}(\hat{\rho}) = 1$ which means that every pure state satisfies $P = \mathrm{Tr}(\hat{\rho}^2) = 1$. In contrast, for a mixed state of the form $\hat{\rho} = \sum_n p_n |n\rangle\langle n|$, one obtains $\hat{\rho}^2 = \sum_n p_n^2 |n\rangle\langle n|$ and therefore $\mathrm{Tr}(\hat{\rho}^2) = \sum_n p_n^2 < 1$ whenever more than one probability contributes [2].

This means that purity measures how concentrated the probability distribution is among the eigenvalues of the density matrix.

4.4.3 Numerical analysis of the normalized second order quantum correlation function, Schmidt Number and Purity

Table 4.1 summarizes the numerical values of $g^{(2)}$, K, and P for the different fiber and pump configurations.

TABLE 4.1: Second order correlation function, Schmidt number, and heralded photon purity for the different fibers and pump configurations.

Fiber	**Case**	$\mathbf{g^{(2)}}$	**K**	**P**
1	A	1.93	1.07	0.93
	B	1.68	1.46	0.68
	C	1.71	1.39	0.71
2	A	1.83	1.20	0.83
	B	1.81	1.23	0.81
	C	1.79	1.26	0.79

Fiber 1 exhibits the largest variation in the Schmidt number, ranging from $K = 1.07$ to $K = 1.46$, with a corresponding decrease in purity from $P = 0.93$ to $P = 0.68$. This indicates that the spectral modal structure is significantly affected by changes in the pump wavelength, leading to different degrees of spectral correlation. By contrast, Fiber 2 shows Schmidt numbers that remain closer to unity and vary more modestly, from $K = 1.20$ to $K = 1.26$, with purity values between $P = 0.83$ and $P = 0.79$. Such behavior suggests that the spectral correlations generated in Fiber 2 are comparatively less sensitive to variations in the pumping conditions, resulting in a more stable modal structure over the analyzed parameter range. Although K, $g^{(2)}$, and P provide useful quantitative measures of the degree of spectral correlation and modal purity, they do not describe the detailed structure of the biphoton state. In particular, two states may display similar Schmidt numbers while having different distributions among their

Schmidt modes. For this reason, the Schmidt decomposition is especially valuable, since it not only quantifies purity but also reveals the full set of orthogonal spectral modes that compose the biphoton state, enabling a more complete physical diagnosis of its quantum correlations [13, 47].

4.5 Analysis on two specific cases of Schmidt mode distribution

As previously established, the Schmidt modes provide a discrete orthogonal modal basis for the continuous spectral Hilbert space, such that,

$$\{|\omega_s\rangle \otimes |\omega_i\rangle\} \rightarrow \{|u_n\rangle_s \otimes |v_n\rangle_i\}. \tag{4.60}$$

The characterization of the correlations between the generated biphoton state in this discrete basis is encoded in the Schmidt coefficients that satisfy the condition,

$$\sum_n \lambda_n = 1. \tag{4.61}$$

Given a general Schmidt decomposed biphoton state generated by SFWM process (Eq. 4.25),

$$|\Psi^{(2)}\rangle = \sum_n \sqrt{\lambda_n}\, |u_n\rangle_s\, |v_n\rangle_i\,. \tag{4.62}$$

Let us analyze two particular cases of Schmidt mode distribution:

a) $\lambda_0 \approx 1$, and $\lambda_{n\geq 1} \approx 0$. Then $K \approx 1$. The Schmidt distribution leads to one dominating mode.

b) $\lambda_0 + \lambda_1 \approx 1$, and $\lambda_{n\geq 2} \approx 0$. Then $K \approx 2$. This Schmidt distribution corresponds to an effectively two mode spectral state.

4.5.1 Pure Heralded Photons

Case a) The biphoton state is:

$$|\Psi^{(2)}\rangle = |u_0\rangle\, |v_0\rangle\,, \tag{4.63}$$

with density operator,

$$\hat{\rho}^{(2)} = (|u_0\rangle\langle u_0|)(|v_0\rangle\langle v_0|). \tag{4.64}$$

By using heralded photon method and trace over idler,

$$\hat{\rho}^s = \mathrm{Tr_i}[\hat{\rho}^{(2)}] = |u_0\rangle \langle u_0| . \tag{4.65}$$

Thus, a **pure single heralded photon** is produced.

For an heralded photon to be pure and useful in quantum applications, and thus without mixing in their internal degrees of freedom. In this case, the Schmidt modes. This pure state is only achievable if and only if the biphotonic state $|\Psi^{(2)}\rangle$ is **factorable** [7, 12]. That is, the JSA can be expressed in the form [8],

$$F(\omega_s, \omega_i) = S(\omega_s)I(\omega_i). \tag{4.66}$$

This may be achieved in the Schmidt mode basis,

$$F(\omega_s, \omega_i) \rightarrow F[u_n(\omega_s), v_n(\omega_i)] = |u_n\rangle_s |v_n\rangle_i . \tag{4.67}$$

This is different from Eq. 4.63. That representation has only one Schmidt mode λ_0. Thus, a pure heralded photon as only a dominant Schmidt coefficient and a factorable JSA. Thus only one factorable eigenvector (state) associated to that coefficient. However, only one spectral mode is accessible [12]. With that in mind, let us analyze the first two Schmidt coefficients (λ_0, λ_1) for each case in Table 4.1

4.5.1.1 Schmidt Coefficients Numerical Analysis

TABLE 4.2: Dominant Schmidt coefficients for the different fibers and cases.

Fiber	**Case**	$\mathbf{g^{(2)}}$	**K**	**P**	$\boldsymbol{\lambda_0}$	$\boldsymbol{\lambda_1}$
1	A	1.93	1.07	0.93	0.96	0.02
	B	1.68	1.46	0.68	0.80	0.14
	C	1.71	1.39	0.71	0.84	0.07
2	A	1.83	1.20	0.83	0.90	0.08
	B	1.81	1.23	0.81	0.90	0.03
	C	1.79	1.26	0.79	0.88	0.03

The numerical analysis of the Schmidt coefficients provides information that goes beyond the Schmidt number itself. In quantum information processing, the most relevant quantity is often not only the value of (K), but rather the modal structure of the generated state. As shown in Table 4.2, some selected cases exhibit Schmidt decomposition is

strongly dominated by a single mode, with $\lambda_0 \gtrsim 0.9$ and remaining coefficients contributing weakly. **This indicates that most of the biphoton probability amplitude is concentrated in a single spectral mode** [2, 38]. In this regime, the biphoton state is effectively single mode, not because all higher order Schmidt modes vanish, but because their relative weights are sufficiently small that they do not significantly affect the reduced single photon statistics. As a result, the heralded photons become highly *indistinguishable*, which is a key requirement for quantum interference experiments and photonic quantum information processing [12]. This requirement is directly related to the fact that when several Schmidt modes contribute with comparable weights, the heralded photon is projected into a mixed spectral state (see Appendix C), which reduces interference visibility and degrades the performance of quantum protocols [44, 48].

In summary, the distribution of Schmidt coefficients determines the effective number of spectral modes K, which in turn quantifies the degree of entanglement and spectral mixing in the generated state. In the regime where a single Schmidt mode dominates, the biphoton state approaches an effectively separable spectral structure, leading to near pure heralded state and, consequently, highly *indistinguishable* single photons upon heralding.

This indistinguishability is directly tested in two-photon interference experiments such as Hong–Ou–Mandel (HOM) interference, where the visibility of the interference dip is fundamentally determined by the overlap of the spectral temporal wavefunctions of the photons [49]. In this sense, HOM visibility can be interpreted as an operational measure of single photon purity and is therefore intrinsically connected to the Schmidt number through $V_{\mathrm{HOM}} \sim \mathrm{Tr}(\hat{\rho}_s^2) = 1/K$ in the ideal symmetric case [48, 50]. For example, for two single photon states described by density operators $\hat{\rho}_1$ and $\hat{\rho}_2$, the HOM interference visibility is determined by their quantum overlap [49]. In the ideal case of identical sources, $\hat{\rho}_1 = \hat{\rho}_2 = \hat{\rho}$, the visibility is given by

$$V_{\mathrm{HOM}} = \mathrm{Tr}(\hat{\rho}^2), \tag{4.68}$$

which coincides with the purity of the heralded single photon state [48, 50]. Since the reduced density matrix obtained from the Schmidt decomposition, it satisfies Eq. 4.59. Then the HOM visibility becomes directly connected to the Schmidt mode structure of the generated biphoton state. Consequently, states dominated by a single Schmidt mode are expected to exhibit high interference visibility, even when small higher-order modal contributions remain present. However, beyond this scalar characterization, a more physically transparent description is provided by the structure of the Schmidt mode distribution itself. As illustrated in Table 4.2, even in cases exhibiting intermediate purity values ($P \sim 0.8$), the decomposition can still be strongly dominated by a

single Schmidt mode, with $\lambda_0 \gtrsim 0.9$ and the remaining coefficients contributing only weak corrections. Thus, the biphoton state is effectively single mode not in the strict mathematical sense, but in an operational sense relevant for measurements: the dominant mode governs the observed statistics, while higher order modes have a negligible impact on interference and heralded state properties [2, 38]. From this perspective, spectral purity alone does not fully capture the physical behavior of the system; But, the degree of modal dominance provides a more refined diagnosis for effective single mode operation. And thus, even moderately mixed states in terms of purity may still exhibit near optimal interference visibility, provided that a well defined leading Schmidt mode dominates the spectral structure. This perspective highlights that engineering the joint spectral amplitude of photon pair sources directly translates into control over photon statistics, *indistinguishability*, and ultimately in the near future the performance of photonic quantum information protocols.

4.5.2 Frequency-bin encoding and Bell state generation from Schmidt modes

...what is proved by impossibility proofs is lack of imagination.

– John Bell [2].

What is a Frequency-bin qubit?

Corresponds to a two dimensional subspace of a single photon in a frequency Hilbert space. The general state of a photon in the frequency basis $|\omega\rangle$ is

$$|\phi\rangle = \int d\omega\, f(\omega)\, |\omega\rangle\,. \tag{4.69}$$

A frequency-bin qubit corresponds to two spectrally localized orthogonal modes centered around different central frequencies ($|\xi_0\rangle$ centered in ω_0), such that,

$$|0\rangle = |\xi_0\rangle\,, \quad |1\rangle = |\xi_1\rangle\,. \tag{4.70}$$

And, as with any qubit, we can express the same state as a superposition:

$$|\phi\rangle = \alpha\,|\xi_0\rangle + \beta\,|\xi_1\rangle\,, \quad \langle\xi_0|\xi_1\rangle = 0. \tag{4.71}$$

In **frequency-domain quantum information** processing, **Schmidt modes** define a natural orthogonal basis for encoding and manipulating photonic states by identifying $|\xi_0\rangle\,,\ |\xi_1\rangle \rightarrow |u_0\rangle\,, |u_1\rangle$. Nevertheless, it is important to emphasize that the potential

of frequency encoding lies in its inherently high dimensional structure [13, 47]. Since frequency is a continuous variable, the associated Hilbert space supports the definition of high dimensional quantum states, **qudits**, in which multiple Schmidt modes can be used as a computational basis under appropriate mode selective control. This feature has motivated significant advances in frequency-bin quantum information processing, including the experimental realization of arbitrary unitary transformations on frequency modes [47], the implementation of quantum logic gates such as frequency-bin controlled-NOT operations [13], and the development of scalable architectures for quantum information processing based on spectral encoding [11].

Bell state generation from a two mode Schmidt spectrum

Case b) The biphoton state is,

$$|\Psi^{(2)}\rangle = \sqrt{\lambda_0}\,|u_0\rangle\,|v_0\rangle + \sqrt{\lambda_1}\,|u_1\rangle\,|v_1\rangle\,. \tag{4.72}$$

This state is entangled since it cannot be written as a product of independent signal and idler states. More generally, a pure bipartite state may be expressed as [38],

$$|\Psi\rangle = C_1\,|a_1\rangle\,|b_1\rangle + C_2\,|a_2\rangle\,|b_2\rangle\,, \tag{4.73}$$

where $\{|a_n\rangle\}$ and $\{|b_n\rangle\}$ denote orthonormal basis states of the two subsystems. Comparing this expression with Eq. (4.72), the Schmidt modes $\{|u_n\rangle\}$ and $\{|v_n\rangle\}$ play the role of the basis states for the signal and idler photons, while the Schmidt coefficients λ_n determine the probability amplitudes associated with each correlated modal pair.

In the particular case in which the first two Schmidt modes dominate the decomposition and contribute with approximately equal weights,

$$\lambda_0 \approx \lambda_1 \approx \frac{1}{2},$$

the state becomes

$$|\Psi^{(2)}\rangle = \frac{1}{\sqrt{2}}\left(|u_0\rangle\,|v_0\rangle + |u_1\rangle\,|v_1\rangle\right). \tag{4.74}$$

Defining the logical basis states

$$|0\rangle_s \equiv |u_0\rangle\,, \qquad |1\rangle_s \equiv |u_1\rangle\,.$$

and

$$|0\rangle_i \equiv |v_0\rangle\,, \qquad |1\rangle_i \equiv |v_1\rangle\,.$$

Eq. (4.74) can be rewritten as

$$|\Psi^{(2)}\rangle = \frac{1}{\sqrt{2}} \left(|0\rangle_s |0\rangle_i + |1\rangle_s |1\rangle_i \right), \tag{4.75}$$

which corresponds to a **maximally entangled frequency-bin Bell state**. Under all the conditions and approximations described, the SFWM process effectively generates a biphoton state confined to a two dimensional spectral subspace, enabling frequency-bin entanglement. This is a pair of **qubits**.

Possible application and practice limitation

Resently, in 2025, the paper "Frequency-bin entanglement-based quantum key distribution" [51], demonstrated an entanglement based QKD experiment (BBM92 protocol) using photons entangled in frequency bins. In their work, two annular resonators on a silicon chip generated a pair of Bell states in frequency, achieving secure key distribution over 26 km of fiber. In general, frequency encoding es compatible with existing fiber optic infrastructure and allows for high dimensional encodings (qudits, previously mentioned) that can be manipulated with standard telecommunications components [47]. In quantum networks, frequency modes offer many spectral channels that can be multiplexed on the same fiber for entanglement distribution. Furthermore, non-local frequency entanglement can be exploited in quantum sensors (for example, sensing non-local delays) and quantum teleportation or entanglement swapping protocols.

Nevertheless, the practical implementation of these states faces challenges. In this work, in particular, it was found that, initially, phase matching in the fiber, determined by scattering and propagation of modes, shapes the amplitude function of the photons, making it difficult to obtain exactly equal Schmidt coefficients. Theoretical studies showed in the citations, and this very work, showed that SFWM in crystal photonic fibers allows flexibility in designing the spectral state by adjusting the dispersion. However, it resulted complex, specially for limitations of time, to simultaneously tune all the fiber parameters to achieve an exact or approximate Bell state.

Another limiting factor that was ignored in this study, is the intrinsic noise: spontaneous Raman scattering in the fiber generates tray photons (Stokes and Anti-Stokes [8, 17]) that degrade quantum purity and limit the usable bandwidth. This effect was not taken in consideration since the end of this work is to analyze SFWM process alone, achieved by simulation. In practice, Ramman scattering **should not be ignored**, since this noise reduces the fidelity of entangled pairs. Additionally, frequency entanglement is sensitive to phase fluctuations induced by thermal variations in the fiber, this can be observed in

QKD experiments previusly mentioned [51], and required real-time phase compensation. Finally, in multimode configurations (or fibers with multiple SFWM process occuring simultaneously) the superposition of various Schmidt modes must be controlled, adding complexity to experimental design. This practice limitations invite to explore the space and nonlinear parameters before considering finding optimal configurations for a wished state, when working with SFWM in PCF.

Proposes

1. **Fiber and waveguide engineering:** Adjusting the microstructure and refractive index profile may provide additional control over the spectral properties of the generated photons pairs, so approach new geometries will be the first option.

2. **Extensive parametric simulations:** Perform systematic numerical studies by varying key parameters like fiber length, pump bandwidth, pump power and rotation of the fiber. Also, optimization techniques based on machine learning could be employed to identify configurations with sufficient data.

3. **Analysis on Non degenerate SFWM configuration:** Investigate pumping schemes involving two different pump frequencies. Breaking the intrinsic symmetry of degenerate SFWM may allow greater flexibility in shaping different configuration of JSA compatibles with the distribution of Schmidt Coefficients desired. Such studies could reveal conditions in which specific frequency-bin entangled states become accessible.

Chapter 5

Conclusions

The results presented throughout this work demonstrate that the implemented JSA model successfully captures the spectral correlations arising from SFWM in PCF and provides a useful framework for analyzing the quantum state of the generated photon pairs. The numerical simulations show that variations fibers geometry and pump wavelength modify the phase matching landscape and consequently alter the orientation, localization, and shape of the JSI distribution. To quantify the modal structure of the biphoton state, a Schmidt decomposition based on the SVD of the JSA was implemented; the numerical analysis allowed the extraction of the Schmidt coefficients, purity, Schmidt number, and second order correlation function, which provided a characterization of the correlations of the biphoton quantum state. All of the analyzed configurations exhibited a dominant Schmidt mode, to a greater or lesser extent, resulting in nearly factorable states, even with cases that presented lower purity. This indicates that the studied PCF configurations constitute promising candidates for the generation of indistinguishable heralded photons.

From this perspective, the Schmidt decomposition serves not only as a characterization tool for spectral correlations, but also as a design and diagnostic framework linking the spectral properties of SFWM sources to potential applications in quantum information processing. By controlling the modal structure of the generated biphoton state through fiber geometry and dispersion engineering, it becomes possible to tailor the source for specific tasks [14]. The increasing interest in frequency-domain quantum technologies further highlights the relevance of this approach.

Future work may explore photonic crystal fiber geometries and dispersion profiles specifically engineered to tailor the Schmidt spectrum toward target quantum states. In particular, configurations supporting two or more significant Schmidt modes could be investigated as potential platforms for frequency-bin entanglement and high-dimensional

photonic encoding schemes. Such possibilities constitute prospective research directions emerging from the analysis developed in this work rather than results demonstrated in the present study.

References

[1] Peter J. Denning and Ted G. Lewis. Exponential laws of computing growth. *Communications of the ACM*, 60(1):54–65, 2017. doi: 10.1145/2994581.

[2] Michael A. Nielsen and Isaac L. Chuang. *Quantum Computation and Quantum Information*. Cambridge University Press, 10th anniversary edition, 2010. ISBN 9781107002173.

[3] Theodore H. Maiman. Stimulated optical radiation in ruby. *Nature*, 187:493–494, 1960. doi: 10.1038/187493a0.

[4] Anthony E. Siegman. *Lasers*. University Science Books, 1986. ISBN 9780935702118.

[5] Warren P. Grice, Alfredo B. U'Ren, and Ian A. Walmsley. Eliminating frequency and space-time correlations in multiphoton states. *Physical Review A*, 64:063815, 2001. doi: 10.1103/PhysRevA.64.063815.

[6] Daniel Rodriguez Guillen. Estudio de correlaciones espectrales en pares de fotones generados por mezcla de cuatro ondas en fibras de cristal fotónico. Master's thesis, Universidad de Guanajuato, León, Guanajuato, México, 2021. URL http://repositorio.ugto.mx/handle/20.500.12059/5010.

[7] Liang Cui, Xiaoying Li, and Ningbo Zhao. Minimizing the frequency correlation of photon pairs in photonic crystal fibers. *Physical Review A*, 85(2):023825, 2012. doi: 10.1103/PhysRevA.85.023825.

[8] Karina Garay Palmett. *Propiedades de enlazamiento espectral de parejas de fotones generadas por mezclado de cuatro ondas espontáneo en fibra óptica*. PhD thesis, Centro de Investigación Científica y de Educación Superior de Ensenada, CICESE, Ensenada, México, 2009.

[9] A.G. de Oliveira, R.M. Gomes, V.C.C. Brasil, N. Rubiano da Silva, L.C. Céleri, and P.H. Souto Ribeiro. Full thermalization of a photonic qubit. *Physics Letters A*, 384 (36):126933, December 2020. ISSN 0375-9601. doi: 10.1016/j.physleta.2020.126933. URL http://dx.doi.org/10.1016/j.physleta.2020.126933.

[10] Tayyab Imran. *Ultrafast Lasers in Quantum Computing*. GoLD, 2025. ISBN 9798287977535.

[11] Joseph M. Lukens and Pavel Lougovski. Quantum information processing with frequency-bin qubits: Progress, status, and challenges. *Optica*, 4(1), January 2017. doi: 10.1364/OPTICA.4.000008.

[12] Christine Silberhorn, Peter J. Mosley, Jeff S. Lundeen, Brian J. Smith, and Ian A. Walmsley. Spectrally resolved photon statistics and purity of heralded single photons. *Physical Review Letters*, 101(19):193601, 2008. doi: 10.1103/PhysRevLett.101.193601.

[13] Hsuan-Hao Lu, Joseph M. Lukens, Brian P. Williams, Poolad Imany, Nicholas A. Peters, Andrew M. Weiner, and Pavel Lougovski. A controlled-not gate for frequency-bin qubits. *npj Quantum Information*, 5:24, 2019. doi: 10.1038/s41534-019-0138-4.

[14] Jesper Bjerge Christensen. *Tailored four-wave-mixing processes for optical quantum information science*. PhD thesis, Technical University of Denmark, 2018. URL https://backend.orbit.dtu.dk/ws/portalfiles/portal/165149068/PhD_JesperBjergeChristensen.pdf.

[15] Anne Rooney. *La historia de la física: De la filosofía natural al enigma de la materia oscura*. Editorial Blume, Barcelona, 2013. ISBN 978-84-15317-72-4.

[16] Henk W. Broer. Bernoulli's light ray solution of the brachistochrone problem through hamilton's eyes. *International Journal of Bifurcation and Chaos*, 24(8):1440009, 2014. doi: 10.1142/S0218127414400094.

[17] Govind P. Agrawal. *Nonlinear Fiber Optics*. Academic Press, 6 edition, 2019. ISBN 9780128170427.

[18] K. Okamoto. *Fundamentals of Optical Waveguides*. Electronics & Electrical. Elsevier Science, 2006. ISBN 9780125250962. URL https://books.google.com.mx/books?id=0SNXgnx6un4C.

[19] K. Thyagarajan and A.K. Ghatak. Fiber and guided wave optics — nonlinear optics. In Robert D. Guenther, editor, *Encyclopedia of Modern Optics*, pages 472–486. Elsevier, Oxford, 2005. ISBN 978-0-12-369395-2. doi: https://doi.org/10.1016/B0-12-369395-0/00700-4.

[20] Robert W. Boyd. *Nonlinear Optics*. Academic Press, 3 edition, 2008. ISBN 9780123694706.

[21] Richard P. Feynman, Robert B. Leighton, and Matthew Sands. *The Feynman Lectures on Physics, Volume I.* Addison-Wesley, Reading, Massachusetts, 1963. ISBN 9780201021158.

[22] P. A. M. Dirac. On the analogy between classical and quantum mechanics. *Reviews of Modern Physics*, 17(2–3):195–199, April 1945. doi: 10.1103/RevModPhys.17.195.

[23] Peter D. Drummond and Mark Hillery. *The Quantum Theory of Nonlinear Optics.* Cambridge University Press, 2014. ISBN 9780521843327.

[24] Max Born and Emil Wolf. *Principles of Optics: Electromagnetic Theory of Propagation, Interference and Diffraction of Light.* Cambridge University Press, Cambridge, 7 edition, 1999. ISBN 9780521642224.

[25] Michele Maggiore. *A Modern Introduction to Classical Electrodynamics.* Oxford University Press, Oxford, United Kingdom, 2023. ISBN 9780192867421. doi: 10.1093/oso/9780192867421.001.0001.

[26] Leonard Mandel and Emil Wolf. *Optical Coherence and Quantum Optics.* Cambridge University Press, 1995. ISBN 9780521417115.

[27] Rodney Loudon. *The Quantum Theory of Light.* Oxford University Press, 3 edition, 2000. ISBN 9708198503102.

[28] Karina Garay-Palmett, Hayden J. McGuinness, Oren Cohen, Jeff S. Lundeen, Rafael Rangel-Rojo, Alfredo B. U'Ren, Michael G. Raymer, Christopher J. McKinstrie, Stojan Radic, and Ian A. Walmsley. Photon pair-state preparation with tailored spectral properties by spontaneous four-wave mixing in photonic-crystal fiber. *Optics Express*, 15:14870–14886, 2007. doi: 10.1364/OE.15.014870.

[29] Christopher Gerry and Peter Knight. *Introductory Quantum Optics.* Cambridge University Press, 2 edition, 2005. ISBN 9780521527357.

[30] Mark Fox. *Quantum Optics: An Introduction.* Oxford University Press, 2006. ISBN 9780198566725.

[31] J.J. Sakurai and J. Napolitano. *Modern Quantum Mechanics.* Cambridge University Press, 2017. ISBN 9781108422413. URL https://books.google.com.mx/books?id=O1OyDwAAQBAJ.

[32] Michael E Peskin and Daniel V Schroeder. *An introduction to quantum field theory.* Addison-Wesley, Reading, MA, 1995. ISBN 9780201503975.

[33] Angela Maria Barragan Diaz. Estados cuanticos de parejas de fotones con entrelazamiento espacial y espectral. *Universidad Nacional Autonoma de Mexico*, 2013. URL https://repositorio.unam.mx/contenidos/118426.

[34] Marvin K. Simon. *Probability Distributions Involving Gaussian Random Variables: A Handbook for Engineers and Scientists*. Springer, 2002. ISBN 978-0-387-47694-0. doi: 10.1007/978-0-387-47694-0.

[35] K.F. Riley, M.P. Hobson, and S.J. Bence. *Mathematical Methods for Physics and Engineering: A Comprehensive Guide*. Cambridge University Press, 2006. ISBN 9781139450997. URL https://books.google.com.mx/books?id=Mq1nlEKhNcsC.

[36] Bin Fang, Offir Cohen, {Jamy B.} Moreno, and Virginia Lorenz. State engineering of photon pairs produced through dual-pump spontaneous four-wave mixing. *Optics Express*, 21(3):2707–2717, February 2013. ISSN 1094-4087. doi: 10.1364/OE.21.002707.

[37] Daniel Rodriguez-Guillen, Antonio Díez, Miguel V. Andrés, and Lorena Velazquez-Ibarra. Inverse design of photonic crystal fibers for dispersion engineering using neural networks. *Optics Communications*, 587:131891, 2025. doi: 10.1016/j.optcom.2025.131891.

[38] Wolfgang Scherer. *Mathematics of Quantum Computing: An Introduction*. Springer, Cham, 2019. ISBN 978-3-030-12357-4. doi: 10.1007/978-3-030-12358-1. Personal copy (print edition).

[39] Michael G. Raymer and Ian A. Walmsley. Temporal modes in quantum optics: Then and now. *Physica Scripta*, 95(6):064002, 2020. doi: 10.1088/1402-4896/ab6153.

[40] Benjamin Brecht, Dileep V. Reddy, Christine Silberhorn, and Michael G. Raymer. Photon temporal modes: A complete framework for quantum information science. *Physical Review X*, 5(4):041017, 2015. doi: 10.1103/PhysRevX.5.041017.

[41] M. V. Fedorov and N. I. Miklin. Schmidt modes and entanglement. *Contemporary Physics*, 55(2):94–109, 2014. doi: 10.1080/00107514.2013.878554.

[42] Ram P. Kanwal. *Linear Integral Equations: Theory and Technique*. Birkhäuser, 2 edition, 2013. doi: 10.1007/978-1-4614-6012-1.

[43] Nicolas Gisin and Rob Thew. Quantum communication. *Nature Photonics*, 1: 165–171, 2007. doi: 10.1038/nphoton.2007.22.

[44] C. K. Law, I. A. Walmsley, and J. H. Eberly. Continuous frequency entanglement: Effective finite hilbert space and entropy control. *Physical Review Letters*, 84(23): 5304–5307, 2000. doi: 10.1103/PhysRevLett.84.5304.

[45] Richard L. Burden and J. Douglas Faires. *Numerical Analysis*. Cengage Learning, 9 edition, 2016. ISBN 9781305253667.

[46] Kendall E. Atkinson. *An Introduction to Numerical Analysis*. John Wiley & Sons, 2 edition, 1989. ISBN 9780471624899.

[47] Hsuan-Hao Lu, Emma M. Simmerman, Pavel Lougovski, Andrew M. Weiner, and Joseph M. Lukens. Fully arbitrary control of frequency-bin qubits. *Physical Review Letters*, 120(3):030502, 2018. doi: 10.1103/PhysRevLett.120.030502.

[48] Peter J. Mosley, Jeff S. Lundeen, Brian J. Smith, Piotr Wasylczyk, Alfred B. U'Ren, Christine Silberhorn, and Ian A. Walmsley. Heralded generation of ultrafast single photons in pure quantum states. *Physical Review Letters*, 100:133601, 2008. doi: 10.1103/PhysRevLett.100.133601.

[49] C. K. Hong, Z. Y. Ou, and L. Mandel. Measurement of subpicosecond time intervals between two photons by interference. *Physical Review Letters*, 59(18):2044–2046, 1987. doi: 10.1103/PhysRevLett.59.2044.

[50] Pieter Kok and Brendon W. Lovett. *Optical Quantum Information Processing*. Cambridge University Press, 2010. ISBN 9780521875342.

[51] Noemi Tagliavacche, Massimo Borghi, Giulia Guarda, Domenico Ribezzo, Marco Liscidini, Davide Bacco, Matteo Galli, and Daniele Bajoni. Frequency-bin entanglement-based quantum key distribution. *npj Quantum Information*, 11(1), April 2025. ISSN 2056-6387. doi: 10.1038/s41534-025-00991-5. URL http://dx.doi.org/10.1038/s41534-025-00991-5.

[52] T. W. Körner. *Fourier Analysis*. Cambridge University Press, 1988. ISBN 9780521389914.

Appendix A

Derivation of the Nonlinear Coupled Mode Equations for Four Wave Mixing

We have the equation,

$$P_j^{(NL)} = \frac{3\epsilon_0}{4}\chi^{(3)} \sum_{i,k,l} F_i F_k F_l^* \, \tilde{A}_i \tilde{A}_k \tilde{A}_l^* \, e^{i(\beta_j z - \omega_j t)} e^{i\Delta\beta z}. \tag{A.1}$$

To isolate the evolution of $\tilde{A}_j(z)$, we project onto the transverse mode $F_j^*(x, y)$ and integrate over the cross section, such as,

$$\iint F_j^* \left[2i\beta_j F_j e^{i(\beta_j z - \omega_j t)} \frac{d\tilde{A}_j}{dz} \right] dxdy = -\frac{\omega_j^2}{c^2\epsilon_0} \iint F_j^* P_j^{(NL)} dxdy \tag{A.2}$$

.

Then,

$$2i\beta_j e^{i(\beta_j z - \omega_j t)} \frac{d\tilde{A}_j}{dz} \iint |F_j|^2 dxdy = \frac{3\epsilon_0}{4}\chi^{(3)} \sum_{i,k,l} \tilde{A}_i \tilde{A}_k \tilde{A}_l^* e^{i(\beta_j z - \omega_j t)} e^{i\Delta\beta z} \iint F_j^* F_i F_k F_l^* dxdy. \tag{A.3}$$

We define the normalization constant as

$$N_j = \iint |F_j(x, y)|^2 dxdy, \tag{A.4}$$

which represents the modal norm associated with the transverse field distribution. This normalization naturally appears when projecting the wave equation onto the $j-$th guided

mode and is directly related to optical power carried to that mode [18]. By substituting into the propagation equation and canceling the exponential factor we obtain,

$$2i\beta_j N_j \frac{d\tilde{A}_j}{dz} = -\frac{3\omega_j^2}{4c^2}\chi^{(3)} \sum_{i,k,l} \tilde{A}_i \tilde{A}_k \tilde{A}_l^* e^{i\Delta\beta z} \iint F_j^* F_i F_k F_l^* dxdy. \tag{A.5}$$

When divide both sides by N_j, we obtain a normalized evolution equation for $\tilde{A}_j(z)$ and introduce the dimensionless overlap integrals

$$2i\beta_j \frac{d\tilde{A}_j}{dz} = -\frac{3\omega_j^2}{4c^2}\chi^{(3)} \sum_{i,k,l} \tilde{A}_i \tilde{A}_k \tilde{A}_l^* e^{i\Delta\beta z} \frac{\iint F_j^* F_i F_k F_l^* dxdy}{N_j}, \tag{A.6}$$

where the modal overlap is defined as

$$\mathcal{O}_{ijkl} = \frac{\iint F_j^* F_i F_k F_l^* \, dxdy}{N_j}. \tag{A.7}$$

This quantity is a dimensionless integral that characterizes the spatial overlap among the interacting modes (j, i, k, l) [17]. It quantifies how efficiently the interacting waves couple through the third order nonlinearity. In the single mode limit, these overlap integrals reduce to the effective area description previously used.

The evolution equation is expressed in terms of field amplitudes $\tilde{A}_j$ with units of electric field, and the nonlinear response appears explicitly through susceptibility $\chi^{(3)}$. However, in nonlinear fiber optics it is customary to express the nonlinear response in terms of the intensity dependent refractive index. Furthermore, the optical intensity I is related to the electric field amplitude through [17],

$$I = \frac{1}{2} n \epsilon_0 c |E|^2 \Rightarrow \; I_j = \frac{1}{2} n_j \epsilon_0 c |\tilde{A}_j|^2. \tag{A.8}$$

Optical power carried by the mode, related to intensity, is obtained by integrating over the transverse plane as,

$$P_j = \iint I_j \, dxdy = \frac{1}{2} n_j \epsilon_0 c |\tilde{A}_j|^2 \iint |F_j|^2 dxdy. \tag{A.9}$$

Thus, obtaining,

$$P_j = \frac{1}{2} n_j \epsilon_0 c N_j |\tilde{A}_j|^2. \tag{A.10}$$

Introduce a new amplitude A_j, known as the normalized amplitude, such that,

$$|A_j|^2 = P_j, \tag{A.11}$$

which directly implies the transformation: $A_j = \tilde{A}_j \sqrt{\frac{n_j \epsilon_0 c N_j}{2}}$. Thus, we can identify the relations,

$$\frac{d\tilde{A}_j}{dz} = \frac{1}{\sqrt{\frac{n_j \epsilon_0 c N_j}{2}}} \frac{dA_j}{dz}, \qquad \tilde{A}_i \tilde{A}_k \tilde{A}_l^* = \frac{A_i A_k A_l^*}{\left(\frac{n_i n_k n_l \epsilon_0^3 c^3 N_i N_k N_l}{2^3}\right)^{1/2}}. \tag{A.12}$$

Substituting these expressions into the propagation equation and multiplying both sides by $(\sqrt{\frac{n_j \epsilon_0 c N_j}{2}})$, the nonlinear coefficient can be rewritten using the relation between the nonlinear refractive index and the third order susceptibility. Eq. 1.21, leads to,

$$\chi^{(3)} = \frac{4}{3} n_j^2 \epsilon_0 c\, n_2$$

and substituting this expression into the nonlinear coefficient give us $\frac{2\omega_j^2}{c^2} n_j^2 \epsilon_0 c\, n_2$.

Furthermore, using the relation $\beta_j = n_j \omega_j / c \Rightarrow \omega_j^2 n_j^2 / c^2 = \frac{\omega_j}{c} \beta_j n_j$, one finds that $\frac{\omega_j^2}{c^2} n_j^2 = \frac{\omega_j}{c} \beta_j n_j$. After these substitutions and dividing both sides by the common factor $2i\beta_j$, the propagation equation becomes,

$$\frac{dA_j}{dz} = i \frac{\omega_j}{c} n_2 \sum_{i,k,l} A_i A_k A_l^* \frac{(n_j^3 N_j)^{1/2}}{(n_i n_k n_l N_i N_k N_l)^{1/2}} \mathcal{O}_{ijkl} e^{i \Delta\beta z}. \tag{A.13}$$

It is convenient at this stage to introduce dimensionless overlap coefficients that account for the transverse modal structure and quantify the strength of the nonlinear coupling among the interacting modes. We therefore define the normalized fourth-order overlap tensor as [17],

$$\tilde{f}_{ijkl} = \frac{\iint F_i F_j^* F_k F_l^* \, dxdy}{(N_i N_j N_k N_l)^{1/2}}, \quad \tilde{f}_{jk} = \frac{\iint |F_j|^2 |F_k|^2 \, dxdy}{N_j N_k}, \tag{A.14}$$

which are particularly useful for describing SPM and XPM processes. When $j = k$, the coefficient characterizes SPM, and when $j \neq k$ it characterizes XPM. These coefficients represent the four mode overlap integral, it measures the efficiency of nonlinear interaction involving the modes, determining how strongly those fields couple through the medium nonlinearity [17].

Using the redefinition,

$$\mathcal{O}_{ijkl} = \tilde{f}_{ijkl} \left(\frac{N_i N_j N_k N_l}{N_j^2} \right)^{1/2}, \tag{A.15}$$

the modal normalization factors cancel, yielding to,

$$\frac{dA_j}{dz} = i\frac{\omega_j}{c} n_2 \sum_{i,k,l} A_i A_k A_l^* \tilde{f}_{ijkl} \left(\frac{n_j^3}{n_i n_k n_l} \right)^{1/2} e^{i\Delta\beta z}. \tag{A.16}$$

For the scalar co-polarized model considered here, all interacting waves are assumed to propagate in the fundamental guided mode of a single-mode fiber [17]. Therefore, within the nonlinear coupling coefficient, the refractive indices may be approximated as,

$$n_i \approx n_k \approx n_l \approx n_j \tag{A.17}$$

Thus, the coupled-amplitude equation then reduces to,

$$\frac{dA_j}{dz} = i\frac{\omega_j}{c} n_2 \sum_{i,k,l} \tilde{f}_{ijkl} A_i A_k A_l^* e^{i\Delta\beta z}. \tag{A.18}$$

Separate the index combinations, analogously index analysis in Chapter 1,

- $i = k = l = j \rightarrow$ SPM: $|A_j|^2 A_j$.
- $i = j,\ k = l \neq j \rightarrow$ XPM: $2|A_k|^2 A_j$.
- $i \neq k \neq l \neq j \rightarrow$ FWM: $2A_i A_k A_l^* e^{i\Delta\beta z}$.

Leading to the general solution [17]:

$$\frac{dA_j}{dz} = \frac{in_2\omega_j}{c} \left[\left(\tilde{f}_{jj}|A_j|^2 + 2\sum_{k\neq j} \tilde{f}_{jk}|A_k|^2 \right) A_j + 2\tilde{f}_{ijkl} A_i A_k A_l^* e^{i\Delta\beta z} \right]. \tag{A.19}$$

Appendix B

Fourier Origin of the Phase Matching sinc Function

The integral represents a coherent sum of infinitesimal phase contributions along the propagation:

$$I = \int_0^L dz\, e^{i\Delta\beta z}. \tag{B.1}$$

Each infinitesimal segment contributes a phase factor $e^{i\Delta\beta z}$. In the complex plane, this expression can be interpreted as a vector rotating along z with angular rate $\Delta\beta$ [17].

- If $\Delta\beta = 0$, all contributions are in phase. The integral then grows linearly with L, corresponding to constructive interference.
- If $\Delta\beta \neq 0$, the phase rotates along z, and the contributions no longer add coherently. The result is an oscillatory behavior due to partial destructive interference.

The Fourier transform of a rectangular function defined on the interval $[A, B]$ is,

$$\mathcal{F}\{\text{rect}(t)\} = \int_A^B e^{ixt}\, dt = \frac{e^{ixB} - e^{ixA}}{ix}. \tag{B.2}$$

If rect(x) is a rectangular function, then rect$(x) = 1 \,\forall\, x \in X := [A, B] \,|\, A, B \in \mathbb{R}$ and rect$(y) = 0 \;\forall\; y \notin X$ [52]. This illustrates a fundamental property of Fourier transforms: spatially bounded interaction produces a sinc-shaped response in the conjugate domain [52]. Let us compute Eq. B.1 explicitly, such as,

$$I = \left[\frac{e^{i\Delta\beta z}}{i\Delta\beta}\right]_0^L = \frac{e^{i\Delta\beta L} - 1}{i\Delta\beta}. \tag{B.3}$$

By factoring the phase term $e^{i\Delta\beta L/2}$, we obtain,

$$I = e^{i\frac{\Delta\beta L}{2}} \frac{e^{i\frac{\Delta\beta L}{2}} - e^{-i\frac{\Delta\beta L}{2}}}{i\Delta\beta}. \tag{B.4}$$

Using the identity $e^{ix} - e^{-ix} = 2i\sin x$ leads to,

$$I = \frac{2\sin\left(\frac{\Delta\beta L}{2}\right)}{\Delta\beta}. \tag{B.5}$$

Therefore,

$$I = L\,\mathrm{sinc}\left(\frac{L\Delta\beta}{2}\right) e^{i\frac{L\Delta\beta}{2}}, \tag{B.6}$$

where the *sinc function* is defined as $\mathrm{sinc}(x) = \frac{\sin x}{x}$.

To visualize the role of the phase-matching function in the generation of photon pairs, Fig. B.1 shows a one dimension cut of the phase-matching term $|\phi|^2$, the pump envelope $|\alpha|^2$, and the resulting Joint Spectral Amplitude $|F|^2$ introduced in Chapter 3. The figure illustrates how the spectral structure of the generated state emerges from the interplay between the pump envelope and the phase-matching condition.

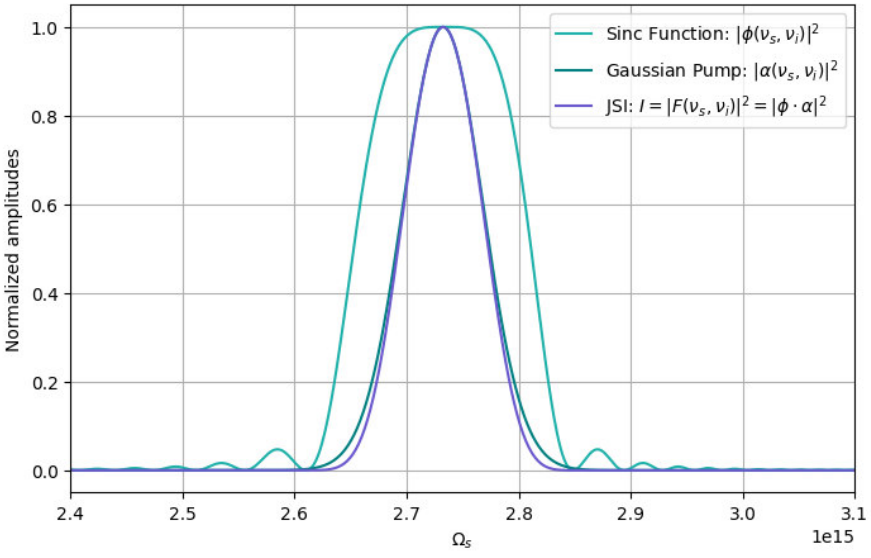

FIGURE B.1: One dimensional cut of the phase matching function $|\phi|^2$, the pump envelope $|\alpha|^2$, and the resulting Joint Spectral Amplitude $|F|^2$ (see Chapter 3). All functions are normalized to their maximum value.

The phase matching function reaches its maximum when $\Delta\beta = 0$ corresponding to perfect phase matching. From Eq. B.6, the generated amplitude is proportional to,

$$\mathrm{sinc}\left(\frac{L\Delta\beta}{2}\right), \tag{B.7}$$

which vanishes whenever,

$$I = 0 \quad \Longleftrightarrow \quad \operatorname{sinc}\left(\frac{L}{2}\Delta\beta\right) = 0. \tag{B.8}$$

Since $L \neq 0$ and $\left|e^{iL\Delta\beta/2}\right| = 1$, the zeros occur at,

$$\Delta\beta = \frac{2\pi m}{L}, \qquad m \in \mathbb{Z} \setminus \{0\}. \tag{B.9}$$

This result is central. The phase-matching function determines how efficiently different frequency combinations contribute to the SFWM process. When $\Delta\beta = 0$, all contributions generated along the fiber remain in phase and add coherently. In this regime, the generated amplitude grows linearly with the interaction length, corresponding to fully constructive interference. When $\Delta\beta \neq 0$, on the other hand, the accumulated phase varies along the propagation direction. Contributions no longer add coherently, and partial cancelation occurs due to destructive interference [17, 20]. As a consequence, the efficiency of photon-pair generation decreases as the phase mismatch increases. This becomes clearer when one recalls that the propagation constant is frequency dependent, i.e., $\beta = \beta(\omega)$ and thus, the propagation constant is itself a function of the signal and idler frequencies. The sinc term then, constrains the momentum conservation condition through the accumulated phase in the propagation and because momentum and frequency are linked through the dispersion relation, the phase-matching function acts as an effective spectral filter [28].

In other words, among all possible biphoton states,

$$|\phi(\omega_s, \omega_i)\rangle\,, \tag{B.10}$$

only those frequency combinations satisfying $\Delta\beta(\omega_s, \omega_i) \approx 0$ contribute significantly to the generated state. These configurations correspond to the solutions of the physical system.

Regions in which $\Delta\beta(\omega_s, \omega_i) \gg 0$ are strongly suppressed. Not strictly forbidden, but frequency pairs associated with larger phase mismatch are progressively suppressed by destructive interference over the finite interaction length resulting in the supression mentioned [17].

This restriction is entirely determined by the dispersion relation $\beta(\omega)$, which encodes the physical properties of the fiber (as discussed in Chapter 1). This is precisely the foundation of **dispersion engineering**: by tailoring $\beta(\omega)$, one can control the regions in

frequency space where $\Delta\beta(\omega_s, \omega_i) = 0$, and therefore shape the generated spectrum [17, 28].

Finally, after understanding these implications, the connection with **Fourier transformations** becomes clear. The finite interaction length of the fiber acts as a rectangular window in real space and the phase matching function emerges as the Fourier transform of this spatially bounded interaction, giving rise to a characteristic sinc profile. From this perspective, the spectral structure of the generated state can be understood as a consequence of the finite spatial extent of the nonlinear medium together with its dispersive properties encoded in $\beta(\omega)$.

Appendix C

Hilbert Spaces, Density Operators and Partial Trace

Hilbert Spaces

Hilbert space is a big place.

- Carlton Caves [2].

Hilbert spaces form the mathematical foundation of quantum mechanics, quantum optics, and quantum field theory. They provide the framework in which quantum states and observables are rigorously defined. A quantum system is therefore described in terms of its associated Hilbert space [38]. This appendix provides a brief and practical introduction to this structure.

The formal mathematical definition is [38]:

Definition A **Hilbert space** $\mathcal{H}$ is a:

1. a complete vector space, i.e., if $\phi, \psi \in \mathcal{H}$ and $a, b \in \mathbb{C}$, then $a\phi + b\psi \in \mathcal{H}$,
2. with a (positive-definite) **scalar product**: $\langle \cdot | \cdot \rangle$, as, $\mathcal{H} \times \mathcal{H} \longrightarrow \mathbb{C}$ and $(\phi, \psi) \longmapsto \langle \phi | \psi \rangle$.

   Such that, $\forall\ \phi, \psi, \phi_1, \phi_2 \in \mathcal{H}$ and $a, b \in \mathbb{C}$:

   - $\langle \phi | \psi \rangle = \langle \psi | \phi \rangle^*$,
   - $\langle \phi | \phi \rangle \geq 0$,
   - $\langle \phi | \phi \rangle = 0 \iff \phi = 0$,
   - $\langle \phi | a\phi_1 + b\phi_2 \rangle = a \langle \phi | \phi_1 \rangle + b \langle \phi | \phi_2 \rangle$.

This scalar product induces the **norm**

$$\begin{aligned} \|\cdot\|\colon \mathcal{H} &\longrightarrow \mathbb{R}, \\ \phi &\longmapsto \sqrt{\langle\phi|\phi\rangle}, \end{aligned} \tag{C.1}$$

in which $\mathcal{H}$ is complete.

A subset $\mathcal{H}_s \subset \mathcal{H}$ that is itself a vector space and inherits the inner product is called a **subspace**.

The structure of a Hilbert space enables the expansion of any quantum state in terms of basis vectors. To make this notion precise, we recall the definitions of linear independence, spanning sets, and orthonormal bases.

Definition 2.3 (Linear independence, basis, and Hilbert space structure) [38].

Let $\mathcal{H}$ be a Hilbert space and I an index set. A set $\{\phi_j \mid j \in I\} \subset \mathcal{H}$ is called **linearly independent** if, for every finite subset $\{\phi_1, \ldots, \phi_n\}$ and coefficients $a_k \in \mathbb{C}$,

$$\sum_{k=1}^{n} a_k \phi_k = 0, \tag{C.2}$$

implies $a_1 = \cdots = a_n = 0$.

A Hilbert space $\mathcal{H}$ is called **finite-dimensional** if it contains at most $\dim \mathcal{H} < \infty$ linearly independent vectors; otherwise, it is **infinite-dimensional**.

A set $\{\phi_j \mid j \in I\}$ is said to **span** $\mathcal{H}$ if every $\phi \in \mathcal{H}$ can be written as

$$\phi = \sum_{j \in I} a_j \phi_j. \tag{C.3}$$

A linearly independent set that spans $\mathcal{H}$ is called a **basis**. If, in addition,

$$\langle e_j | e_k \rangle = \delta_{jk}, \tag{C.4}$$

the basis is said to be **orthonormal**. A Hilbert space is called **separable** if it admits a countable orthonormal basis.

The previous definition is purely mathematical. Physically, a Hilbert space should not be interpreted as a spatial or geometrical space, but rather as an abstract space in which quantum states are represented as vectors. This structure is essential because it provides

a consistent framework to describe superposition, measurement, and observable quantities in quantum mechanics. To see this let us analyze the **First Quantum Postulate of Quantum Mechanics** [2, 38]:

> ***Postulate 1*** *(Observables and Pure States). Associated with any isolated physical system is a complete vector space with inner product (i.e., a Hilbert space), known as the state space of the system. The system is completely described by its state vector.*

This postulate establishes that quantum states are represented as vectors in a Hilbert space. A more detailed formulation [38] further specifies that physical observables are represented by self-adjoint operators acting on this space, and that the expectation value of an observable A in a normalized state $|\psi\rangle$ is given by:

$$\langle A\rangle_{\psi} = \langle\psi|A|\psi\rangle\,. \tag{C.5}$$

If the statistical properties of a system can be completely described by a single state vector, the system is said to be in a **pure state**.

Therefore, the Hilbert space provides the complete framework in which all possible states of a given quantum system are defined, while physical observables correspond to operators acting on these states. The outcomes of measurements are obtained through expectation values and probability amplitudes derived from the state vector. In practice, a specific physical system does not explore the entire Hilbert space, but rather a restricted subset determined by the boundary conditions, symmetries, and initial preparation of the system.

Density Operators

However, pure states are not the most general form in which quantum systems can appear. A quantum system must be described by a mixed state when it is in one of a set of states $\{|\psi_j\rangle\}$, but we do not know which one. Instead, we only know the probabilities p_j associated with each state. The statistical properties of such an ensemble are described by a **mixed state** [38].

Mathematically, the most general description of a quantum system, encompassing both pure and mixed states, is given by the so-called **density operator**. *The density operator contains complete statistical information about the quantum system* [2, 27, 29].

Let us introduce the **Fifth Postulate of Quantum Mechanics** [38]:

> ***Postulate 5*** *(Mixed States). In general, a quantum mechanical system is described by an operator $\hat{\rho}$ acting on a Hilbert space $\mathcal{H}$. The operator $\hat{\rho}$ is called the* ***density operator****. The set of all density operators on $\mathcal{H}$ is denoted by $D(\mathcal{H})$, defined as*
>
> $$D(\mathcal{H}) := \left\{ \hat{\rho} \in L(\mathcal{H}) \;\middle|\; \hat{\rho}^\dagger = \hat{\rho},\ \hat{\rho} \geq 0,\ \mathrm{Tr}(\hat{\rho}) = 1 \right\}. \tag{C.6}$$
>
> *The states described by density operators in $D(\mathcal{H})$ are called* ***mixed states****.*

Where $L(\mathcal{H})$ is the set of linear operators on $\mathcal{H}$.

What is this **density operator**? We have seen that physical observables are represented by self-adjoint operators acting on a state, what physical observable does this operator represent? Well, the density operator more like a mathematical equivalent representation of the vector state, useful under certain specifications. Working with the vector state, or it's density operator gives the same physical information.

For pure states, the density operator can be written as:

$$\hat{\rho} = |\psi\rangle \langle\psi| . \tag{C.7}$$

However, the density operator provides a more general description, allowing the representation of statistical mixtures of states.

For example, let $\hat{M}$ be a measurement operator (Kraus operator) [2]. The measurement of a physical observable using state vectors is described through expectation values such as $\langle \hat{M} \rangle_\psi$. For well-defined observables represented by self-adjoint operators [38], one has the eigenvalue equation:

$$\hat{M} |\psi\rangle = m |\psi\rangle , \tag{C.8}$$

where m is an eigenvalue of $\hat{M}$.

On the other hand, in the density operator formalism, measurements are described more generally. If $|\psi_i\rangle$ is the initial state, the probability of obtaining the outcome associated with $\hat{M}$ is:

$$p(m|i) = \langle \psi_i | \hat{M}^\dagger \hat{M} | \psi_i \rangle = \mathrm{Tr}\left[\hat{M}^\dagger \hat{M} \hat{\rho} \right]. \tag{C.9}$$

The post-measurement state is given by:

$$|\psi_i^m\rangle = \frac{\hat{M} |\psi_i\rangle}{\sqrt{\langle \psi_i | \hat{M}^\dagger \hat{M} | \psi_i \rangle}}. \tag{C.10}$$

Thus, after the measurement, the system is described by a set of states $|\psi_i^m\rangle$ with associated probabilities. In the density operator formalism, the updated state is:

$$\hat{\rho}_m = \frac{\hat{M}\hat{\rho}\hat{M}^\dagger}{\mathrm{Tr}\left[\hat{M}^\dagger\hat{M}\hat{\rho}\right]}. \tag{C.11}$$

In general, the density operator can be written as a convex combination of states:

$$\hat{\rho} = \sum_i p_i \left|\psi_i\right\rangle \left\langle\psi_i\right|, \tag{C.12}$$

or, more generally,

$$\hat{\rho} = \sum_i p_i \hat{\rho}_i, \quad \hat{\rho}_i = \sum_j p_{j,i} \left|\psi_{ij}\right\rangle \left\langle\psi_{ij}\right|. \tag{C.13}$$

Reduced Density Operator

For subsystems of a composite quantum system, one defines the reduced density operator. Suppose we have two physical systems A and B, whose joint state is described by $\hat{\rho}^{AB} \in \mathcal{H}^A \otimes \mathcal{H}^B$. The reduced density operator for system A is defined as:

$$\hat{\rho}^A \equiv \mathrm{Tr}_B\left[\hat{\rho}^{AB}\right]. \tag{C.14}$$

Here, Tr_B denotes the **partial trace** over subsystem B [2]. The partial trace is defined by its action on product operators:

$$\mathrm{Tr}_B\left[\left|a_1\right\rangle\left\langle a_2\right| \otimes \left|b_1\right\rangle\left\langle b_2\right|\right] \equiv \left|a_1\right\rangle\left\langle a_2\right| \ \mathrm{Tr}\left(\left|b_1\right\rangle\left\langle b_2\right|\right), \tag{C.15}$$

and extended linearly to arbitrary operators. Thus, the partial trace acts only on subsystem B, leaving subsystem A unchanged (Ignore B).

It is not immediately obvious that the reduced density operator $\hat{\rho}^A$ provides a complete description of subsystem A. To illustrate this, consider a product state of the form $\hat{\rho}^{AB} = \hat{\rho}\otimes\hat{\sigma}$, where $\hat{\rho}$ and $\hat{\sigma}$ are the density operators of systems A and B, respectively [2]. Then,

$$\hat{\rho}^A = \mathrm{Tr}_B\left[\hat{\rho}\otimes\hat{\sigma}\right] = \hat{\rho}\,\mathrm{Tr}(\hat{\sigma}) = \hat{\rho}. \tag{C.16}$$

Appendix D

SVD and Schmidt Decomposition

Information is physical.

- Rolf Landauer [2].

For a pure state of a composite system, the many important properties of quantum systems will be the same for both systems. This has no obvious symmetry property, and is a consequence of the Schmidt decomposition [2]

Let us give proof for the case where two systems A and B have state spaces of the same dimension, with the set of orthonormal basis: $\{|j\rangle, |k\rangle\}$ for such systems, respectively. Then the bipartite state $|\psi\rangle$ may be expanded as:

$$|\psi\rangle = \sum_{jk} a_{jk} |j\rangle |k\rangle . \tag{D.1}$$

For some matrix a of complex numbers a_{jk}. By the singular value decomposition,

$$a = UDV^*. \tag{D.2}$$

Where D is a diagonal matrix with non-negative elements, and U and V are unitary matrices. Thus

$$|\psi\rangle = \sum_{ijk} U_{ji} D_{ii} V^\dagger_{ik} |j\rangle |k\rangle . \tag{D.3}$$

If we define

$$\begin{aligned} |i_A\rangle &\equiv \sum_j U_{ji} |j\rangle , \\ |i_B\rangle &\equiv \sum_k V^*_{ki} |k\rangle . \end{aligned} \tag{D.4}$$

And define the elements in d as

$$s_i \equiv d_{ii}. \tag{D.5}$$

Therefore, the state may be written as

$$|\psi\rangle \equiv \sum_i \sqrt{\lambda_i}\, |i_A\rangle\, |i_B\rangle\,. \tag{D.6}$$

Where $\lambda_i \equiv s_i^2$, this is the **Schmidt Decomposition** for a normalized quantum state. Thus, the Schmidt decomposition is obtained directly from the singular value decomposition of the coefficient matrix. Where $|i_A\rangle$ forms an orthonormal set, from the unitary of u and the orthonormality of $|j\rangle$, similarly that $|i_B\rangle$ form an orthonormal set.